UNIVERSITÀ DEGLI STUDI DI PADOVA

Dipartimento di ingegneria civile, edile e ambientale

Technische Universität Carolo Wilhelmina zu Braunschweig

Laurea Magistrale in Ingegneria Civile

A numerical approach for modelling fracture in variably saturated porous media

Relatore: Prof. Lorenzo SANAVIA

Correlatore: Prof.ssa Laura DE LORENZIS

Laureanda:

Francesca MARCON 1058705

ANNO ACCADEMICO 2014-2015

Ringraziamenti

In primis volevo ringraziare il Professor Lorenzo Sanavia per la pazienza e il tempo dedicatomi alla realizzazione di questa tesi e la Professoressa Laura de Lorenzis per l'aiuto e la collaborazione nel periodo a Braunschweig.

I miei genitori per avermi permesso di intraprendere e ultimare quest'avventura e mia sorella Michela per essermi stata vicina durante tutto questo percorso.

Gli amici della compagnia di Silea, tutte le mie coinquiline, i miei compagni di studi e tutti gli amici che in questi anni non solo universitari hanno reso possibile questo traguardo.

Alberto per essermi stato vicino come solo lui sa fare supportandomi e rubandomi sempre un sorriso.

Un grazie di cuore a tutti perché senza tutti voi ora non sarei qui a poter festeggiare la fine di bellissimo percorso.

Index

Chapter 1 – Introduction

This thesis, developed in cooperation with the Institute of Applied Mechanics, Technische Universität Braunschweig (Germany), aspires to couple a model of porous media with a phase field model for fracture.

In recent years, the interest in thermos-hydromechanics of partially saturated porous media is increased and several mathematical models were therefore implemented, neglecting however some relevant aspects of the problem, which involves gas phase, water phase and the solid matrix.

In this dissertation we take in account only two phases, i.e. the solid matrix and water, omitting the effects of the gas in the mixture. The implemented model consists in balance equations of mass, linear momentum and energy, as well as of the appropriate constitutive equations.

The macroscopic balance equations will be discretized both in space (using the finite element method) and both in time.

The discretized equations in matrix form will be therefore solved by means of a Newton-Raphson type procedure.

Some examples, simpler before and more and more complex and complete later, will be carried out in order to validate the model step by step, comparing it to analytical results or with the help of some benchmarks.

From the case of fully saturated model, the dissertation will arrive to discuss the case of a partially saturated model.

When the model of the porous media is completed and validated, it is time to introduce the concept of phase field, for the study of the development of the fracture in the material.

In order to briefly introduce the phase field model (better explained in Chapter 4), we can describe it like a model where the fracture is indicated with a scalar order parameter, which is able to change the stiffness of the material, thanks to its link with the material properties.

In particular, the order parameter assumes the value zero where the material is broken (and the stiffness will be consequently reduced), and the value one for the undamaged material. At interface between broken and undamaged material, the order parameter interpolates between zero and one.

The Institute of Applied Mechanics, Technische Universität Braunschweig (Germany), and in particular its Professor and Director, Prof. Dr.-Ing. Laura De Lorenzis, supplied a Matlab code in which the phase field model was implemented.

In this model, in addition to the displacement vector, the phase field order parameter is treated as a supplementary nodal degree of freedom. Usual linear shape functions can be used, together with four noded element.

In every time step, the nonlinear coupled system of equations formed by the discretized elasto-mechanincal field equations and the evolution equation is solved using a Newton-Raphson algorithm.

The objective was therefore to introduce in this code the porous media model, briefly descripted before, and to make the two fit together in order to couple the two approaches and study the fracture in a porous material.

Chapter 2 – Theory of the porous media

2.1. Governing equations for dynamic behaviour of saturated-unsaturated porous media

2.1.1. Introduction

Biot was the first who established the essence of the mathematical theory governing the behavior of saturated porous media. He formulated the solid-fluid interaction for linear elastic materials by a straightforward physical approach.

Later, Zienkiewicz and Shiomi extended the Biot's theory with large strain and non-linear material behavior of saturated porous media.

This thesis uses a further expansion of the Biot's theory where the principle of effective stress is extended to unsaturated zones and the air pressure is assumed to be zero.

The dynamic unsaturated context presents the most difficult situation and the formulation is given in this case. The other phenomena (slow consolidation or saturated behaviors) can be treated like special cases.

Throughout this thesis the stress is defined as tension positive and the pressure as compression negative.

2.1.2. General assumption for behavior of porous media

Porous media are composed of a mass of solid grains separated by spaces or voids. These voids are filled with air or water or both. The porous media is dry when only air is present, it is saturated when only water is present. When both water and air are present the porous media is said to be partially saturated.

S_w , the degree of water saturation and S_a, the degree of air saturation are defined as:

$$\begin{cases} S_w = \frac{volume\ of\ water}{volume\ of\ voids} \\ S_a = \frac{volume\ of\ air}{volume\ of\ voids} \end{cases} \quad (2.1)$$

If the porous media is dry, saturated or partially saturated the sum of S_w and S_a is always equal to unity:

$$S_w + S_a = 1. \quad (2.2)$$

The mechanics of porous media is described on a macroscopic scale so that a continuum approach can be used in the analysis, assuming the porous medium to be continuous everywhere, with air, water and solid grains forming an overlapping continuum.

If the air flow is not significant and the air pressure is nearly uniform over the domain considered, it may be assumed that the air pressure p_a in the unsaturated zones remains at atmospheric pressure, or:

$$p_a = 0 \quad (2.3)$$

2.1.3. Description of skeleton deformation and fluid flow

A Cartesian coordinate system is used as a reference for all displacements, velocities and accelerations. There are two different description: Lagrangian and Eulerian. In the first one the attention is focused on what is happening to a particular material with its initial coordinate $\underline{X}$. In the second one we concentrate on events at a particular point $\underline{x}$ in the space.

In small strain and small displacement analysis it makes no difference which description is used. But if the finite deformation of the soil skeleton is to be considered, a Lagrangian description is used for the solid phase.

The displacement vector $\underline{u}$ of a typical particle from its initial position $\underline{X}$ to its position at time t is:

$$\underline{u} = \underline{x} - \underline{X} \tag{2.4}$$

Coupled problems in soil mechanics are generally focused on water flow. $\underline{\dot{w}}$ is the water velocity relative to the solid phase and it is defined as the rate of water flow across unit gross area of the solid-fluid ensemble. The relative velocity of water is $\frac{\underline{\dot{w}}}{(nS_w)}$.

n is the porosity of the solid which is defined as:

$$n = \frac{volume\ of\ voids}{total\ volume\ of\ soil} \tag{2.5}$$

The absolute velocity of water $\underline{\dot{U}}$ is:

$$\underline{\dot{U}} = \underline{\dot{u}} + \frac{\dot{\underline{w}}}{(nS_w)} \tag{2.6}$$

Where $\underline{\dot{u}}$ is the velocity of the solid phase.

2.1.4. Effective stress in partially saturated soils

For saturated soil Terzaghi, who introduced the concept of effective stress, related it to the total stress $\underline{\sigma}$ and the water pressure p_w as:

$$\underline{\sigma} = \underline{\sigma}' + \underline{m}\, p_w \tag{2.7}$$

Where $\underline{m}^T = [1\ 1\ 1\ 0\ 0\ 0]$.

The principle of effective stress is extended to the unsaturated zones and the Bishop's law is adopted:

$$\underline{\sigma} = \underline{\sigma}' + \underline{m}\, \bar{p} \tag{2.8}$$

With:

$$\bar{p} = \chi\, p_w + (1 - \chi)\, p_a \tag{2.9}$$

χ is the Bishop's parameter and it was suggested to be dependent on the degree of water saturation, and other factors. $\bar{p}$ can be treated like the approximation of the pressure acting on the soil grains.

χ may be approximated as:

$$\chi \cong S_w \tag{2.10}$$

Substituting equations (2.10) and (2.1) into equation (2.9) gives:

$$\bar{p} = S_w\, p_w + S_a\, p_a \tag{2.11}$$

Assuming the air pressure equals to zero, the equation becomes:

$$\bar{p} = S_w\, p_w \tag{2.12}$$

A modification of the equation (2.8) can be introduced to account for the compressibility of the solid grains:

$$\underline{\sigma} = \underline{\sigma}'' - \underline{m}\, \alpha\, \overline{p} \tag{2.13}$$

$\underline{\sigma}''$ is the real effective stress.

For the concrete α is in the range of 0.4 – 0.6 and in this case it is important to take the effect of solid grain compressibility into account.

2.1.5. Partial saturation and capillary pressure

A liquid surface resists tensile forces because of the attraction between adjacent molecules in the surface. The phenomenon of capillarity is caused by such surface tension. The height of water column a soil can thus support, depends on the capillarity pressure difference p_c which is defined as:

$$p_c = p_a - p_w \tag{2.14}$$

The value of capillarity forces is inversely proportional to the size of soil void at the air-water interface. There is great difference in the capillarity tensions owing to the great difference in the particle size within sands and clays. There can be very large capillarity tensions within clays, but only very small capillarity tensions can exist within sands.

If the air pressure is zero, (2.14) can be written as :

$$p_w = -p_c \tag{2.15}$$

Negative water pressures are thus maintained in the partially saturated soils through the mechanism of capillarity forces. From equations (2.8), (2.12) and (2.15) the effective stress can be written as:

$$\underline{\sigma}' = \underline{\sigma} - \underline{m}\, S_w\, p_c \tag{2.16}$$

The apparent cohesion $S_w\, p_c$ is a significant component of strength for some soils in which the strength is proportional to the effective confining stress.

Since the capillarity pressure is dependent on the size of soil void, for a given granular material with specific void ratio and under isothermal conditions we can assume that a unique function defines:

$$p_c = p_c(S_w) \tag{2.17a}$$

or

$$S_w = S_w(p_c) \tag{2.17b}$$

The permeability coefficient $\underline{k}_w$ is, by similar arguments, again a unique function.

$$\underline{k}_w = \underline{k}_w(S_w) \tag{2.18a}$$

or

$$\underline{k}_w = \underline{k}_w(p_c) \tag{2.18b}$$

2.1.6. Constitutive relation

In the absence of significant rotation, the constitutive law relating the effective stress change $d\underline{\sigma}'$ and the total strain change $d\underline{\varepsilon}$ can be written as:

$$d\underline{\sigma}' = \underline{\underline{D}} \left(d\underline{\varepsilon} - d\underline{\varepsilon}^0 - d\underline{\varepsilon}^p \right) \tag{2.19}$$

Where the matrix $\underline{\underline{D}}$ is the general dependent on the history and current state of stress, as well as on the loading direction, $d\underline{\varepsilon}^0$ is the change of 'initial' strain due to non-stress effects such as temperature, creep and soil wetting. In this thesis it is assumed that $d\underline{\varepsilon}^0$ is not present.

$d\underline{\varepsilon}^p$ is the change of volumetric strain due to the uniform compression of the solid grains:

$$d\underline{\varepsilon}^p = -\underline{m}\, d\overline{p}/3K_s \tag{2.20}$$

In which K_s is the average bulk modulus of the grains.

Substituting equation (2.20) into (2.19) and neglecting the initial strain, we obtain:

$$d\underline{\sigma}' = \underline{\underline{D}} \left(d\underline{\varepsilon} + \underline{m}\, d\overline{p}/3K_s \right) \tag{2.21}$$

It is more convenient to write the constitutive relation as:

$$d\underline{\sigma}'' = \underline{\underline{D}}\, d\underline{\varepsilon} \tag{2.22}$$

Comparing equation (2.8), (2.13), (2.21) and (2.22) it follows:

$$\alpha\, \underline{m} = \underline{m} - \frac{\underline{\underline{D}}\, \underline{m}}{3\, K_s} \tag{2.23}$$

Premultiplying equation (2.23) with $\underline{m}^T$, we obtain:

$$\alpha = 1 - \frac{\underline{m}^T\, \underline{\underline{D}}\, \underline{m}}{9\, K_s} \tag{2.24}$$

In this case the material is isotropic so the quantity of $\underline{m}^T\, \underline{\underline{D}}\, \underline{m}$ is equal to $9\, K_s$, and K_s is the bulk modulus of the overall soil mixture. Equation (2.24) can be simplified as:

$$\alpha = 1 - \frac{K_t}{K_s} \tag{2.25}$$

For small strain analysis, the change of total strain $d\underline{\varepsilon}$ is related to the change of displacement $d\underline{u}$ of the soil skeleton as:

$$d\varepsilon_{ij} = (\, du_{i,j} + du_{j,i})/2 \tag{2.26a}$$

or

$$d\underline{\varepsilon} = \underline{\underline{L}}\, d\underline{u} \tag{2.26b}$$

And the differential operator $\underline{\underline{L}}^T$ is defined as:

$$\underline{\underline{L}}^T = \begin{bmatrix} \frac{\partial}{\partial x} & 0 & 0 \\ 0 & \frac{\partial}{\partial y} & 0 \\ 0 & 0 & \frac{\partial}{\partial z} \\ \frac{\partial}{\partial y} & \frac{\partial}{\partial x} & 0 \\ 0 & \frac{\partial}{\partial z} & \frac{\partial}{\partial y} \\ \frac{\partial}{\partial z} & 0 & \frac{\partial}{\partial x} \end{bmatrix} \tag{2.27}$$

2.1.7. Momentum equilibrium equations

Assuming that the coordinate system moves with the solid phase the convective acceleration is applied only to the fluid. For a unit volume of the soil mixture, the overall equilibrium equation relates the total stress $\underline{\sigma}$ and the body force $\underline{b}$ to the acceleration of the soil skeleton and the relative acceleration of water in this form:

$$\underline{\underline{L}}^T \underline{\sigma} + \rho\, \underline{b} = \rho\, \underline{\ddot{u}} + \rho_w\, n\, S_w\, \frac{\underline{\underline{D}}}{Dt}\left(\frac{\dot{w}}{n\, S_w}\right) \tag{2.28}$$

ρ_w is the density of the water and ρ is the density of the soil mixture written as:

$$\rho = \rho_s\, (1 - n) + \rho_w\, n\, S_w \tag{2.29}$$

ρ_s is the density of the solid grain.

In the case of water passing through soil, the validity of Darcy law is assumed. For a unit volume of water, the Darcy law in the generalized form can be written as:

$$\underline{\underline{k}}_w^{-1}\,\underline{\dot{w}} = -\underline{\nabla} p_w + p_w\left(\underline{b} - \frac{D\underline{\dot{U}}}{Dt}\right) \tag{2.30}$$

$\underline{\underline{k}}_w$ is the dynamic permeability matrix of water. For isotropic case it is conveniently replaced by a single k_w value. $\underline{\dot{U}}$ is the actual velocity of water as indicated in equation 6 and the acceleration of water is given as:

$$\frac{D\underline{\dot{U}}}{Dt} = \underline{\ddot{u}} + \frac{D}{Dt}\left(\frac{\underline{\dot{w}}}{n\,S_w}\right) \tag{2.31}$$

Since the air pressure has been assumed to be zero, the equation (2.30) is not need in the present analysis approach.

2.1.8 Water flow continuity equation

For a unit volume of soil mixture, the rate of water inflow is given by:

$$-\underline{\nabla}^T \underline{\dot{w}} \tag{2.32}$$

There are five factors that contribute to the change of water stored in the unit volume of the solid-fluid ensemble:

1. Volumetric strain of the soil skeleton:

$$\underline{m}^T \frac{\partial \underline{\varepsilon}}{\partial t} \tag{2.33a}$$

2. Compressive volumetric strain of the grain due to pressure changes:

$$\frac{(1-n)}{K_s}\,\frac{\partial \overline{p}}{\partial t} \tag{2.33b}$$

3. Compressive volumetric strain of water:

$$n\,\frac{S_w}{K_w}\,\frac{\partial p_w}{\partial t} \tag{2.33c}$$

4. Increase of water storage due to saturation changes:

$$n\,\frac{\partial S_w}{\partial t} = n\,\frac{\partial S_w}{\partial p_w}\frac{\partial p_w}{\partial t} = C_s\,\frac{\partial p_w}{\partial t} \tag{2.33d}$$

Where C_s is the specific moisture capacity, which can be evaluated from $S_w - p_w$ curves as $n\,\frac{\partial S_w}{\partial p_w}$.

5. Compressive volumetric strain of grain due to effective stress:

$$-\frac{1}{3K_s}\underline{m}^T\frac{\partial \underline{\sigma}'}{\partial t} = -\frac{1}{3K_s}\underline{m}^T\underline{\underline{D}}\frac{\partial \underline{\varepsilon}}{\partial t} - \underline{m}^T\underline{\underline{D}}\,\underline{m}\,\frac{1}{(3K_s)^2}\frac{\partial \overline{p}}{\partial t} \tag{2.33e}$$

The final continuity equation for water flow becomes:

$$-\underline{\nabla}^T\underline{\dot{w}} = n\,\frac{S_w}{K_w}\frac{\partial p_w}{\partial t} + C_s\,\frac{\partial p_w}{\partial t} + S_w\left(\underline{m}^T - \frac{\underline{m}^T\underline{\underline{D}}}{3K_s}\right)\frac{\partial \underline{\varepsilon}}{\partial t} + S_w\left[\frac{(1-n)}{K_s} + \right.$$

$$\left. - \underline{m}^T\underline{\underline{D}}\,\underline{m}\,\frac{1}{(3K_s)^2}\right]\frac{\partial \overline{p}}{\partial t} \tag{2.34}$$

Using the definition of $\overline{p}$ in the equation (2.12) an of α in equation (2.23), equation (2.34) becomes:

$$-\underline{\nabla}^T\underline{\dot{w}} = n\,\frac{S_w}{K_w}\frac{\partial p_w}{\partial t} + C_s\,\frac{\partial p_w}{\partial t} + S_w\alpha\,\underline{m}^T\frac{\partial \underline{\varepsilon}}{\partial t} + S_w\frac{(\alpha-n)}{K_s}\left(S_w + \frac{C_s}{n}p_w\right)\frac{\partial p_w}{\partial t} \tag{2.35}$$

This is a general equation for continuity of water flow through a partially saturated porous medium.

2.1.9. Summary of governing equations

1. Equilibrium of the soil mixture:

$$\underline{\underline{L}}^T\underline{\sigma} + \rho\,\underline{b} = \rho\,\underline{\ddot{u}} + \rho_w\,n\,S_w\,\frac{\underline{\underline{D}}}{Dt}\left(\frac{\dot{w}}{n\,S_w}\right) \tag{2.36a}$$

2. Equilibrium of water:

$$\underline{\underline{k}}_w^{-1}\,\dot{w} = -\underline{\nabla}p_w + p_w\left(\underline{b} - \underline{\ddot{u}} - \frac{D}{Dt}\left(\frac{\dot{w}}{n\,S_w}\right)\right) \tag{2.36b}$$

3. Continuity of water flow:

$$-\underline{\nabla}^T \underline{\dot{w}} = n\,\frac{S_w}{K_w}\,\frac{\partial p_w}{\partial t} + C_s\,\frac{\partial p_w}{\partial t} + S_w \alpha\,\underline{m}^T \frac{\partial \underline{\underline{\varepsilon}}}{\partial t} +$$

$$+S_w \frac{(\alpha - n)}{K_s}\left(S_w + \frac{C_s}{n} p_w\right)\frac{\partial p_w}{\partial t} \qquad (2.36c)$$

4. The real 'effective stress':

$$\underline{\sigma} = \underline{\sigma}'' - \underline{m}\,\alpha\,S_w\,p_w \qquad (2.36d)$$

5. Constitutive relation:

$$d\underline{\sigma}'' = \underline{\underline{D}}\,d\underline{\varepsilon} \qquad (2.36e)$$

6. Incremental strain:

$$d\underline{\varepsilon} = \underline{\underline{L}}\,d\underline{u} \qquad (2.36f)$$

7. Partial saturation relationships:

$$S_w = S_w(p_c), \quad \underline{k}_w = \underline{k}_w(p_c)\ and\ C_s = n\,\frac{\partial S_w}{\partial p_w} \qquad (2.36g)$$

The above system of equations is the generalized Biot formulation for dynamic behavior of saturated-unsaturated porous media. It can be solved incrementally for most problems with appropriate boundary and initial conditions such as:

Boundary conditions

a. Prescribed displacement

$$\underline{u} = \overline{\underline{u}} \quad on\ \Gamma_u\ \ at\ \ t \geq 0 \qquad (2.37)$$

b. Prescribed traction

$$\underline{t} = \overline{\underline{t}} \quad on\ \Gamma_t\ \ at\ \ t \geq 0 \qquad (2.38a)$$

i.e.

$$\underline{\underline{l}}^T \underline{\sigma} = \overline{\underline{t}} \quad on\ \Gamma_t\ \ at\ \ t \geq 0 \qquad (2.38b)$$

In which the matrix $\underline{\underline{l}}$ is related to the unit normal vector

$\underline{n} = [n_x, n_y, n_z]^T$ by

$$\underline{\underline{l}} = \begin{bmatrix} n_x & 0 & 0 \\ 0 & n_y & 0 \\ 0 & 0 & n_z \\ n_y & n_x & 0 \\ 0 & n_z & n_y \\ n_z & 0 & n_x \end{bmatrix} \tag{2.38c}$$

c. Prescribed water flow:

$$\underline{\dot{w}} = \overline{\underline{\dot{w}}} \;\; on \;\; \Gamma_w \;\; at \;\; t \geq 0 \tag{2.39a}$$

or from the equation (2.33b) it is given that:

$$\underline{k}_w \left(-\underline{\nabla} p_w + p_w \left(\underline{b} - \underline{\ddot{u}} - \frac{D}{Dt}\left(\frac{\underline{\dot{w}}}{n\, S_w} \right) \right) \right) = \overline{\underline{\dot{w}}} \tag{2.39b}$$

d. Prescribed water pressure:

$$p_w = \overline{p}_w \;\; on \;\; \Gamma_{p_w} \;\; at \;\; t \geq 0 \tag{2.40}$$

Initial conditions

$$\underline{u} = \underline{u}_0 \tag{2.41a}$$

$$\underline{\dot{u}} = \underline{\dot{u}}_0 \;\; in \;\; \Omega \;\; and \; on \; \Gamma \;\; at \; t = 0 \tag{2.41b}$$

$$p_w = p_{w_0} \tag{2.41c}$$

There are nine variables in the system (2.36). They are named $\underline{u}$, $\underline{w}$, $\underline{\varepsilon}$, $\underline{\sigma}$, $\underline{\sigma}''$, S_w, K_w and C_s. A direct numerical solution to equations (2.36) can be obtained by taking $\underline{u}$ and $\underline{w}$ as primary variables with other variables eliminated. Solving these equations for nonlinear dynamic problems can be very expensive. Therefore, under certain conditions, an

approximation to the system (2.36) is useful and indeed more economical for the practical use.

2.1.10. Two simplifying approximations

Partially saturated dynamic u-p formulation

When the relative acceleration of the water with respect to the soil skeleton is not significant, the variable $\underline{w}$ can be eliminated by dropping the acceleration terms associated with $\underline{w}$ on the assumption that:

$$\frac{D\underline{\dot{w}}}{Dt} \ll \underline{\ddot{u}} \quad or \quad \frac{D}{Dt}\left(\frac{\underline{\dot{w}}}{n\,S_w}\right) \ll \underline{\ddot{u}} \tag{2.42}$$

For most problems in earthquake response analysis, this approximation is sufficiently accurate. The equation system (2.36) can now be reduced by eliminating $\underline{\dot{w}}$ between (2.36b) and (2.36c) to:

$$\underline{\underline{L}}^T \underline{\sigma} + \rho\,\underline{b} = \rho\,\underline{\ddot{u}} \tag{2.43a}$$

$$\underline{\nabla}^T\left[\underline{k}_w\left(\underline{\nabla} p_w - \rho_w(\underline{b} - \underline{\ddot{u}})\right)\right] = n\,\frac{S_w}{K_w}\frac{\partial p_w}{\partial t} + C_s\,\frac{\partial p_w}{\partial t} + S_w \alpha\,\underline{m}^T\frac{\partial \underline{\varepsilon}}{\partial t} + \\ + S_w\frac{(\alpha - n)}{K_s}\left(S_w + \frac{C_s}{n}p_w\right)\frac{\partial p_w}{\partial t} \tag{2.43b}$$

$$\underline{\sigma} = \underline{\sigma}'' - \underline{m}\,\alpha\,S_w\,p_w \tag{2.43c}$$

$$d\underline{\sigma}'' = \underline{\underline{D}}\,d\underline{\varepsilon} \tag{2.43d}$$

$$d\underline{\varepsilon} = \underline{\underline{L}}\,d\underline{u} \tag{2.43e}$$

$$S_w = S_w(p_c), \quad \underline{k}_w = \underline{k}_w(p_c) \; and \; C_s = n \, \frac{\partial S_w}{\partial p_w} \tag{2.43f}$$

This is the dynamic u-p formulation partially saturated porous media, where the displacement $\underline{u}$ and water pressure p_w are taken as primary variables.

Partially saturated consolidation form

This is the case developed in this thesis. The problem is very slow and all the acceleration forces are found to be negligible:

$$\frac{D}{Dt}\left(\frac{\dot{\underline{w}}}{n\, S_w}\right) \rightarrow \underline{0} \quad and \quad \ddot{\underline{u}} \rightarrow \underline{0} \tag{2.44}$$

The consolidation equations are obtained:

$$\underline{\underline{L}}^T \underline{\sigma} + \rho \, \underline{b} = \underline{0} \tag{2.45a}$$

$$\underline{\nabla}^T \left[\underline{k}_w \left(\underline{\nabla} p_w - \rho_w \underline{b}\right)\right] = n \, \frac{S_w}{K_w} \, \frac{\partial p_w}{\partial t} + C_s \, \frac{\partial p_w}{\partial t} + S_w \alpha \, \underline{m}^T \frac{\partial \underline{\varepsilon}}{\partial t} +$$

$$+ S_w \frac{(\alpha - n)}{K_s} \left(S_w + \frac{C_s}{n} p_w\right) \frac{\partial p_w}{\partial t} \tag{2.45b}$$

$$\underline{\sigma} = \underline{\sigma}'' - \underline{m} \, \alpha \, S_w \, p_w \tag{2.45c}$$

$$d\underline{\sigma}'' = \underline{\underline{D}} \, d\underline{\varepsilon} \tag{2.45d}$$

$$d\underline{\varepsilon} = \underline{\underline{L}} \, d\underline{u} \tag{2.45e}$$

$$S_w = S_w(p_c), \quad \underline{k}_w = \underline{k}_w(p_c) \; and \; C_s = n \, \frac{\partial S_w}{\partial p_w} \tag{2.45f}$$

There are the same equations of the system (2.44) but with terms containing $\underline{\ddot{u}}$ omitted.

2.2. Discretization of governing equations

2.2.1. Introduction

In Section 2.1, the governing equations for the coupled problem of saturated-unsaturated flow in deforming porous media have been presented.

Because of the eventually complex geometry and arbitrary nonlinearity in these kind of problems, the use of the finite element method is the most recommended, and is therefore used in this thesis.

In this Section, the numerical solution to the governing equations of static behaviour of saturated-unsaturated porous media is discussed. First, the time discretization and the iterative Newton-Raphson procedure is described. Then the finite element method is applied to the generalized Biot equations for the spatial discretization.

2.2.2. Discretization in time

Generally, a boundary value problem can be represented as:

$$\underline{A}(\underline{u}) = \underline{\underline{C}}\,\underline{u} + \underline{p} = 0 \qquad in\ \Omega \tag{2.46a}$$

and

$$\underline{B}(\underline{u}) = \underline{\underline{D}}\,\underline{u} + \underline{q} = 0 \qquad on\ \Gamma \tag{2.46b}$$

Where C and D are linear or nonlinear differential operators, p and q are functions defined in the domain Ω and on the boundary Γ and u is the exact solution to the governing equation (2.46a) subject to the boundary condition (2.46b).

Due to the impossibility of finding the exact solution, some approximations must be done.

This is the reason for the introduction of the Weighted Residual Method, which assumes that a solution can be approximated analytically or piecewise analytically. In general, a solution of the problem can be expressed as a linear combination of a base set of functions where the coefficients are determined by a chosen method, and the method attempts to minimize the approximation error.

Indeed, the approximation $\underline{u^*}$, substituted into (2.46a) and (2.46b), usually do not satisfy them with the creation of a residual in the domain:

$$\underline{R_\Omega} = \underline{A}(\underline{u^*}) = \underline{\underline{C}}\,\underline{u} + \underline{p} = 0 \qquad in\ \Omega \tag{2.47a}$$

and

$$\underline{R_\Omega} = \underline{B}(\underline{u^*}) = \underline{\underline{D}}\,\underline{u} + \underline{q} = 0 \qquad on\ \Gamma \tag{2.47b}$$

The residuals can be made zero in some weighted sense writing:

$$\int_{\Omega} \underline{W}^T \underline{R}_{\Omega}\, d\Omega + \int_{\Gamma} \overline{\underline{W}}^T \underline{R}_{\Gamma}\, d\Gamma \tag{2.48}$$

or

$$\int_{\Omega} \underline{W}^T \left(\underline{\underline{C}}\, \underline{u} + \underline{p}\right) d\Omega + \int_{\Gamma} \overline{\underline{W}}^T \left(\underline{\underline{D}}\, \underline{u} + \underline{q}\right) d\Gamma \tag{2.49}$$

where the weighted functions $\underline{W}$ and $\overline{\underline{W}}$ can be, in general, chosen independently.

In what follows, the weighted residual method is applied in the case of the partially saturated dynamic u-p formulation of (2.43).

Applying the integral equation (2.49) to the equilibrium equation (2.43a) and the boundary condition (2.38b), we obtain:

$$\int_{\Omega} \underline{W}^T \left(\underline{L}^T \underline{\sigma} + \rho \underline{b} - \rho \underline{\ddot{u}}\right) d\Omega + \int_{\Gamma} \overline{\underline{W}}^T \left(\underline{l}^T \underline{\sigma} - \overline{\underline{t}}\right) d\Gamma = 0 \tag{2.50}$$

The boundary condition (2.37) of $\underline{u} = \overline{\underline{u}}$ on Γ_u is satisfied by the choice of the approximation of $\underline{u}$.

By using the Green's theorem, the first term of the equation (2.50) becomes:

$$-\int_{\Omega} \left(\underline{L}\, \underline{W}\right)^T \underline{\sigma}\, d\Omega + \int_{\Gamma_u + \Gamma_t} \overline{\underline{W}}^T \underline{l}^T \underline{\sigma}\, d\Gamma \tag{2.51}$$

Forcing the weighting functions to be like:

$$\underline{W} = 0 \quad on \quad \Gamma_u \tag{2.52a}$$

$$\overline{\underline{W}} = -\underline{W} \quad on \quad \Gamma_t \tag{2.52b}$$

the equation (2.50) is reduced to:

$$\int_\Omega \left(\underline{L}\,\underline{W}\right)^T \underline{\sigma}\, d\Omega + \int_\Omega \underline{W}^T \rho\, \underline{\ddot{u}}\, d\Omega = \int_\Omega \underline{W}^T \rho \underline{b}\, d\Omega + \int_\Gamma \overline{\underline{W}}^T \overline{\underline{t}}\, d\Gamma \tag{2.53}$$

The continuity equation of water flow can be rewritten substituting equation (2.43e) into (2.43b) as:

$$\underline{\nabla}^T\left[-\underline{k}_w\, \underline{\nabla}\, p_w + \underline{k}_w\, \rho_w \left(\underline{b} - \underline{\ddot{u}}\right)\right] + S_w\, \alpha\, \underline{m}^T \underline{L}\, \underline{\dot{u}} + \frac{1}{Q^*}\, \underline{\dot{p}} = 0 \tag{2.54}$$

where

$$\frac{1}{Q^*} = C_s + n\, \frac{S_w}{K_w} + S_w\, \frac{(\alpha - n)}{K_s} \left(S_w + \frac{C_s}{n}\, p_w\right) \tag{2.55}$$

As regards the boundary condition (2.39b), it can be simplified using the assumption (2.44) for the dynamic u-p formulation. The result is:

$$\underline{k}_w \left[-\underline{\nabla}\, p_w + \rho_w \left(\underline{b} - \underline{\ddot{u}}\right)\right] = \overline{\dot{w}} \quad on \quad \Gamma_w \tag{2.56}$$

It is possible now to apply the weighted residual method to the equations (2.54) and (2.56), obtaining:

$$\int_\Omega \underline{W}^{*T} \left\{\underline{\nabla}^T\left[-\underline{k}_w\, \underline{\nabla}\, p_w + \underline{k}_w\, \rho_w \left(\underline{b} - \underline{\ddot{u}}\right)\right] + S_w\, \alpha\, \underline{m}^T \underline{L}\, \underline{\dot{u}} + \frac{1}{Q^*}\, \underline{\dot{p}}\right\} d\Omega +$$
$$+ \int_\Gamma \overline{\underline{W}}^{*T} \left\{\left[-\underline{k}_w \underline{\nabla}\, p_w + \underline{k}_w\, \rho_w \left(\underline{b} - \underline{\ddot{u}}\right) - \overline{\dot{w}}\right]^T \underline{n}\right\} d\Gamma = 0 \tag{2.57}$$

where $\underline{W}^*$ and $\overline{\underline{W}}^*$ are arbitrary weighting functions.

The boundary condition (2.40) of $p_w = \overline{p_w}$ on Γ_w is satisfied by the choice of the approximation of p_w.

By applying the Green's theorem to the first term of the first integral of the equation (2.57), and limiting the choice of the weighting functions so that:

$$\underline{W^*} = 0 \quad on \quad \Gamma_p \tag{2.58a}$$

$$\underline{\overline{W^*}} = -\underline{W^*} \quad on \quad \Gamma_u \quad on \quad \Gamma_w \tag{2.58b}$$

the equation (2.57) is now written as:

$$\int_\Omega \left\{-\left(\underline{\nabla W^*}\right)^T\left[-\underline{k_w}\,\underline{\nabla}\,p_w + \underline{k_w}\,\rho_w\left(\underline{b} - \underline{\ddot{u}}\right)\right] + \underline{W^{*T}} S_w\,\alpha\,\underline{m}^T\underline{L}\,\underline{\dot{u}} + \right.$$
$$\left. + \underline{W^{*T}}\frac{1}{Q^*}\,\underline{\dot{p}}\right\} d\Omega + \int_{\Gamma_w} \underline{W^{*T}}\,\underline{\overline{w}}^T\,\underline{n}\; d\Gamma = 0 \tag{2.59}$$

At the end the equations weighted are:

$$\int_\Omega \left(\underline{LW^*}\right)^T \underline{\sigma}\; d\Omega - \int_\Omega \left(\underline{W^*}\right)^T \rho\underline{b}\; d\Omega - \int_\Gamma \underline{\overline{W}}^T\underline{\overline{t}}\; d\Gamma = 0 \tag{2.60a}$$

$$\int_\Omega \left\{-\left(\underline{\nabla W^*}\right)^T\left[-\underline{k_w}\,\underline{\nabla}\,p_w + \underline{k_w}\,\rho_w\,\underline{b}\right] + \underline{W^{*T}} S_w\,\alpha\,\underline{m}^T\underline{L}\,\underline{\dot{u}} + \right.$$
$$\left. + \underline{W^{*T}}\frac{1}{Q^*}\,\underline{\dot{p}}\right\} d\Omega + \int_{\Gamma_w} \underline{W^{*T}}\,\underline{\overline{\dot{w}}}^T\,\underline{n}\; d\Gamma = 0 \tag{2.60b}$$

With:

$$\underline{\sigma} = \underline{\sigma'} + S_w\,\alpha\,\underline{m\dot{p}} \tag{2.61a}$$

$$\rho = \rho_s(1-n) + nS_w\underline{\dot{p}} \tag{2.61b}$$

It is assumed that the differential equations are to be satisfied at each discrete time station.

The derived terms are substituted with their incremental ratio in the following way:

$$\underline{\dot{\overline{u}}} = \left(\frac{d\underline{\overline{u}}}{dt}\right)_{n+1} = \frac{\underline{\overline{u}}_{n+1} - \underline{\overline{u}}_n}{\Delta t} \tag{2.62a}$$

$$\underline{\dot{\overline{p}}} = \left(\frac{d\underline{\overline{p}}}{dt}\right)_{n+1} = \frac{\underline{\overline{p}}_{n+1} - \underline{\overline{p}}_n}{\Delta t} \tag{2.62b}$$

$$\underline{\dot{S}}_{n+1} = \frac{\underline{S}_{n+1} - \underline{S}_n}{\Delta t} \tag{2. 62c}$$

Eq. 2.70c can be written as:

$$\underline{\dot{S}}_{n+1} = \frac{\partial S}{\partial p}\underline{\dot{p}} \tag{2.62d}$$

where the suffix 'w' is now omitted for simplicity.

Inserting the (2.62a) and (2.62b) into the equations (2.60a) and (2.60b), the result is:

$$\int_\Omega \left(\underline{\underline{L}}\,\underline{\underline{W}}^*\right)^T \underline{\sigma}'_{n+1} d\Omega - \int_\Omega \left(\underline{\underline{L}}\,\underline{\underline{W}}^*\right)^T S_w\, \alpha\, \underline{m}\,\underline{\overline{p}}_{n+1}\, d\Omega - \int_\Omega \left(\underline{\underline{W}}^*\right)^T \left[(1 - n)\rho_s + nS_{w_{n+1}}\rho_w\right]\underline{b}\, d\Omega - \int_\Gamma \underline{\overline{W}}^T \underline{\overline{t}}\, d\Gamma = 0 \tag{2.63a}$$

$$\nabla t \int_\Omega \left(\underline{\underline{\nabla}}\,\underline{\underline{W}}^*\right)^T \underline{\underline{k}}_w\, \underline{\nabla}\, p_{w_{n+1}} d\Omega - \nabla t \int_\Omega \left(\underline{\underline{\nabla}}\,\underline{\underline{W}}^*\right)^T \underline{\underline{k}}_w\, \rho_w\, \underline{b}\, d\Omega + \int_\Omega \underline{\underline{W}}^{*T} S_w\, \alpha\, \underline{m}^T \underline{\underline{L}}\, \underline{\overline{u}}_{n+1}\, d\Omega - \int_\Omega \underline{\underline{W}}^{*T} S_w\, \alpha\, \underline{m}^T \underline{\underline{L}}\, \underline{\overline{u}}_n\, d\Omega + \int_\Omega \underline{\underline{W}}^{*T} \frac{1}{Q^*} \underline{\overline{p}}_{n+1}\, d\Omega - \int_\Omega \underline{\underline{W}}^{*T} \frac{1}{Q^*} \underline{\overline{p}}_n\, d\Omega + \nabla t \int_{\Gamma_w} \underline{\underline{W}}^{*T}\, \underline{\dot{\overline{w}}}^T\, \underline{n}\, d\Gamma = 0 \tag{2.63b}$$

The system of equation now obtained is a non-linear system. To be solved, it needs some iterative procedure. We decided to use the Newton-Raphson method.

Eq. (2.63a) can be written as $R_1\left(\underline{\overline{u}}_{n+1}, \underline{\overline{p}}_{n+1}\right)$ and Eq. (2.63b) as $R_2\left(\underline{\overline{u}}_{n+1}, \underline{\overline{p}}_{n+1}\right)$.

The next passage is the differentiation of the two equations of the (2.63), in order to obtain a system with the following structure:

$$\begin{bmatrix} \left(\frac{\partial R_1}{\partial u_{n+1}}\right)^{(i)} \underline{\Delta u}_{n+1}{}^{(i+1)} & \left(\frac{\partial R_1}{\partial p_{n+1}}\right)^{(i)} \underline{\Delta p}_{n+1}{}^{(i+1)} \\ \left(\frac{\partial R_2}{\partial u_{n+1}}\right)^{(i)} \underline{\Delta u}_{n+1}{}^{(i+1)} & \left(\frac{\partial R_2}{\partial p_{n+1}}\right)^{(i)} \underline{\Delta p}_{n+1}{}^{(i+1)} \end{bmatrix} = -\begin{bmatrix} R_1^{(i)} \\ R_2^{(i)} \end{bmatrix} \tag{2.64}$$

where the index (i) identifies the respective Newton-Raphson iteration.

Each term of the matrix in (2.64) is reported below:

$$\frac{\partial R_1}{\partial u_{n+1}} \underline{\Delta u}_{n+1} = \int_\Omega \left(\underline{\underline{L W^*}}\right)^T \frac{\partial \sigma'_{n+1}}{\partial \varepsilon_{n+1}} \frac{\partial \varepsilon_{n+1}}{\partial u_{n+1}} \underline{\Delta u}_{n+1} d\Omega = \int_\Omega \left(\underline{\underline{L W^*}}\right)^T \frac{\partial \sigma'_{n+1}}{\partial \varepsilon_{n+1}} \underline{L}\, \underline{\Delta u}_{n+1} d\Omega \tag{2.65}$$

$$\frac{\partial R_1}{\partial p_{n+1}} \underline{\Delta p}_{n+1} = -\int_\Omega \left(\underline{\underline{L W^*}}\right)^T \frac{\partial S_w}{\partial p_{n+1}}\, \alpha\, \underline{m}\, \underline{\Delta p}_{n+1}\, \underline{\overline{p}}_{n+1}\, d\Omega -$$
$$\int_\Omega \left(\underline{\underline{L W^*}}\right)^T S_{w_{n+1}}\, \alpha\, \underline{m}\, \frac{\partial \underline{\overline{p}}_{n+1}}{\partial \underline{\overline{p}}_{n+1}}\, \underline{\Delta p}_{n+1}\, d\Omega + -\int_\Omega \left(\underline{W^*}\right)^T \frac{\partial S_w}{\partial p_{n+1}} n \rho_w \underline{b}\, \underline{\Delta p}_{n+1}\, d\Omega \tag{2.66}$$

$$\frac{\partial R_2}{\partial u_{n+1}} \underline{\Delta u}_{n+1} = \int_\Omega \underline{W^*}^T S_w\, \alpha\, \underline{m}^T \underline{L}\, \frac{\partial \underline{\overline{u}}_{n+1}}{\partial \underline{\overline{u}}_{n+1}} \underline{\Delta u}_{n+1}\, d\Omega \tag{2.67}$$

$$\frac{\partial R_2}{\partial p_{n+1}} \underline{\Delta p}_{n+1} = \Delta t \int_\Omega \left(\underline{\nabla W^*}\right)^T \frac{\partial \underline{k}_w}{\partial \underline{\overline{p}}_{n+1}} \underline{\Delta p}_{n+1}\, \underline{\nabla}\, p_{w_{n+1}} d\Omega +$$
$$\Delta t \int_\Omega \left(\underline{\nabla W^*}\right)^T \frac{\partial \underline{\overline{p}}_{n+1}}{\partial \underline{\overline{p}}_{n+1}} \underline{k}_w \underline{\Delta p}_{n+1}\, d\Omega + -\Delta t \int_\Omega \left(\underline{\nabla W^*}\right)^T \frac{\partial \underline{k}_w}{\partial \underline{\overline{p}}_{n+1}} \underline{\Delta p}_{n+1}\, \rho_w\, \underline{b}\, d\Omega +$$
$$\int_\Omega \underline{W^*}^T \frac{\partial S_w}{\partial p_{n+1}} \underline{\Delta p}_{n+1}\, \alpha\, \underline{m}^T \underline{L}\, \underline{\overline{u}}_{n+1}\, d\Omega +$$
$$-\int_\Omega \underline{W^*}^T \frac{\partial S_w}{\partial p_{n+1}} \underline{\Delta p}_{n+1}\, \alpha\, \underline{m}^T \underline{L}\, \underline{\overline{u}}_n\, d\Omega + \int_\Omega \underline{W^*}^T \frac{\partial \frac{1}{Q^*}}{\partial p_{n+1}} \underline{\Delta p}_{n+1}\, \underline{\overline{p}}_{n+1}\, d\Omega +$$
$$+\int_\Omega \underline{W^*}^T \frac{1}{Q^*} \frac{\partial \underline{\overline{p}}_{n+1}}{\partial \underline{\overline{p}}_{n+1}} \underline{\Delta p}_{n+1}\, d\Omega - \int_\Omega \underline{W^*}^T \frac{\partial \frac{1}{Q^*}}{\partial p_{n+1}} \underline{\Delta p}_{n+1}\, \underline{\overline{p}}_n\, d\Omega \tag{2.68}$$

The structure for the Newton- Raphson method is:

$$\begin{bmatrix} \left(\frac{\partial R_1}{\partial u_{n+1}}\right)^{(i)} & \left(\frac{\partial R_1}{\partial p_{n+1}}\right)^{(i)} \\ \left(\frac{\partial R_2}{\partial u_{n+1}}\right)^{(i)} & \left(\frac{\partial R_2}{\partial p_{n+1}}\right)^{(i)} \end{bmatrix} \begin{bmatrix} \underline{\Delta u}_{n+1} \\ \underline{\Delta p}_{n+1} \end{bmatrix}^{(i+1)} = - \begin{bmatrix} R_1^{(i)} \\ R_2^{(i)} \end{bmatrix} \tag{2.69}$$

where the index (i) identifies the respective Newton-Raphson iteration.

The matrix on the left is the so called stiffness matrix, and is simplified as:

$$\underline{K} = \begin{bmatrix} K_{11} & K_{12} \\ K_{21} & K_{22} \end{bmatrix} \tag{2.70}$$

2.2.3. Finite Element spatial discretization

The standard procedure of the finite element method requires the division of the domain Ω into subdomains (elements). Then, the displacements and pore water pressure fields of each element are expressed as linear combination of a finite number of nodal values. The coefficients of this particular combinations are called shape functions. The result is the following:

$$\underline{u}^e = \sum_{i=1}^{m} \underline{N_u}_i{}^e \, \overline{\underline{u}}_i{}^e = \underline{N_i}^e \overline{\underline{u}}^e \tag{2.71a}$$

$$\underline{p_w}^e = \sum_{j=1}^{n} \underline{N_p}_j{}^e \, \overline{p}^e{}_{w\,j} = \underline{N_p}^e \overline{\underline{p}}^e{}_w \tag{2.71b}$$

where the superscript ‘e’ denotes the element we are taking in consideration and

$\overline{\underline{u}}_i{}^e = [u_{ix}, u_{iy}, u_{iz}]^T$ is the displacement at node i

$\underline{\overline{u}}^e = \left[\underline{\overline{u}}_1^{\,eT} \ldots \underline{\overline{u}}_i^{\,eT} \ldots \underline{\overline{u}}_m^{\,eT}\right]^T$	is the nodal displacement vector
$\overline{p}^e{}_{w_j}$	is the water pressure at node j
$\underline{\overline{p}}^e{}_w = \left[\, p_{w1}^e \ldots p_{wj}^e \ldots p_{wm}^e\right]^T$	is the nodal water pressure vector
m	is the number of nodes per element for the displacement shape function
n	is the number of nodes per element for the water pressure shape function
$\underline{N_u}^e = \left[N_{u1}^e \underline{I_3} \ldots N_{ui}^e \underline{I_3} \ldots N_{um}^e \underline{I_3}\right]$	is the shape function for the displacements ($\underline{I_3}$ is a 3x3 identity matrix)
$\underline{N_p}^e = \left[N_{p1}^e \ldots N_{pj}^e \ldots N_{pn}^e\right]$	is the shape function for the water pressure

As the whole domain is concerned, the summation of all element contributions can be represented in terms of global shape functions as:

$$\underline{u} = \underline{N_u}\,\underline{\overline{u}} \tag{2.72a}$$

$$p_w = \underline{N_p}\underline{\overline{p}}_w \tag{2.72b}$$

$$\Delta \underline{u} = \underline{N_u} \Delta \underline{\overline{u}} \tag{2.71c}$$

$$\Delta p_w = \underline{N_p} \Delta \underline{\overline{p}}_w \tag{2.71d}$$

$$\underline{W^*} = \underline{N_u} \underline{W^*} \tag{2.71e}$$

The type of elements can be chosen in many different ways. In this thesis we work with isoparametric elements, that is using the same shape functions both for the interpolation of the coordinates within an element and in the displacement representation (2.70).

As concerning the displacement shape functions and the water pressure ones, they can be different (therefore we use two different notation, $\underline{N_u}$ and $\underline{N_p}$ respectively). Even if analysis indicates that it is usually necessary to use higher order of interpolation for $\underline{u}$ than for p_w, in the first part of our dissertation we will use the same shape function for both of them, losing accuracy, but making the problem simpler.

Substituting the approximations (2.71a,b,c,e)) for the displacement and water pressure into equations (2.65), (2.66), (2.67), (2.68) :

$$\frac{\partial R_1}{\partial u_{n+1}} \underline{\Delta u}_{n+1} = \int_\Omega \left(\underline{L}\, \underline{N_u} \right)^T \frac{\partial \sigma'_{n+1}}{\partial \varepsilon_{n+1}} \underline{L}\, \underline{N_u}\, \underline{\Delta u}_{n+1} d\Omega \tag{2.72a}$$

$$\frac{\partial R_1}{\partial p_{n+1}} \underline{\Delta p}_{n+1} = -\int_\Omega \left(\underline{L}\, \underline{N_u} \right)^T \frac{\partial S_w}{\partial p_{n+1}}\, \alpha\, \underline{m}\, \underline{N_u}\, \underline{\Delta p}_{n+1} \underline{N_u}\, \underline{\overline{p}}_{n+1}\, d\Omega +$$
$$-\int_\Omega \left(\underline{L}\, \underline{N_u} \right)^T S_{w\,n+1}\, \alpha\, \underline{m}\, \frac{\partial \underline{\overline{p}}_{n+1}}{\partial \underline{\overline{p}}_{n+1}}\, \underline{N_u} \underline{\Delta p}_{n+1}\, d\Omega - \int_\Omega \left(\underline{N_u} \right)^T \frac{\partial S_w}{\partial p_{n+1}} n \rho_w \underline{b}\, \underline{N_u}\, \underline{\Delta p}_{n+1} d\Omega \tag{2.72b}$$

$$\frac{\partial R_2}{\partial u_{n+1}} \underline{\Delta u}_{n+1} = \int_\Omega\, \underline{N_p}^T S_w\, \alpha\, \underline{m}^T \underline{L}\, \underline{N_u}\, \frac{\partial \underline{\overline{u}}_{n+1}}{\partial \underline{\overline{u}}_{n+1}} \underline{\Delta u}_{n+1}\, d\Omega \tag{2.72c}$$

$$\frac{\partial R_2}{\partial p_{n+1}}\underline{\Delta p}_{n+1} = \Delta t \int_\Omega \left(\underline{\nabla N_p}\right)^T \frac{\partial \underline{k}_w}{\partial \underline{\overline{p}}_{n+1}} \underline{\Delta p}_{n+1} \underline{\nabla N_p}\ \underline{\nabla}\ p_{w\,n+1} \underline{N_p} d\Omega +$$

$$\Delta t \int_\Omega \left(\underline{\nabla N_p}\right)^T \frac{\partial \underline{\overline{p}}_{n+1}}{\partial \underline{\overline{p}}_{n+1}} \underline{k}_w \underline{\Delta p}_{n+1}\ \underline{N_p} d\Omega + -\Delta t \int_\Omega \left(\underline{\nabla N_p}\right)^T \frac{\partial \underline{k}_w}{\partial \underline{\overline{p}}_{n+1}} \underline{N_p} \underline{\Delta p}_{n+1}\ \rho_w\ \underline{b}\ d\Omega +$$

$$+ \int_\Omega\ \underline{N_p}^T \frac{\partial S_w}{\partial p_{n+1}} \underline{\Delta p}_{n+1}\ \alpha\ \underline{m}^T \underline{L}\ \underline{N_u}\ \underline{\overline{u}}_{n+1} \underline{N_p}\ d\Omega +$$

$$- \int_\Omega\ \underline{N_p}^T \frac{\partial S_w}{\partial p_{n+1}}\ \underline{\Delta p}_{n+1}\ \alpha\ \underline{m}^T \underline{L}\ \underline{N_u}\ \underline{\overline{u}}_n \underline{N_p}\ d\Omega + \int_\Omega\ \underline{N_p}^T \frac{\partial \frac{1}{Q^*}}{\partial p_{n+1}} \underline{\Delta p}_{n+1} \underline{N_p}\ \underline{\overline{p}}_{n+1} \underline{N_p}\ d\Omega +$$

$$+ \int_\Omega\ \underline{N_p}^T \frac{1}{Q^*} \frac{\partial \underline{\overline{p}}_{n+1}}{\partial \underline{\overline{p}}_{n+1}}\ \underline{N_p} \underline{\Delta p}_{n+1}\ d\Omega - \int_\Omega\ \underline{N_p}^T \frac{\partial \frac{1}{Q^*}}{\partial p_{n+1}} \underline{\Delta p}_{n+1} \underline{N_p}\ \underline{\overline{p}}_n \underline{N_p}\ d\Omega \tag{2.72d}$$

To keep on making all the terms of equations (2.72) explicit, some constitutive relations for the concrete are needed. In order to have a benchmark to validate the model, the program is implemented using some constitutive laws for the soil. In particular, the approximated equations of the Liakopoulus saturation of water-capillary pressure and relative permeability of water-capillary pressure relationships of the following form:

$$S_w = 1 - 1.9722 \cdot 10^{-11} p_c^{2.4279} \tag{2.73}$$

$$kr_w = 1 - 2.207(1 - S_w)^{1.0121} \tag{2.74}$$

were applied.

As a consequence the term C_s assumes the configuration

$$C_s = n(-4.8768 \cdot 10^{-11} p_c^{1.4279}) \tag{2.75}$$

The capillary pressure is $p_c = -p_w$ only when the water pressure p_w is negative. Otherwise $p_c = 0$. In this case the material is fully saturated,

the saturation of water-capillary pressure takes value one, as well as the relative permeability.

It is possible now to describe each term of the K_{ii} parts of the matrix $\underline{K}$.

All the needed elements are now examined. In the next Chapter some exemples will be carried on.

Chapter 3 – Modelling of the porous media

3.1. Summary of the examples

The model described in the previous Chapter 2 is implemented using a Matlab code.

In order to not neglect any kind of mistake in the different part of the code, several steps are done, before coming to the definitive and complete model for the porous media.

In Section 3.2. all these "preparing steps" are described. Here a brief summary of these steps is given:

- Step one. Fully saturated soil. Control of displacements.
- Step two. Fully saturated soil. Control of pressure.
- Step three. Fully saturated soil. Control of the coupling between displacements and pressure.
- Step four. Fully saturated soil. Control of the model development in time.
- Step five. Fully saturated soil. Addition of a mechanical load.

In Section 3.3. the final test is described, carried on in conditions of partial saturation.

3.2. Initial steps

3.2.1. Step 1

This first case wants to analyze the mechanical behavior of the model. In particular the precision of the results in terms of displacements are investigated, without considering the effects of pressure on them.

A concrete column with a displacement applied on the top will be therefore modeled, fixing the parameter $\alpha = 0$. In this way the $K_{12}$and K_{21}elements of the stiffness matrix assume null values and the problem is uncoupled, i.e. there are no interactions between displacements and pressures.

The column is 2.00 m high and 1.00 m wide with a constant load of 1 mm. This column is completely saturated and the problem is two dimensional. Nodes on the base are fixed in both directions while others nodes are fixed in the horizontal direction only.

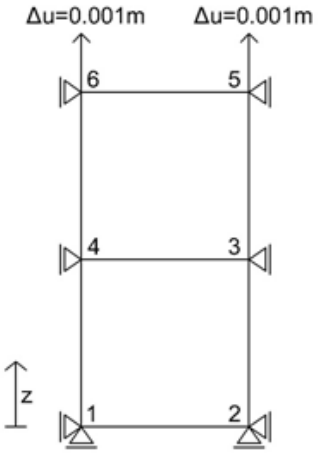

Material parameters:

$$\rho^s = 2000 \frac{kg}{m^3}$$

$$\rho^w = 1000\ kg/m^3$$

$$E = 2 \cdot 10^{10} Pa$$

$$v = 0{,}001\ m$$

Figure 3. 1. - Representation of the geometry and list of material parameters

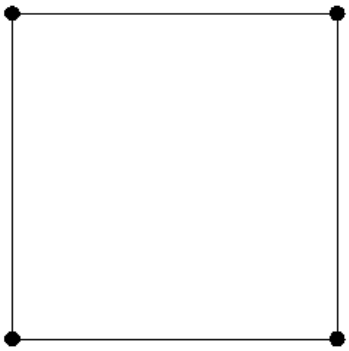

Figure 3. 1. - Element type

For the discretization, the column is spatial divided into 2 isoparametric elements. These ones have 4 nodes and dimensions 1m x 1m.

The only two degrees of freedom that must be calculated are the displacements of node 3 and 4.

The results of the Matlab Code are compared to the analytical calculations, computed with the help of Excel.

- Excel

ITER 1:

The system is solved using only the parts of matrix and vectors which correspond to the free degrees of freedom, in this case the vertical displacements of nodes 3 and 4.

When the Euclidean norm of the residuals vector decreases below the tolerance (in this case 10^{-8}), the iterative Newton-Raphson process can be considered concluded.

Stiffness Matrix of the free DOFs			Free DOFs		Residuals
20000,1685	-0,1685		Δv3	=	10
0,0000	20000,1685		Δv4		10
Inverse of the Stiffness Matrix			Residuals		Δv
5,00E-05	4,21E-10		10	=	0,0005
0	5,00E-05		10		0,000499996
	v new		Euclidean norm		
v3	0,0005		14,14213562		
v4	0,000499996				

Table 3. 1. - Iter one. Analytical results.

ITER 2:

Stiffness Matrix of the free DOFs			Free DOFs		Residuals
20000,1685	-0,1685		Δv3	=	-8,88E-16
0,0000	20000,1685		Δv4		8,43E-05
Inverse of the Stiffness Matrix			Residuals		Δv
5,00E-05	4,21E-10		10	=	3,55E-14
0	5,00E-05		10		4,21E-09
	v new		Euclidean norm		
v3	0,0005		8,43E-05		
v4	0,0005				

Table 3. 2. - Iter two. Analytical results.

ITER 3:

Stiffness Matrix of the free DOFs			Free DOFs		Residuals
20000,1685	-0,1685		Δv3	=	8,88E-16
0,0000	20000,1685		Δv4		7,11E-15
Inverse of the Stiffness Matrix			Residuals		Δv
5,00E-05	4,21E-10		8,88E-16	=	4,44E-20
0	5,00E-05		7,11E-15		3,55E-19
	v new		Euclidean norm		
v3	0,0005		7,16E-15		
v4	0,0005				

Table 3. 3. - Iter three. Analytical results.

In three iterations the system of equations converges and the norm goes to zero. The result is what we expected to have.

- Matlab Code

DOF	VALUE
U1	0
V1	0
P1	0
U2	0
V2	0
P2	0
U3	0
V3	**5*10^-4**
P3	0
U4	0
V4	**5*10^-4**
P4	0
U5	0
V5	1*10^-3
P5	0
U6	0
V6	1*10^-3
P6	0

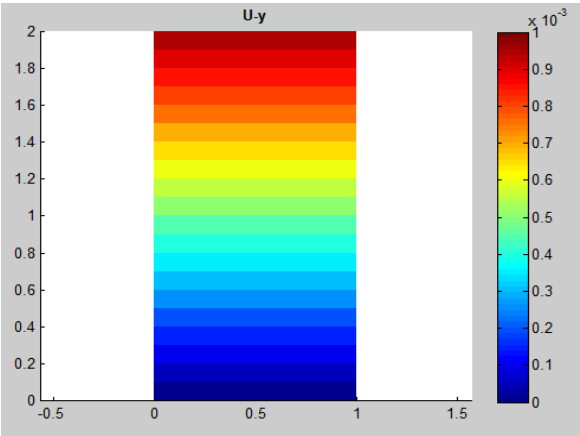

Figure 3. 2. - Spectrum of displacements

Table 3. 4. - Numerical results.

The vector with all the degrees of freedom and the diagram of displacements along the two-element column show how the code perfectly fits to the analytical solution.

This output is obtained after to iterations only:

```
n_iter: 2  resi: 7.4506e-09
```

After the second iteration in fact the Euclidian norm is decreased below the tolerance.

In this particular comparison a geometrical model formed by two elements only is created, to have a more simple system and make the analytical computations simpler. Analogue results are however reached also considering a different mesh formed by more elements.

3.2.2. Step 2

The aim of this second sub-case is checking the pressures alone. In other words we want to control the element K_{22} of the global stiffness matrix.

For this reason the parameter α, which links displacements and pressures, is maintained equal to zero.

Even the geometry is maintained the same of the previous example. The changes are in terms of applied load. There are no more displacements applied on the top, but the gravity $g = 9{,}81\ m/s^2$ is the only external load. It will not be applied on the nodes, but it becomes part of the

equations themselves, in particular of the term f^p in correspondence of the vector; previously named $\underline{b}$.

The boundary conditions infect the pressure on the top (nodes 5 and 6) and are fixed to zero.

What we expect at the end of this simulation, is an hydrostatic distribution of pressures along the entire high of the column.

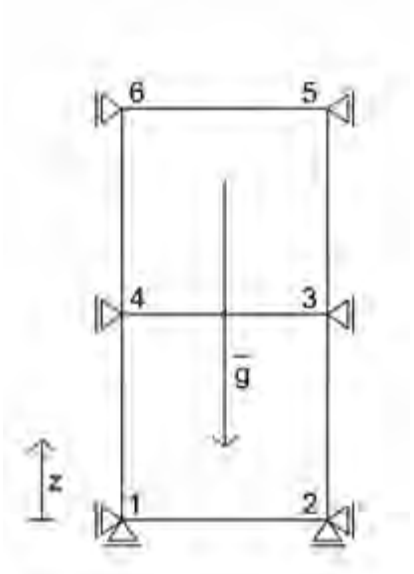

$$\rho^s = 2000\frac{kg}{m^3}$$

$$\rho^w = 1000\ kg/m^3$$

$$E = 2 \cdot 10^{10} Pa$$

$$g = 9{,}81\ m/s^2$$

Figure 3. 4. - Representation of the geometry and list of material parameters

ITER 1

Stiffness Matrix of the free DOFs					Free DOFs		Residuals
2,666689205	-0,666689106	-1,33331084	-0,666689106		Δp1		0
-0,666689106	2,666689205	-0,66668911	-1,333310844		Δp2	=	0
-1,333310844	-0,666689106	5,333378411	-1,333378212		Δp3		0
-0,666689106	-1,333310844	-1,33337821	5,333378411		Δp4		0
Inverse of the Stiffness Matrix					Residuals		Δp
0,653058555	0,346941247	0,265304559	0,234695304		19620		19620
0,346941247	0,653058555	0,234695304	0,265304559		19620	=	19620
0,265304559	0,234695304	0,326529277	0,173470623		0		9810
0,234695304	0,265304559	0,173470623	0,326529277		0		9810

	p new		Euclidean norm
p1	19620		7,16E-15
p2	19620		
p3	9809,997		
p4	9809,997		

Table 3. 5. – Iter 1. Analytical results.

ITER 2

Stiffness Matrix of the free DOFs					Free DOFs		Residuals
2,666689205	-0,666689106	-1,33331084	-0,666689106		Δp1		5,46E-12
-0,666689106	2,666689205	-0,66668911	-1,333310844		Δp2	=	8,19E-12
-1,333310844	-0,666689106	5,333378411	-1,333378212		Δp3		3,18E-12
-0,666689106	-1,333310844	-1,33337821	5,333378411		Δp4		4,09E-12
Inverse of the Stiffness Matrix					Residuals		Δp
0,653058555	0,346941247	0,265304559	0,234695304		5,46E-12		8,21E-12
0,346941247	0,653058555	0,234695304	0,265304559		8,19E-12	=	9,07E-12
0,265304559	0,234695304	0,326529277	0,173470623		3,18E-12		5,12E-12
0,234695304	0,265304559	0,173470623	0,326529277		4,09E-12		5,34E-12

	p new		Euclidean norm
p1	19620		1,11E-09
p2	19620		
p3	9809,997		
p4	9809,997		

Table 3. 6. – Iter 2. Analytical results.

Like expected the pressure is the hydrostatic one and depends on the height.

In two iterations the system of equations converges and the norm goes to zero.

- Matlab Code

DOF	VALUE
P1	0
P2	0
P3	9810
P4	9810
P5	19620
P6	19620

Table 3. 7. – Numerical results.

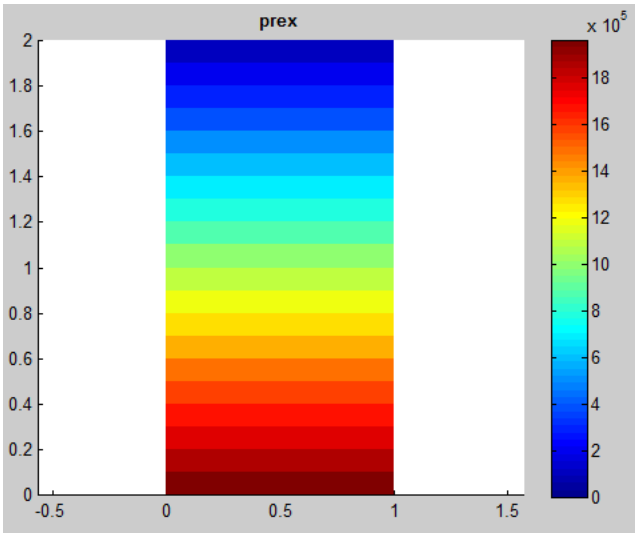

Figure 3. 4. – Spectrum of pressures.

The results showed, both in the table and both in the colored diagram, are right and the same of the analytical calculations.

The precise solution is reached in two iterations:

```
n_iter: 2   resi: 1.5619e-09
```

3.2.3. Step 3

After the validation of the program respectively in the decoupled case of displacements alone or pressure alone, the coupled case is considered.

Fixed the parameter $\alpha = 0$, the $K_{21}$and K_{21}elements of the stiffness matrix begin to be significant and assume values different from zero.

The case of a column, 10m high, composed by ten square elements 1x1 is considered. The only contribute of the external forces is due to the gravity.

First, the analytical solution has to be calculated, in order to have a basis for comparison.

The analysed system and the material parameters used in this example are summarized in Figure 3.6..

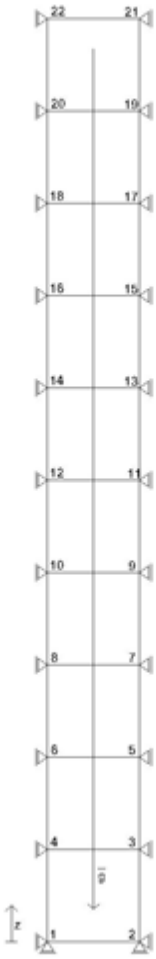

$$\rho^s = 2000 \frac{kg}{m^3}$$

$$\rho^w = 1000\ kg/m^3$$

$$E = 2 \cdot 10^{10} Pa$$

$$g = 9{,}81\ m/s^2$$

Figure 3. 5. – Representation of geometry and list of the material parameters.

The width of the elements is the unit, in order to assume the plane stress state.

As already said, the only external force is the weight force of the grains themselves. The effective stress $\sigma(z)'$ is therefore calculated as:

$$\sigma'(z) = \gamma' z \tag{3.1}$$

where $\gamma'$is effective part of the specific weight γ of the global material. It can be in fact written as:

$$\gamma' = \gamma - \gamma^w \tag{3.2}$$

where $\gamma^w$is the water specific weight.

The terms above can be rewritten using respectively the mixture density ρ_{mix} and the water density ρ^w:

$$\gamma = \rho_{mix} g = (1-n)\rho^s + n\rho^w \tag{3.3}$$

$$\gamma^w = \rho^w g \tag{3.4}$$

with ρ^s density of the solid skeleton.

The effective part of the specific weight is therefore explicated as:

$$\gamma' = [(1-n)\rho^s + (n-1)\rho^w]g = 6891{,}52\ N/m^2 \tag{3.5}$$

It is now necessary to find the law for the strain $\varepsilon(z)$ and to integrate it in order to obtain the relative displacements ΔL.

The strain law can be deduced by the stress one:

$$\varepsilon(z) = \frac{\sigma(z)}{E} \tag{3.6}$$

and the stretching is therefore:

$$\Delta L(z) = \int_0^z \varepsilon \, dz = \int_0^z \frac{\gamma' z}{E} dz = \frac{\gamma'}{E} \int_0^z z \, dz = \frac{\gamma'}{E} \frac{z^2}{d} \tag{3.7}$$

We can now calculate for example the hugest stretching, that is the incremental displacement of the superior element (nodes 21-22), which is:

$$\Delta L(z = 10) = \frac{\gamma'}{E} \frac{h^2}{2} = 0{,}0000072288125 \, m \tag{3.8}$$

The next step is therefore the comparison between this result and the numerical output of Matlab Code.

The gait of pressure and displacement is reported in the following images:

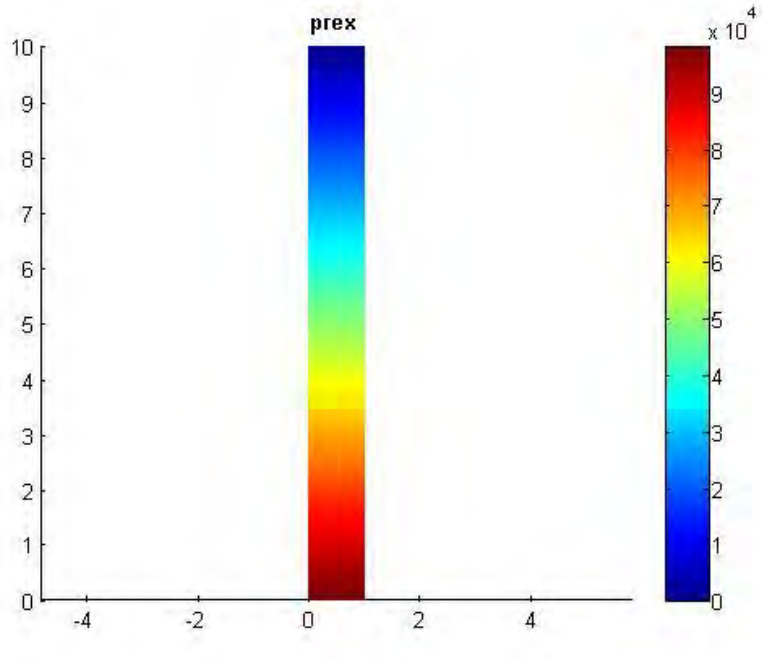

Figure 3. 6. Spectrum of pressures

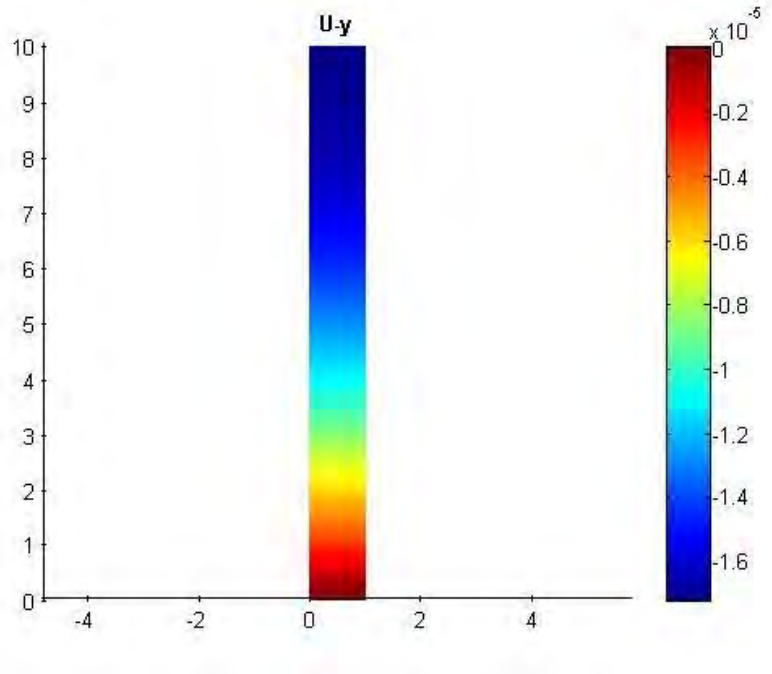

Figure 3. 7. – Spectrum of Displacements.

The numerical values of pressure and displacements are listed in Table 3.8.

NODO	SPOSTAMENTO IN Y	PRESSIONE
1	0	9.809999999999968e+04
2	0	9.809999999999968e+04
3	-3.273474375000019e-06	8.828999999999968e+04
4	-3.273474375000019e-06	8.828999999999968e+04
5	-6.202372500000039e-06	7.847999999999968e+04
6	-6.202372500000039e-06	7.847999999999968e+04
7	-8.786694375000053e-06	6.866999999999969e+04
8	-8.786694375000053e-06	6.866999999999969e+04
9	-1.102644000000007e-05	5.885999999999972e+04

10	-1.102644000000007e-05	5.885999999999972e+04
11	-1.292160937500009e-05	4.904999999999976e+04
12	-1.292160937500009e-05	4.904999999999976e+04
13	-1.447220250000010e-05	3.923999999999981e+04
14	-1.447220250000010e-05	3.923999999999981e+04
15	-1.567821937500010e-05	2.942999999999986e+04
16	-1.567821937500010e-05	2.942999999999986e+04
17	-1.653966000000011e-05	1.961999999999991e+04
18	-1.653966000000011e-05	1.961999999999991e+04
19	-1.705652437500011e-05	9.809999999999953e+03
20	-1.705652437500011e-05	9.809999999999953e+03
21	**-1.722881250000012e-05**	0
22	**-1.722881250000012e-05**	0

Table 3. 8. – Numerical results.

As expected, pressures keep their hydrostatic behaviour.

The displacements results are validated too. Their values in correspondence of nodes 21 and 22 (highlighted in bold in Table 3.8.) are in fact the same calculated in (3.8) with the analytical method.

3.2.4. Step 4

This step contains the validation of the model in the same load and geometrical conditions of “step 3”, comparing the results at each time step with the program Comes-GeoPZ. The aim is checking the right transmission of the load in time.

The material parameters in this example are the following:

$\rho_w = 1000\ kg/m^3$	water density
$\rho_s = 2000\ kg/m^3$	grains density
$E = 30 \cdot 10^6 Pa$	Young modulus of the soil
$\nu = 0$	Posson ratio of the soil
$K_s = 6.78 \cdot 10^9 Pa$	bulk modulus of the grains
$K_{wa} = 0.2 \cdot 10^9\ Pa$	bulk modulus of the water
$kwi = 4.5 \cdot 10^{-13} m^2$	intrinsic permeability
$\mu_w = 0.001 \frac{kg}{m \cdot s}$	water viscosity

The analysis is carried on using steps of time of 100s.

Previously, the program Comes-GeoPZ is run. Noticed that the complete consolidation is reached after 238 steps, our steps are fixed at the number of 250.

Next, the results after step 1, 50, 150 and 250 are copied out.

We compare the results of the two programs in terms of maximum pressure, measured at the bottom of the column.

In Comes-GeoPz the water pressure p_c is calculated, while with the Matlab Code the output is the water pressure. The modulus is the same, only the sign obviously changes.

Time step 1 t=100 s

- *Comes*

```
*****************************************************************
 STEP :     1 - DTIME : 0.100000E+03 s - TIME : 0.100000E+03 s
*****************************************************************

ACT. DTIME : 0.100000E+03 s - TIME : 0.100000E+03 s

IT.NORM EUCLID. ER. NAT.       PG          PC          T        UX          UY         DEQP
001 0.1000E+01 0.1000E+01 0.1013E+06-0.1582E+06  293.15  0.0000E+00 -0.3099E-03  0.0000E+00
002 0.7613E-13 0.5705E-12 0.1013E+06-0.1582E+06  293.15  0.0000E+00 -0.3099E-03  0.0000E+00
```

Figure 3. 8. – Time step 1. Numerical results with Comes.

- *Matlab*

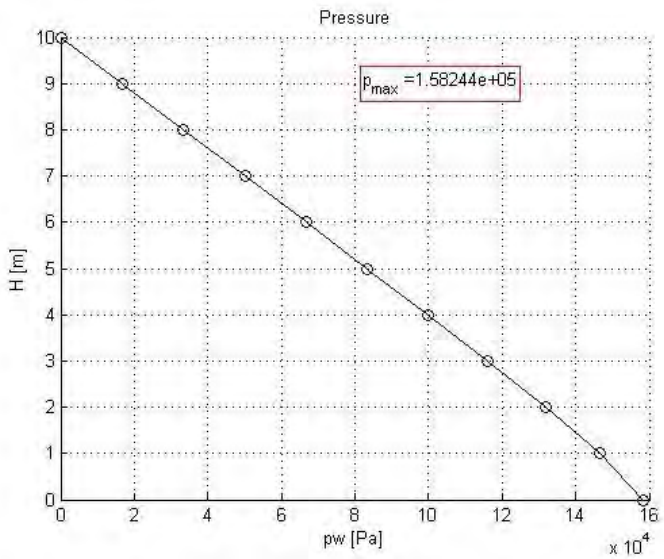

Figure 3. 9. Time step 1. Numerical results for pressure with Matlab code.

Time step 50 t=5000s

- *Comes*

```
*****************************************************************
 STEP :    50 - DTIME : 0.100000E+03 s - TIME : 0.500000E+04 s
*****************************************************************

ACT. DTIME : 0.100000E+03 s - TIME : 0.500000E+04 s

IT.NORM EUCLID. ER. NAT.       PG          PC          T        UX          UY         DEQP
001 0.6563E-02 0.6802E-02 0.1013E+06-0.1060E+06  293.15  0.0000E+00 -0.8180E-02  0.0000E+00
002 0.1230E-14 0.1531E-14 0.1013E+06-0.1060E+06  293.15  0.0000E+00 -0.8180E-02  0.0000E+00
```

Figure 3. 10. Time step 50. Numerical results with Comes.

- *Matlab*

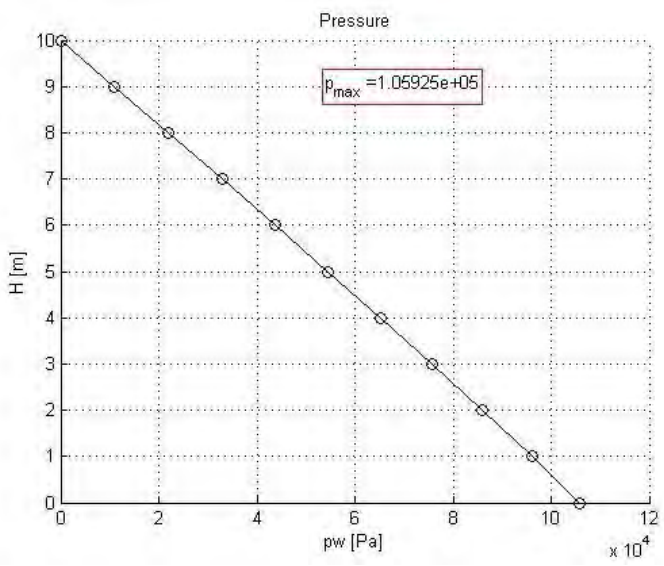

Figure 3.11. – Time step 50. Numerical results for pressure with Matlab code.

Time step150 t=15000s

- *Comes*

```
*****************************************************************
 STEP :   150 - DTIME : 0.100000E+03 s - TIME : 0.150000E+05 s
*****************************************************************

ACT. DTIME : 0.100000E+03 s - TIME : 0.150000E+05 s

IT.NORM EUCLID. ER. NAT.       PG          PC          T        UX          UY         DEQP
001 0.1122E-03 0.1157E-03 0.1013E+06-0.9826E+05  293.15  0.0000E+00 -0.9544E-02  0.0000E+00
002 0.8679E-15 0.1238E-14 0.1013E+06-0.9826E+05  293.15  0.0000E+00 -0.9544E-02  0.0000E+00
```

Figure 3. 12. – Time step 150. Numerical results with Comes.

- *Matlab*

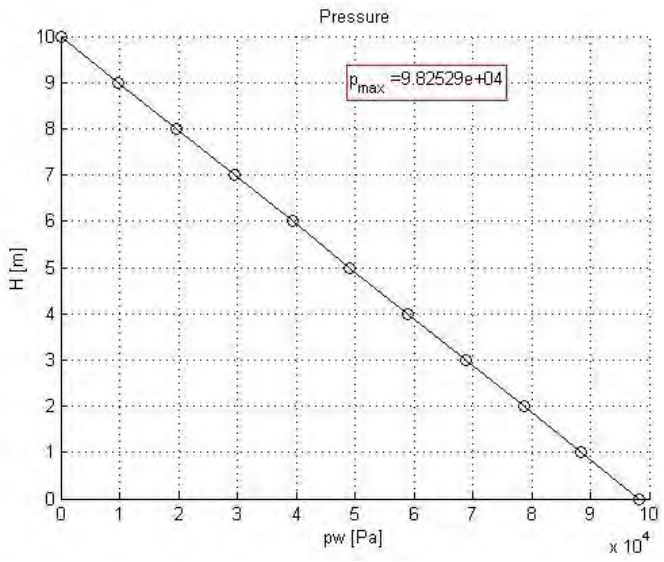

Figure 3. 13. – Time step 150. Numerical results for pressure with Matlab code.

Time step250 t=25000s

- *Comes*

```
****************************************************************
 STEP :   250 - DTIME : 0.100000E+03 s - TIME : 0.250000E+05 s
****************************************************************

ACT. DTIME : 0.100000E+03 s - TIME : 0.250000E+05 s

IT.NORM EUCLID. ER. NAT.       PG          PC          T        UX          UY
001 0.2222E-05 0.2291E-05 0.1013E+06-0.9810E+05  293.15  0.0000E+00 -0.9571E-02
002 0.1311E-15 0.4220E-15 0.1013E+06-0.9810E+05  293.15  0.0000E+00 -0.9571E-02
```

Figure 3. 14. – Time step 250. Numerical results with Comes.

- *Matlab*

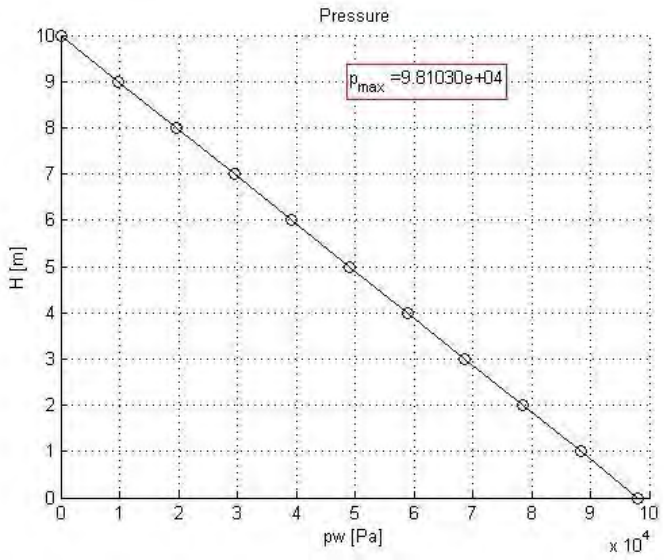

Figure 3. 15. – Time step 250. Numerical results for pressure with Matlab code.

The two models are comparable. We can easily notice that the process of consolidation is not really finished at step 250. The decimal places neglected by Comes are not null yet.

Going on with the time steps, the solution slowly tends to the precise expected value of 98100 Pa.

The results in terms of pressure and displacements at the 400th time step are therefore given (Figure 3.17).

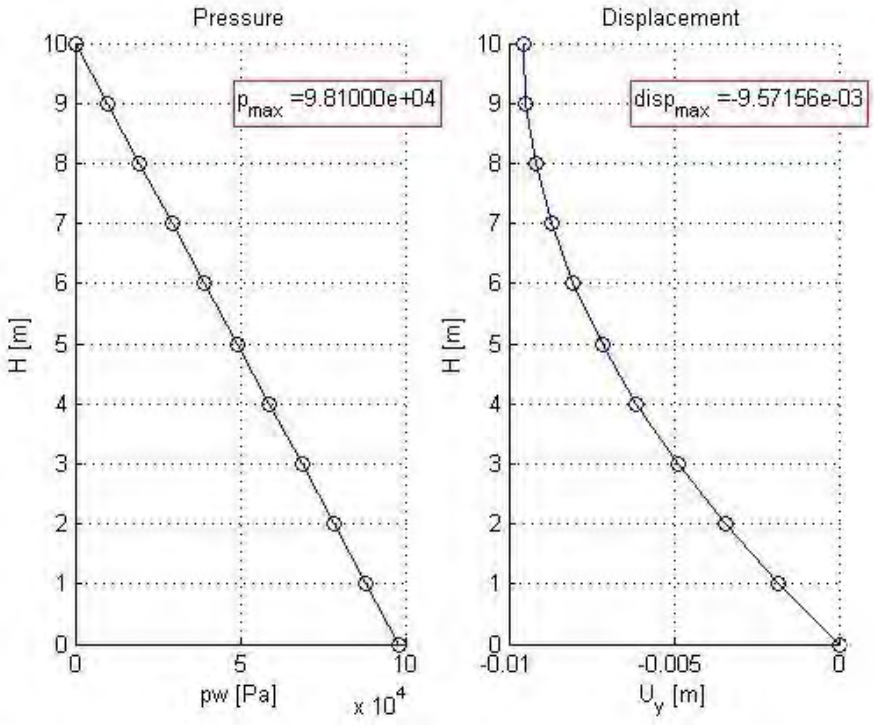

Figure 3. 16 – Time step 400. Numerical results with Matlab code.

3.2.5. Step 5

In this last example with a fully saturated condition of flow, the load conditions and the initial conditions change, while the geometry and the spatial constraints remain the same.

At time $t = 0$, the process of consolidation is considered finished. As initial conditions, the hydrostatic trend of pressure and the deformation field at the end of the consolidation process are assumed. In other words the results of previous Step 4 can be considered the start of this new case.

As for the applied load, a mechanical vertical load of 10.000 Pa is acting on the top of the ten elements-column.

The system is represented in Figure (3.18).

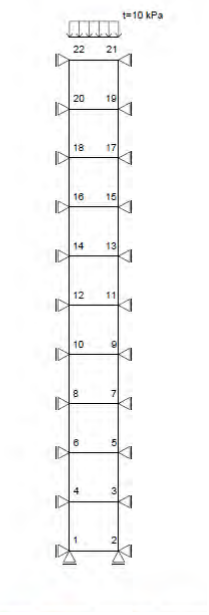

Figure 3. 18. – Representation of the geometry.

The development of the water pressure we expect to find, is the following one, described by Figure (3.19).

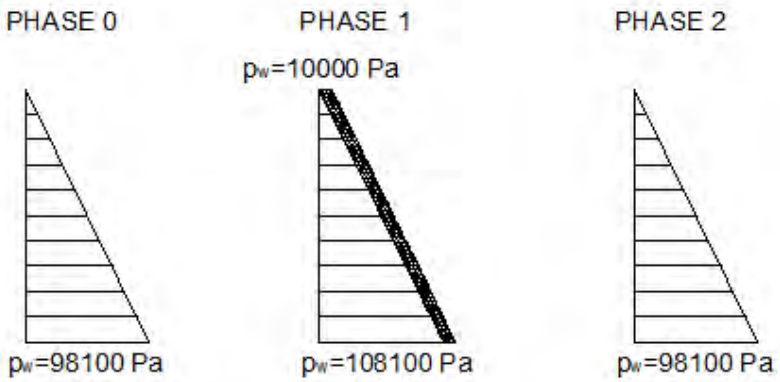

Figure 3. 19. – Representation of the geometry.

Starting from an hydrostatic configuration (phase 0), water pressures should initially adsorb the whole entity of the applied load (phase 1), and then pass it on to the solid skeleton, returning therefore to the initial condition (phase 2).

In this particular case, in order to fix a boundary condition for the water pressure, this last one is fixed zero on the nodes 21 and 22. This creates a discrepancy in the trend in correspondence of the superior part of the column between Figure 3.19 and the numerical implementation.

The applied load is inserted into the code, by adding it to the residual term of the first momentum equilibrium equation.

It needs his own loop of integration between node 21 and 22, using the interpolation functions of a two-node element.

Next, the results at some significant time-steps are reported. Even in this case, they are compared to the outputs of an existent model for the consolidation in Comes.

Time step1 t=100s

This is the initial step, in which the water takes all the load.

The water pressure value at nodes 1 and 2 must be the sum between the initial hydrostatic pressure and the applied tension:

$$p_w(node\ 1) = 98100 + 10000 = 108100Pa = 1{,}081 \cdot 10^5 Pa$$

Indeed, both Comes and Matlab give this result, as shown in Figure (3.20-3.21).

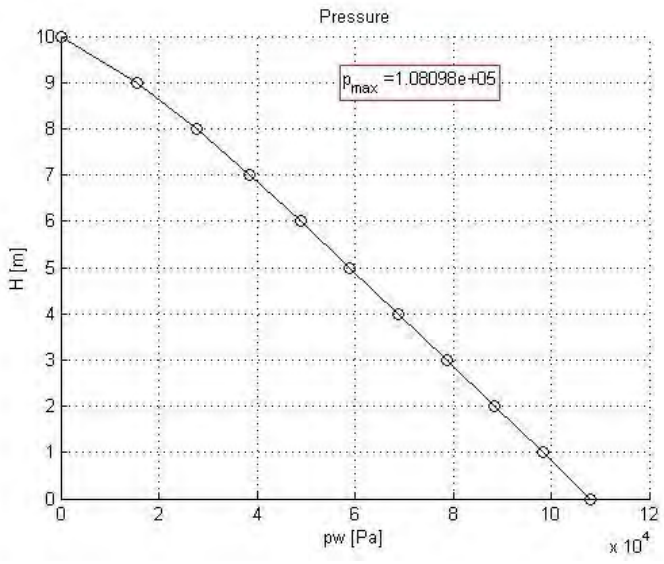

Figure 3. 20. – Time step 1. Numerical results for pressure with Matlab code.

```
*****************************************************************
 STEP :     1 - DTIME : 0.100000E+03 s - TIME : 0.251000E+05 s
*****************************************************************

ACT. DTIME : 0.100000E+03 s - TIME : 0.251000E+05 s

IT.NORM EUCLID. ER. NAT.       PG          PC          T        UX          UY          DEQP
001 0.1351E+00 0.3988E+00 0.1013E+06-0.1081E+06  293.15  0.0000E+00 -0.9925E-02  0.0000E+00
002 0.1034E-14 0.3901E-14 0.1013E+06-0.1081E+06  293.15  0.0000E+00 -0.9925E-02  0.0000E+00
```

Figure 3. 21. – Time step 1. Numerical results for pressure with Comes.

Time step50 t=5000s

Matlab results are firstly shown. Therefore the comparison between it and Comes is represented in a graph.

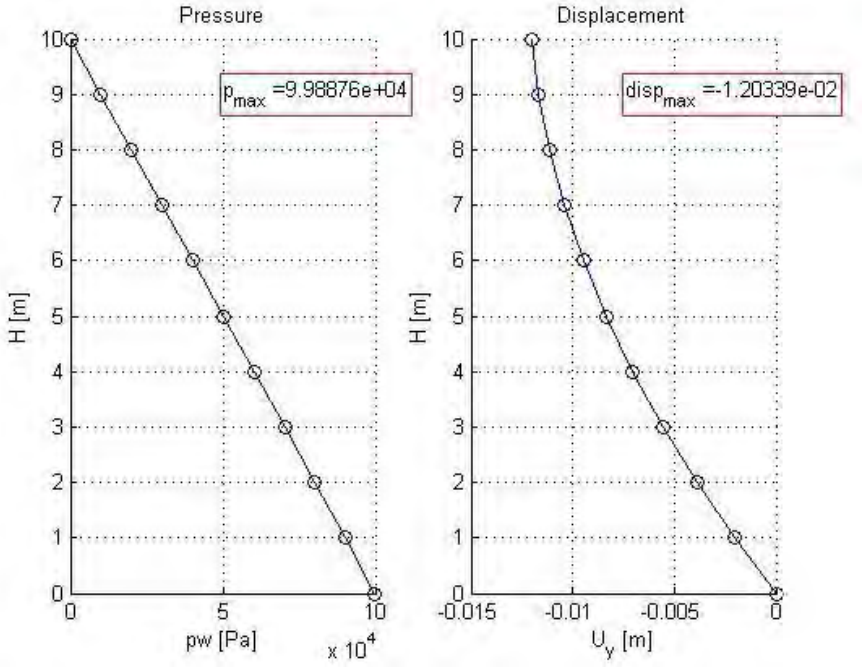

Figure 3. 22. – Time step 50. Numerical results with Matlab code.

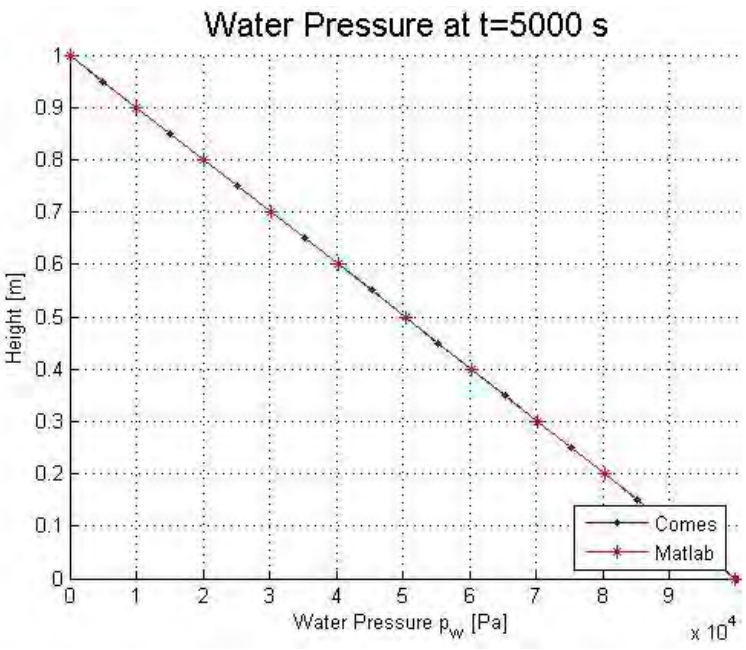

Figure 3. 23. – Time step 50. Comparison Matlab/Comes for pressures.

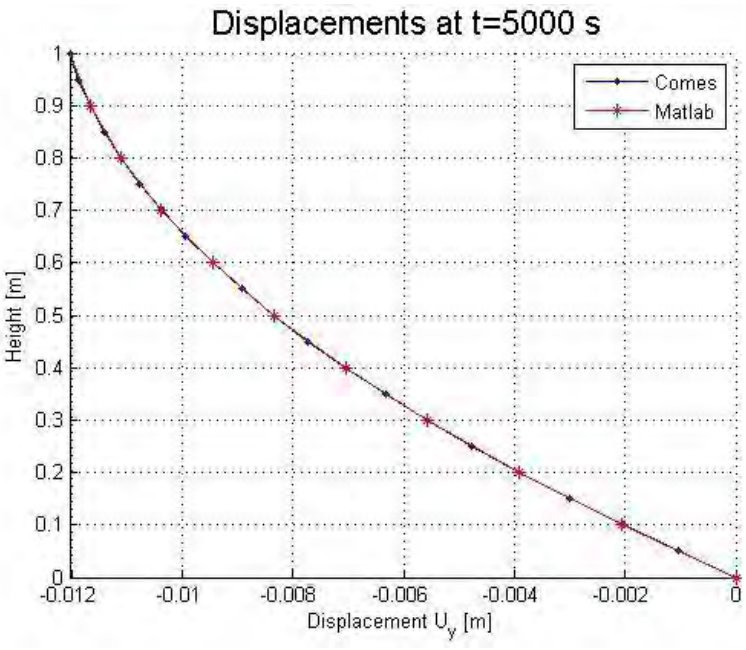

Figure 3. 24. – Time step 50. Comparison Matlab/Comes for displacements.

Time step100 t=10000s

Matlab results are firstly shown. Therefore the comparison between it and Comes is represented in a graph.

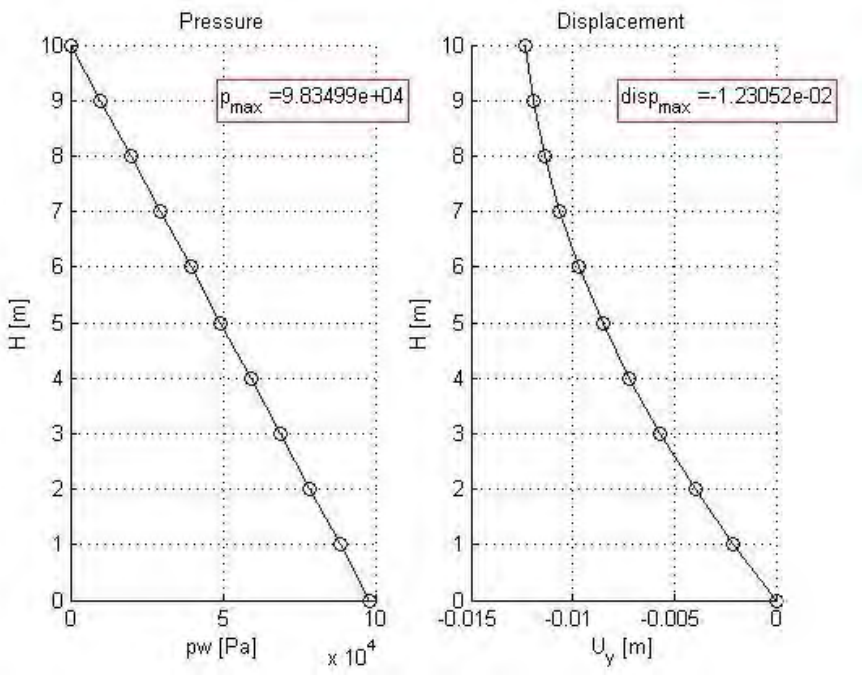

Figure 3. 25. – Time step 100. Numerical results with Matlab code.

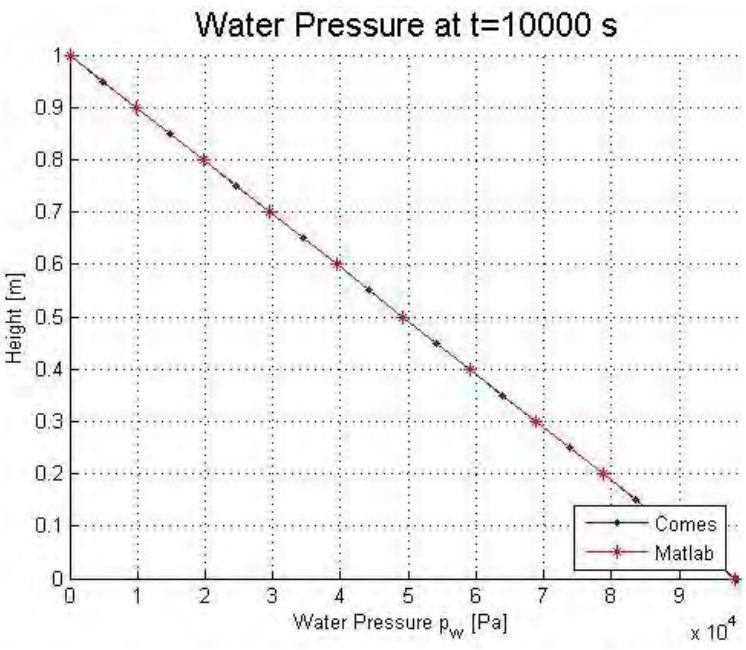

Figure 3. 26. – Time step 100. Comparison Matlab/Comes for pressures.

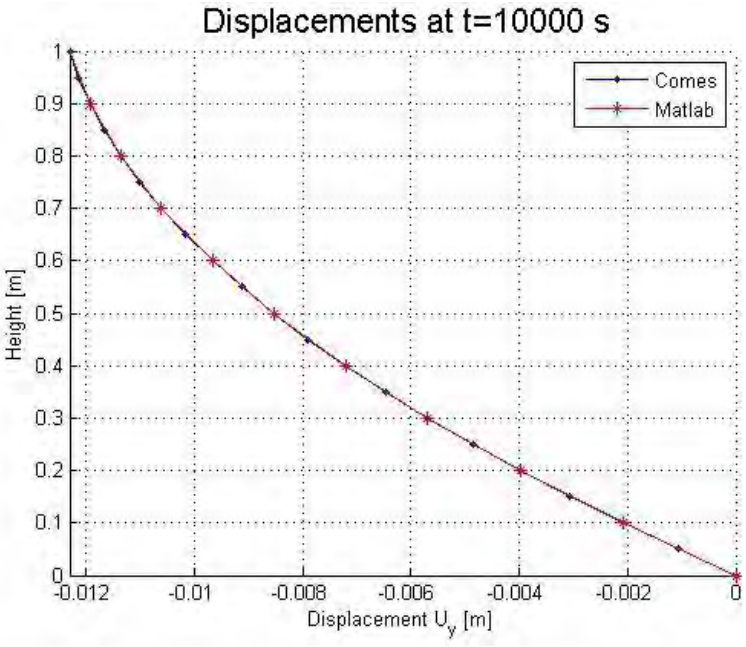

Figure 3. 27. – Time step 100. Comparison Matlab/Comes for displacements.

Time step250 t=25000s

Matlab results are firstly shown. Therefore the comparison between it and Comes is represented in a graph.

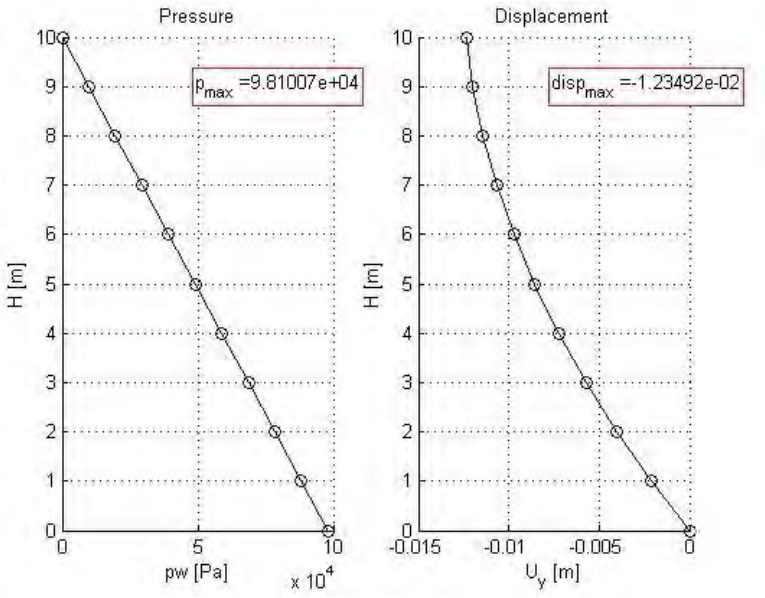

Figure 3. 28. – Time step 250. Numerical results with Matlab code.

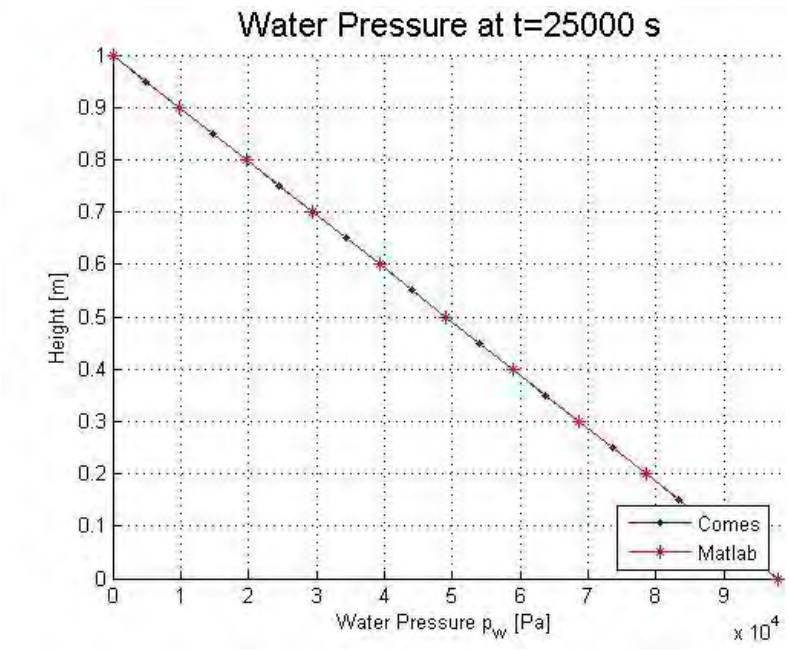

Figure 3. 29. – Time step 250. Comparison Matlab/Comes for pressure.

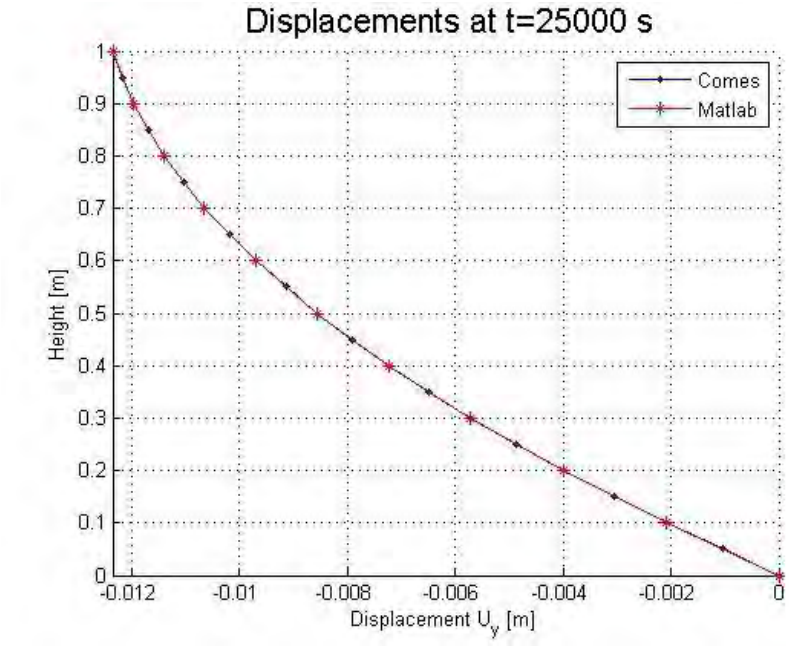

Figure 3. 30. – Time step 250. Comparison Matlab/Comes for displacements.

Conclusions

After 250 time step, that is after 25000 seconds, the load is completely transmitted from the water to the solid skeleton.

Water pressures settle themselves again in their hydrostatic trend, while the displacements reach the maximum value on the top of -1,235 cm. Purified of the initial displacement due to the process of consolidation (-0.957 cm), the maximum displacement caused by the applied load has a value of -1.139 cm.

The code can be considered validated in fully saturated conditions, as the comparison with Comes at different time steps proves.

3.3. Partially Saturated conditions

3.3.1. Explanation of the benchmark

In this last test, the aim was the validation of the model in condition of partially saturated soil.

It is difficult to choose appropriate tests to validate the model developed in the previous sections and its implementation in the computer code. Indeed there are no analytical solution for this type of coupled problems, where deformations of the solid skeleton are studied with saturated-unsaturated flow of mass transfer. There are also very few documented laboratory experiments.

One of these is the experiment conducted by Liakopoulos on the isothermal drainage of water from a vertical column of water saturated

sand. The column is one meter high, subdivided into ten quadrilateral elements of 0.1 x 0.1 meters. All the nodes of the column are fixed along the horizontal direction. The base of the column is also fixed for the vertical displacements.

The column was packed by Del Monte sand and instrumented to measure the moisture tension at several points along the column. Before starting the experiment (t < 0) water was continuously added from the 28 The Erwin Stein Award top and was allowed to drain freely at the bottom through a filter. The flow was carefully regulated until the tensiometers read zero pore pressure. At t = 0 the water supply was ceased and the tensiometers reading were recorded.

Only the porosity and the hydraulic properties of Del Monte sand were measured by an independent set of experiments. Material parameters and the experimental constitutive laws for $S_w(p_c)$ and $kr_w(p_c)$ used in the computation are listed in (Table 3.9.).

PARAMETER	VALUE
Porosity	$n = 0.2975$
Isotropic permeability	$k = 4.3 \cdot 10^{-6} m/s$
Solid grain density	$\rho_s = 2000\ kg/m^3$
Water density	$\rho_w = 1000\ kg/m^3$
Gravity acceleration	$g = 9.806\ m/s$
Water saturation	$S_w = 1 - 1.9722 \cdot 10^{11} p_c^{2.4279}$
Relative permeability for water	$k_{rw} = 1 - 2.207(1 - S_w)^{1.0121}$
Solid bulk modulus	$K = 2166.77\ kN/m^3$

Table 3. 9. – Parameters.

3.3.2. Implementation: results and validation

Liakopoulus' column is made of consolidated sand. As initial condition for modelling, the pressures and the dispalcements obtained after Step 4 (consolidation) are imposed. Water pressure at the bottom is fixed zero, to simulate the dreinage of water.

The simulation is divided into time steps of $t = 10s$.

The compairson with the Liakopoulus test implemented with Comes are done at different time steps: 5, 30, 60 and 120 minutes.

The results in terms of water pressure, displacement and saturation degree are shown below.

- **Water pressure**

A compairson between Matlab code and Comes at each time step will be described in the next graphs.

After them, another diagram will show the evolution of water pressure during the time.

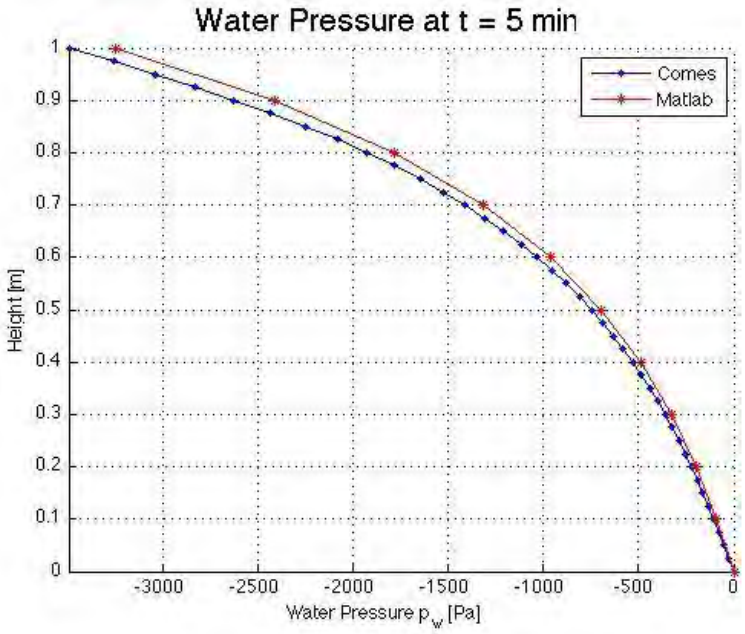

Figure 3. 31. – Time step 30. Comparison Matlab/Comes for pressure.

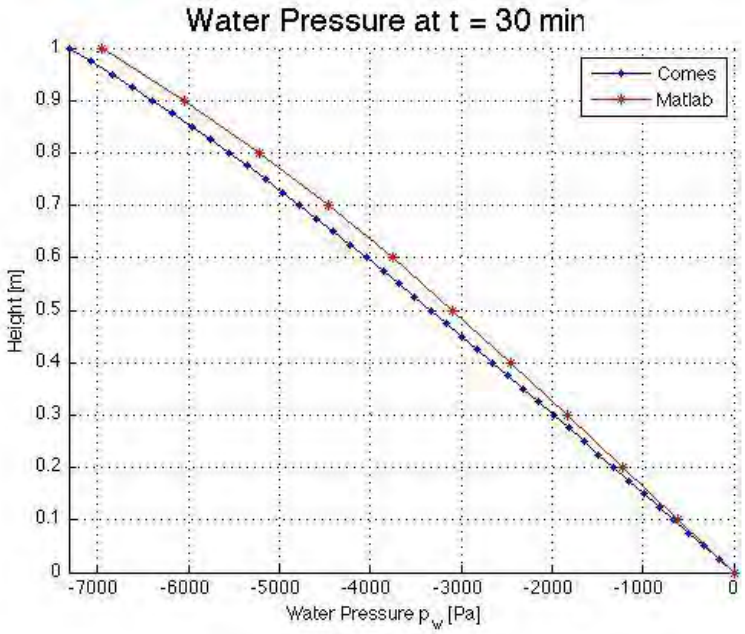

Figure 3. 32. – Time step 180. Comparison Matlab/Comes for pressure.

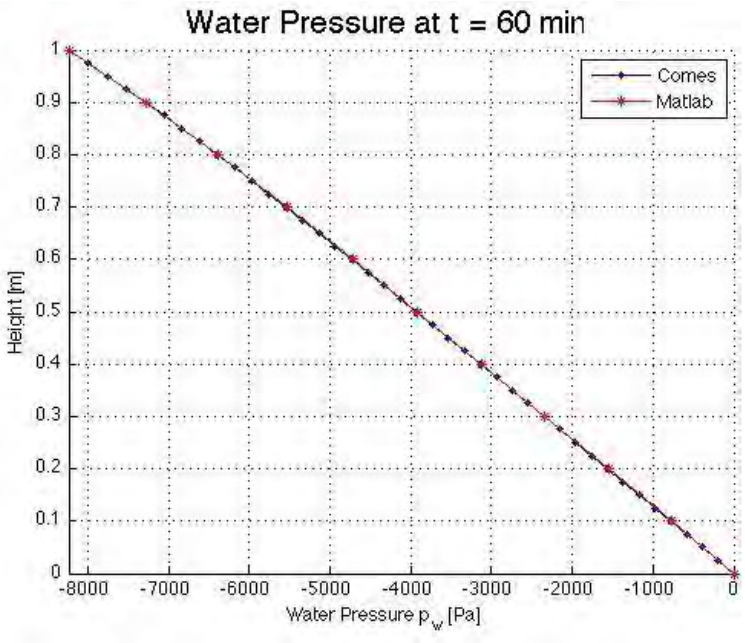

Figure 3. 33. – Time step 360. Comparison Matlab/Comes for pressure.

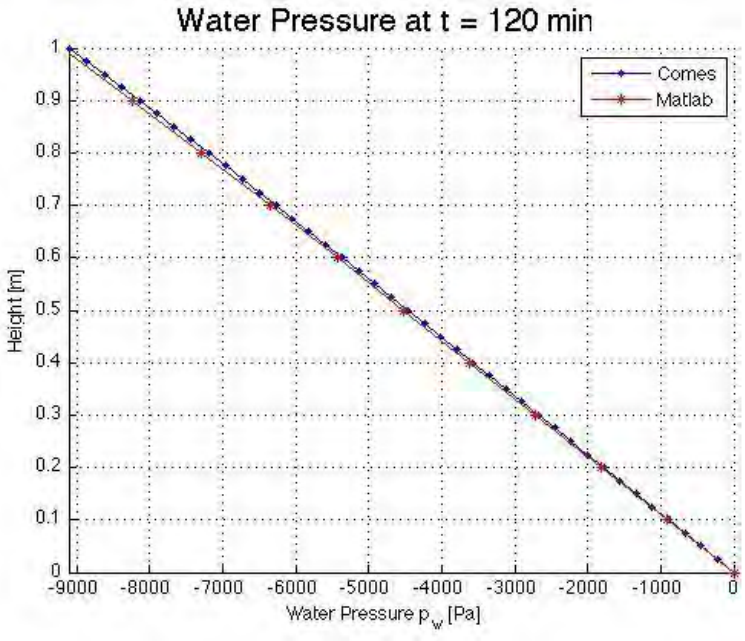

Figure 3. 34. – Time step 720. Comparison Matlab/Comes for pressure.

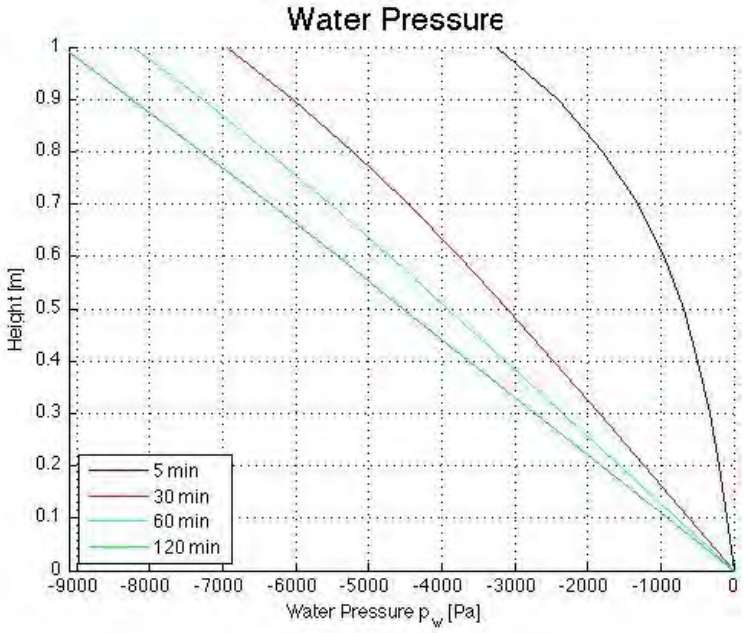

Figure 3. 35. – Evolution in time of water pressure.

- **<u>Saturation degree</u>**

A compairson between Matlab code and Comes at each time step will be described in the next graphs. After them, another diagram will show the evolution of saturation degree S_w during the time.

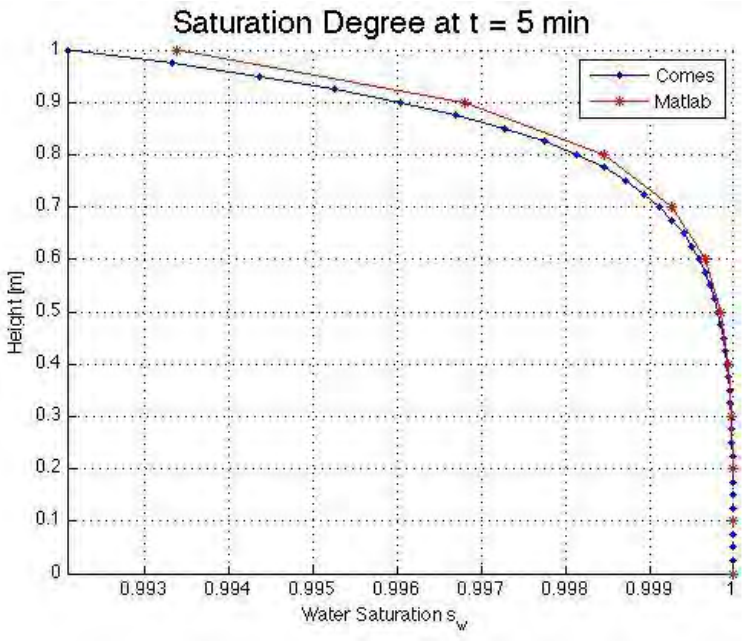

Figure 3. 36. – Time step 30. Comparison Matlab/Comes for Sw.

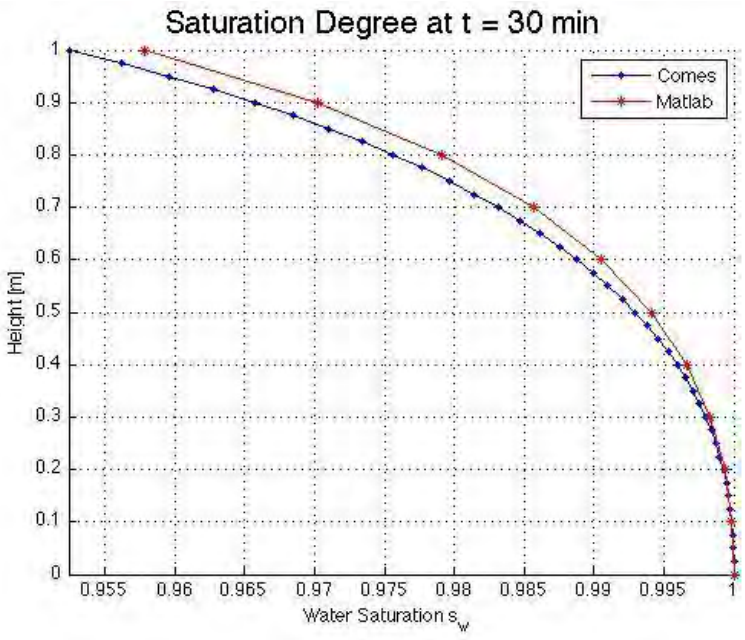

Figure 3. 37. – Time step 180. Comparison Matlab/Comes for Sw.

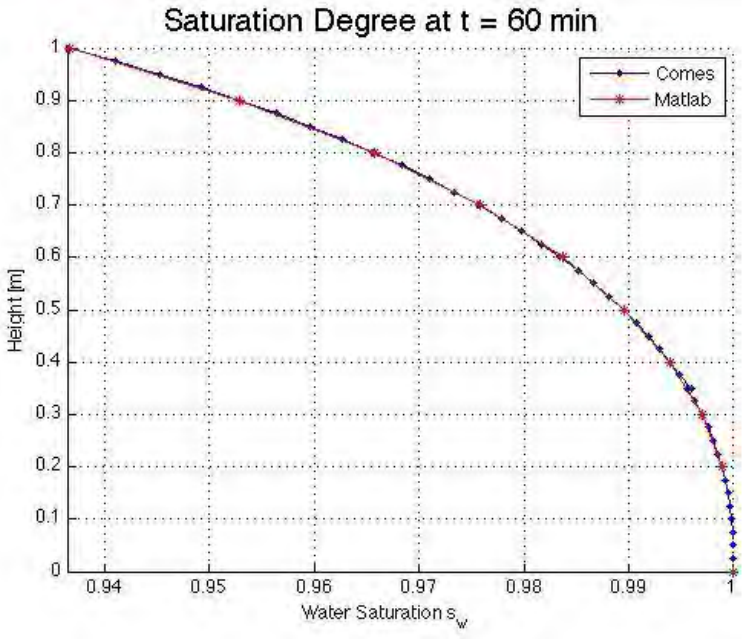

Figure 3. 38. – Time step 360. Comparison Matlab/Comes for Sw.

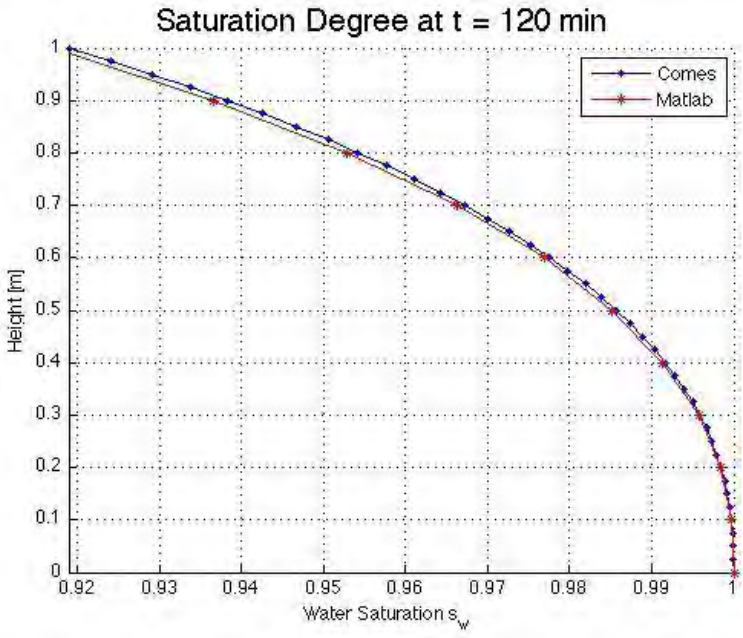

Figure 3. 39. – Time step 720. Comparison Matlab/Comes for Sw.

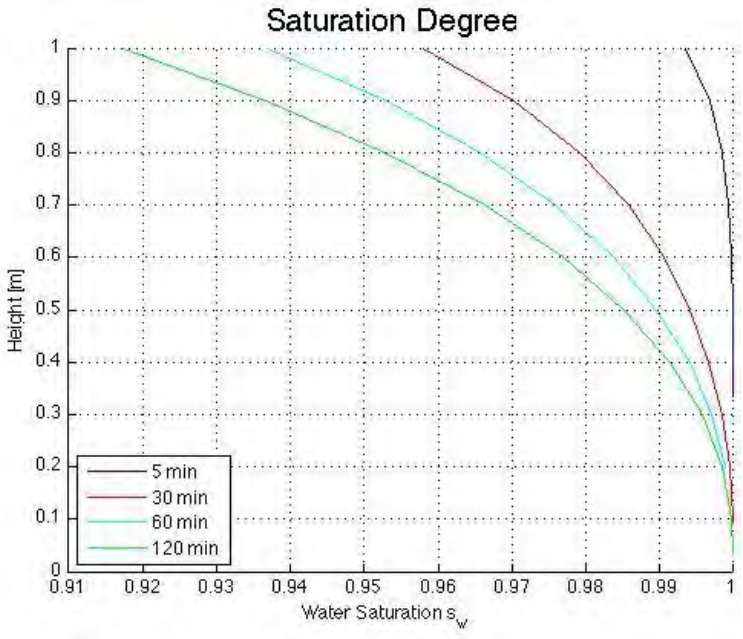

Figure 3. 40. – Evolution in time of saturation degree.

- **<u>Displacements</u>**

A compairson between Matlab code and Comes at each time step will be described in the next graphs. After them, another diagram will show the evolution of displacments during the time.

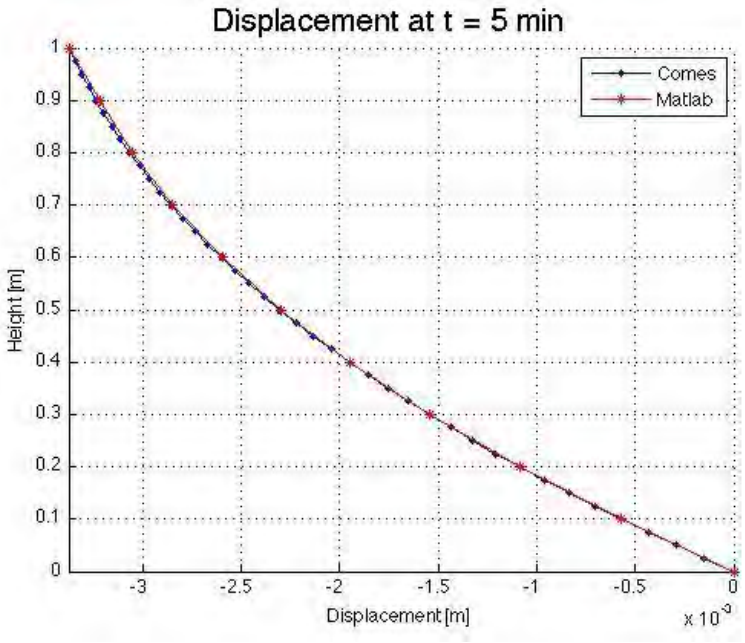

Figure 3. 41. – Time step 30. Comparison Matlab/Comes for displacements.

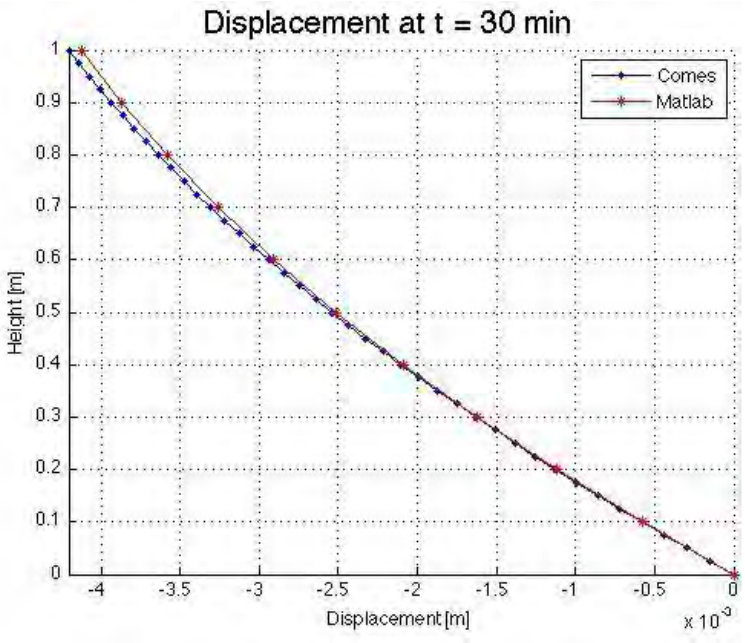

Figure 3. 42. – Time step 180. Comparison Matlab/Comes for displacements.

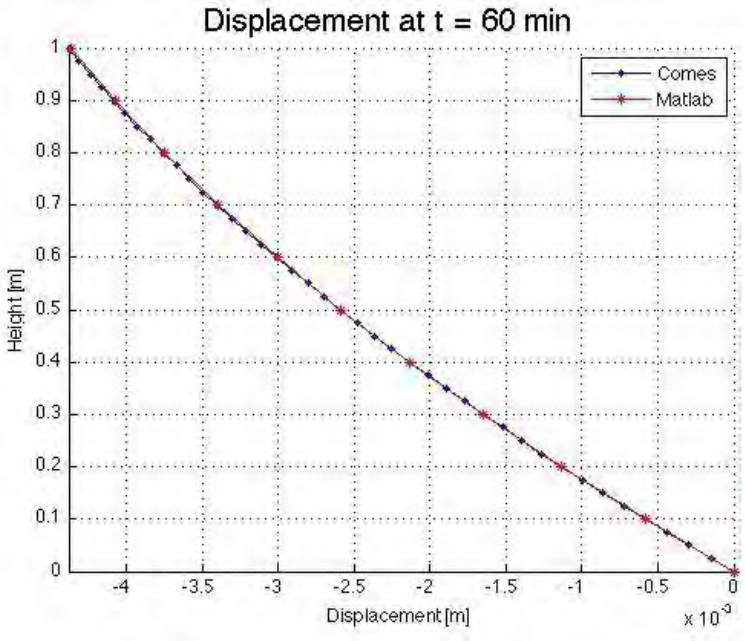

Figure 3. 43. – Time step 360. Comparison Matlab/Comes for displacements.

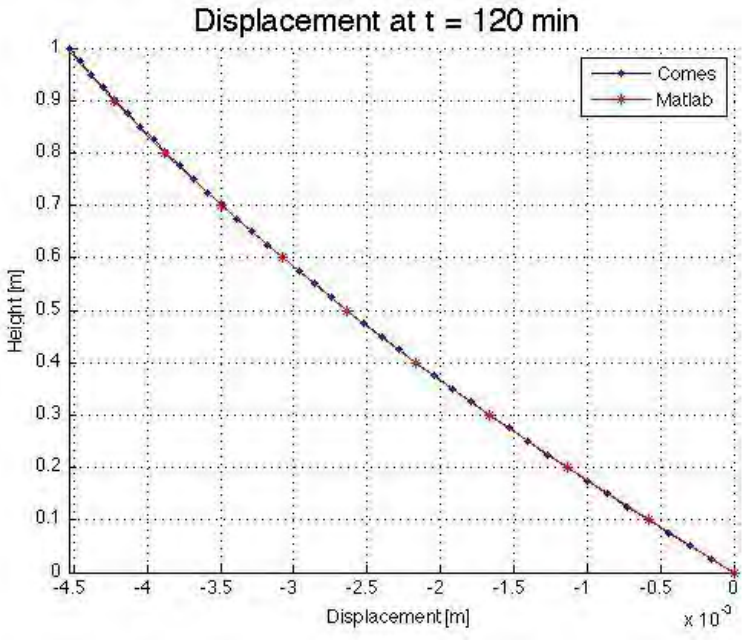

Figure 3. 44. – Time step 720. Comparison Matlab/Comes for displacements.

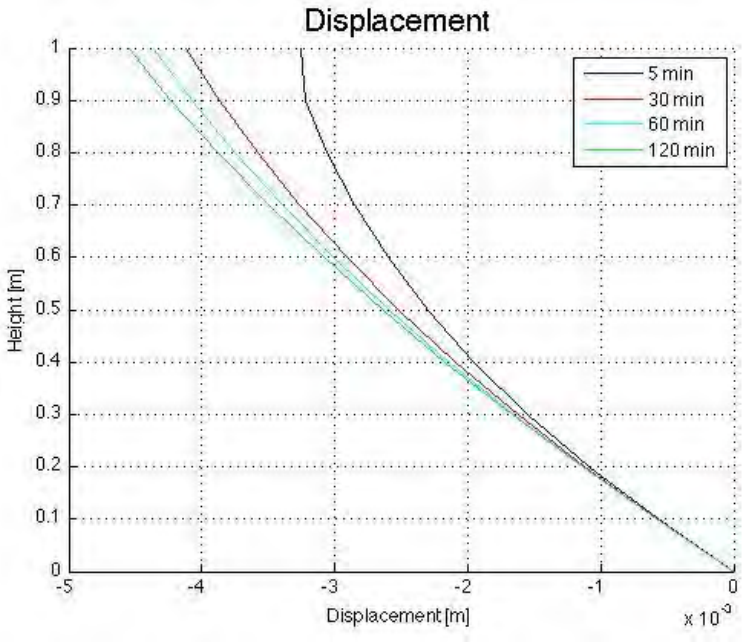

Figure 3. 45. – Evolution in time of displacements.

3.3.3. Conclusions

After 2 hours the process is almost concluded. The water pressure on the top should in fact reach the value of $p_w = -9810\,Pa$, linearly decreasing his absolute value until reaching the null pressure at the bottom.

The model implemented in Matlab can be considered validated. It fits in fact with the Comes results.

Chapter 4 - The phase-field description of dynamic brittle fracture

4.1. Introduction to phase field

As experimental tests are expensive and time consuming, they cannot be carried out at all stages of a design process in an efficient and economical way. Thus, conclusions drawn from numerical simulations often play a crucial role in design decisions. This happens even in the case of the study of material fractures.

As a consequence, lots of research effort is put into the development of reliable fracture models and the numerical implementation thereof. The key objective of these fracture models is the prediction of the fracture evolution in a given loading situation. On the one hand, this requires criteria for the onset of crack extension of pre-existing cracks and for the nucleation of new cracks in originally undamaged material. On the other hand, the geometry of the crack path, including possible kinking of a crack or bifurcation into several crack branches, needs to be predicted. In dynamic fracture mechanics, also the velocity of crack propagation is an issue.

The theoretical foundations of the contemporary theory of brittle fracture were laid in the works of Griffith [1921] and Irwin [1957]. Griffith was the first to link the energy necessary for the breaking of atomic bonds to an energy density of crack surfaces. As a consequence, he formulated an energetic fracture criterion, where crack propagation results from the

competition of elastic energy stored in the solid and surface energy needed to create new fracture surfaces. The actual breakthrough of this new concept was achieved through the works of Irwin. Besides a refinement of the surface energy density proposed by Griffith, he characterized the loading of a crack in terms of singular stresses at the crack tip, and proved the equivalence of his method and Griffith's energetic approach. This link allows to evaluate cracks using the tools of classical continuum mechanics and opened the door to practical applications of the new concepts and to further research in the field of theoretical fracture mechanics.

Besides the development of physically sound and appropriate models of crack propagation, numerical instruments are needed to describe the elastic deformations of complex structures, which generally cannot be obtained analytically. To this end, particularly the finite element method (FEM) is widely used in industrial applications. The essential characteristic of this method is the discretization of a continuous structure into a set of sub-domains referred to as elements with a certain number of element nodes. The partial differential equations for the unknown field variables are then recast into a finite dimensional set of equations for the discrete nodal values. In between the element nodes, the unknown field variables are usually approximated by means of continuous shape functions. Consequently, finite elements do not cope well with field discontinuities. This challenges their application in the context of fracture mechanics, because at a crack the displacement field

may suffer jump discontinuities.

In this regard, a conceptually different modeling approach to fracture has gained importance in recent years. The so called phase field method bases on concepts elaborated by Ginzburg and Landau [1959] and was originally introduced by Collins and Levine [1985] and Caginalp and Fife [1986] in order to model solidification processes. The general idea of this modeling approach is the incorporation of an additional continuous field variable – the phase field order parameter – whose value describes the condition of the system. At interfaces between different material phases, the order parameter interpolates smoothly between the values assigned to the different phases, avoiding discontinuous jumps. The width of the diffuse transition zone between different material phases is controlled by a model inherent length scale. If this length scale becomes infinitesimal small, the underlying sharp interface model is recovered. In a phase field model, the motion of the interfaces is given implicitly by the solution of a partial differential equation for the order parameter. This so called evolution equation is coupled to the elastic field equations in order to model the mutual interaction between the phase state and the elastic properties of the material. This coupling also has the effect that the boundary conditions at phase interfaces are automatically satisfied, thus avoiding an explicit treatment thereof. This property is also very advantageous concerning numerical simulations and significantly facilitates the study of structures with more complex interface geometries. Thus, the phase field method is a very powerful numerical tool to solve moving boundary problems.

4.2. General remarks

In this thesis a continuum approach to brittle fracture is used. This means that the material is treated as a continuum, and fracture is predicted on the basis of an analysis of macroscopic quantities stress, energy and strain. from this point of view, a crack is a cut in the body at the scale of the structure. The dimension of a crack is considered to be one dimension lower than the geometrical dimension of the surrounding material.

A crack is a line and its end point is called *crack tip*, in two-dimensional media. In three-dimensional media, a crack forms a surface ending at the crack front. The opposite boundaries of a crack are called crack faces. These ones are considered to be traction free in most applications.

The loading of a crack can be described with three independent components according to the figure. Mode one is a symmetric crack opening orthogonal to the local fracture surface. It is the most important case for practical application. In mode two, the crack surface slide relatively to each other in the plane of the crack and perpendicular to the crack front, causing shear stresses. In mode three, crack surfaces separate in the plane of the crack, but parallel to the crack front.

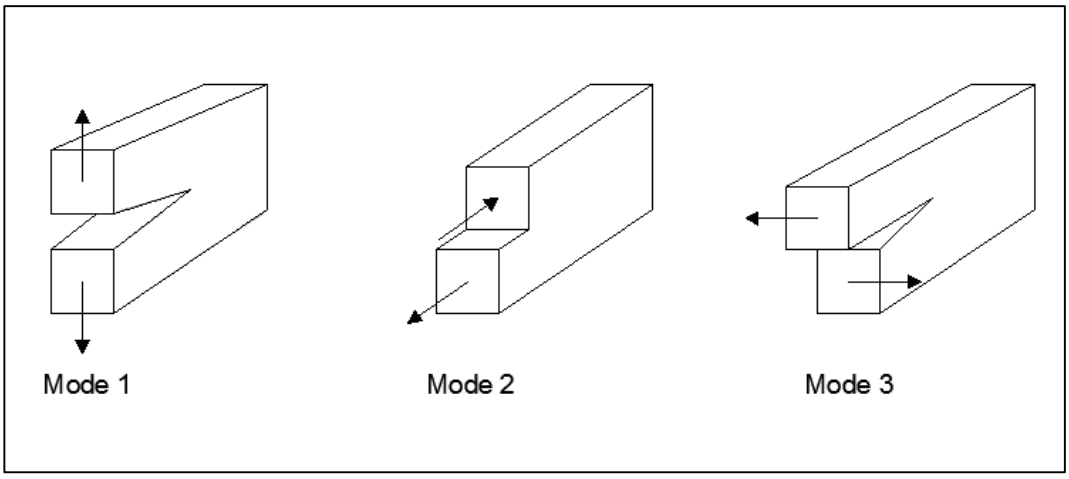

Figure 4. 1. Crack opening modes.

4.3. Model assumption in LEFM

The complex processes of bond breaking in front of the crack front or crack tip are not explicitly described by continuum approaches to fracture. Therefore, the process zone, in which these events take place, must be negligibly small compared to all macroscopic dimensions of the investigated structure. This assumption holds true for many brittle materials and is a typical feature of metals.

In reality, the material will deform inelastically in the so called yielding zone around the crack tip. Thus, linear theory is applicable, if the yielding zone is limited to a very small area around the crack. Which holds true for many brittle but not for ductile materials.

4.4. Griffith's theory of brittle fracture

An arbitrary body $\Omega \subset R^d$ (with $d \in \{1,,2,3\}$) with external boundary $\partial\Omega$ and internal discontinuity boundary Γ is considered.

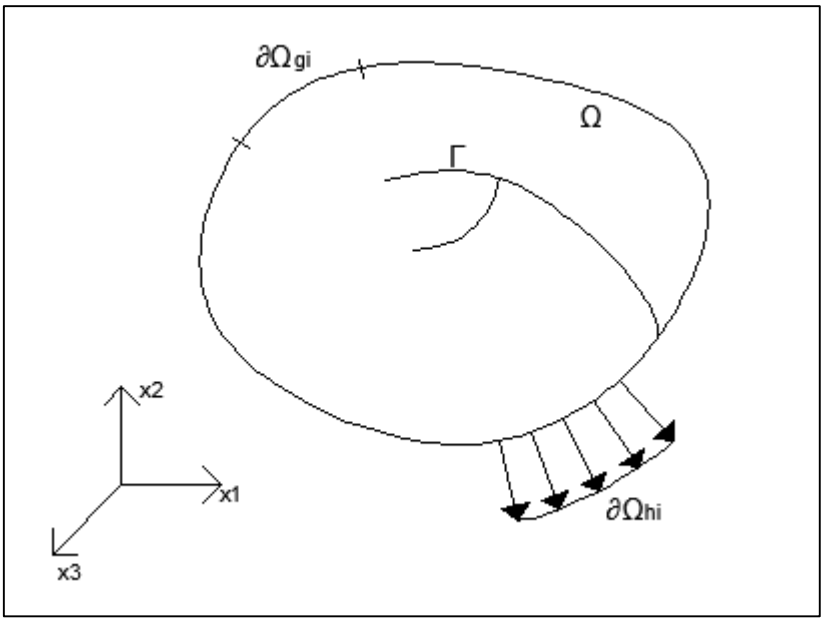

Figure 4. 2. Schematic representation of a solid body X with internal discontinuity boundaries Γ.

The displacement of a point $x \in \Omega$ at time $t \in [0, T]$ is denoted by $i, j = 1, \dots, d$. The displacement field satisfies time-dependent Dirichlet boundary conditions, $u_i(x,t) = g_i(x,t)$, on $\partial\Omega_{g_i} \subseteq \partial\Omega$, and time-dependent Neumann boundary conditions on $\partial\Omega_{h_i} \subseteq \partial\Omega$. Small deformations and deformation gradients are assumed, and the infinitesimal strain tensor is defined as $\varepsilon(x,t) \in R^{dxd}$, with components

$$\varepsilon_{ij} = u_{(i.j)} = \frac{1}{2}\left(\frac{\partial u_i}{\partial x_i} + \frac{\partial u_j}{\partial x_j}\right) \tag{4.1}$$

as an appropriate deformation measure, isotropic linear elasticity is assumed, such that the elastic energy density is given by:

$$\psi_e(\varepsilon) = \frac{1}{2}\lambda\varepsilon_{ii}\varepsilon_{jj} + \mu\varepsilon_{ii}\varepsilon_{jj} \tag{4.2}$$

with λ and μ the Lamé constants. The Einstein summation convention is used on repeated indices.

The evolving internal discontinuity boundary, Γ(t), represent a set of discrete cracks. In according with Griffith's theory of brittle fracture, the energy required to create a unit area of fracture surface is equal to the critical fracture energy density $\mathcal{G}_c$. The total potential energy of the body, ψ_{pot}, being the sum of the elastic energy and the fracture energy, is the given by

$$\psi_{pot}(u,\Gamma) = \int_{\Omega} \psi_e(\nabla^s u)dx + \int_{\Gamma} \mathcal{G}_c dx \qquad (4.3)$$

the symmetric gradient operator, $\nabla^s: u \rightarrow \varepsilon$, is defined as a mapping from the displacement field to the strain field. Since brittle fracture is assumed, the fracture energy contribution is merely the critical fracture energy density integrated over the fracture surface. In the case of small deformations, irreversibility of the fracture process dictates that $\Gamma(t) \subseteq \Gamma(t+\Delta t)$ for all $\Delta t > 0$. Hence, translation of cracks through the domain is prohibited, but cracks can extend, branch and merge.

The kinetic energy of the body Ω is given by:

$$\psi_{kin}(\dot{u}) = \frac{1}{2}\int_{\Omega} \rho \dot{u}_i \dot{u}_i dx \qquad (4.4)$$

with $\dot{u} = \frac{\partial u}{\partial t}$ and ρ the mass density of the material. Combined with the potential energy this renders the Lagrangian for the discrete fracture problem as:

$$L(u,\dot{u},\Gamma) = \psi_{kin}(\dot{u}) - \psi_{pot} = \int_{\Omega} \left[\frac{1}{2}\rho\dot{u}_i\dot{u}_i - \psi_e(\nabla^s u)\right] dx - \int_{\Gamma} \mathcal{G}_c dx \tag{4.5}$$

The Euler-Lagrange equations of this functional determine the motion of the body. From a numerical standpoint, tracking the evolving discontinuity boundary, Γ, often requires complex and costly computations. This is particularly so when interactions between multiple cracks, or complex shaped cracks in three dimensions are considered.

4.5. Phase-field approximation

4.4.1. Phase field theory

In order to circumvent the problems associated with numerically tracking the propagating discontinuity representing a crack, the fracture surface, Γ, is approximated by a phase-field, $s(x,t) \in [0,1]$. The value of this phase field is equal to 1 away from the crack and is equal to 0 inside the crack. As in Bourdin the fracture energy is approximated by:

$$\int_{\Gamma} \mathcal{G}_c dx \approx \int_{\Omega} \mathcal{G}_c \left[\frac{(s-1)^2}{4l_0} + l_0 \frac{\partial s}{\partial x_i}\frac{\partial s}{\partial x_i}\right] dx \tag{4.6}$$

where $l_0 \in \mathbb{R}^+$is a model parameter that controls the width of the smooth approximation of the crack. From Eq (4.6) it is clear that a crack is represented by regions where the phase field goes to zero. As elaborated by Bourdin n the limit of the length scale l_0 going to zero, the phase field approximation converges to the discrete fracture surface.

To model the loss of material stiffness in the failure zone, it is followed Miehe and the elastic energy is defined as:

$$\psi_e(\varepsilon, s) = [(1-k)s^2 + k]\psi_e^+(\varepsilon) + \psi_e^-(\varepsilon) \tag{4.7}$$

where $\psi_e^+(\varepsilon)$ and $\psi_e^-(\varepsilon)$ are the strain energies computed from the positive and negative components of the strain tensor, respectively, defined through a spectral decomposition of strain. Let:

$$\varepsilon = P\Lambda P^T \tag{4.8}$$

where P consists of the orthonormal eigenvectors of ε and $\Lambda = diag(\lambda_1, \lambda_2, \lambda_3)$ is a diagonal l matrix of principal strains. Defining:

$$\varepsilon^+ = P\Lambda^+ P^T \tag{4.9}$$

$$\varepsilon^- = P\Lambda^- P^T \tag{4.10}$$

where:

$$\Lambda^+ = diag(\langle\lambda_1\rangle, \langle\lambda_2\rangle, \langle\lambda_3\rangle) \tag{4.11}$$

$$\Lambda^- = \Lambda - \Lambda^+ \tag{4.12}$$

and

$$\langle x\rangle = \begin{cases} x & x > 0 \\ 0 & x \leq 0 \end{cases} \tag{4.13}$$

Then:

$$\psi_e^+(\varepsilon) = \frac{1}{2}\lambda\langle tr\varepsilon\rangle^2 + \mu tr[(\varepsilon^+)^2] \tag{4.14}$$

and

$$\psi_e^-(\varepsilon) = \frac{1}{2}\lambda(tr\varepsilon + \langle tr\varepsilon\rangle)^2 + \mu tr[(\varepsilon - \varepsilon^+)^2]. \tag{4.15}$$

the intent of the model is to maintain resistance in compression and, in particular, during crack closure. All calculations in this model set $k = 0$ because its inclusion is unnecessary.

Substitution of the phase field approximations for the fracture energy (4.6) and the elastic energy density (4.7) into Lagrange energy functional (4.5) yields:

$$L(u, \dot{u}, \Gamma) = \int_{\Omega} \left(\frac{1}{2} \rho \dot{u}_i \dot{u}_i - [(1-k)s^2 + k] \psi_e^+ (\nabla^s u) - \psi_e^- (\nabla^s u) \right) dx - \int_{\Omega} \mathcal{G}_c \left[\frac{(s-1)^2}{4l_0} + l_0 \frac{\partial s}{\partial x_i} \frac{\partial s}{\partial x_i} \right] dx \quad (4.17)$$

In order to conserve mass kinetic energy term is unaffected by the phase field approximation. The dependence of Lagrange energy functional on the propagating discontinuity boundary id now captured by the phase field, $s(x,t)$, which simplifies the numerical treatment of the model. Miehe uses an additional viscosity contribution but hence this term is omitted for brevity.

The Lagrangian is formulated in terms of the independent fields $u(x,t)$ and $s(x,t)$, the Euler-Lagrange equations are used to arrive at the strong form equations of motion:

$$\begin{cases} \frac{\partial \sigma_{ij}}{\partial x_j} = \rho \ddot{u}_i & on\ \Omega \times]0, T[\\ \left(\frac{4l_0(1-k)\psi_e^+}{\mathcal{G}_c} + 1 \right) s - 4l_0^2 \frac{\partial^2 s}{\partial x_i^2} = 1 & on\ \Omega \times]0, T[\end{cases} \quad (4.18)$$

where $\ddot{u} = \frac{\partial^2 u}{\partial t^2}$ and the Cauchy stress tensor $\sigma \in \mathbb{R}^{d \times d}$ is defined by

$$\sigma_{ij} = [(1-k)s^2 + k] \frac{\partial \psi_e^+}{\partial \varepsilon_{ij}} + \frac{\partial \psi_e^-}{\partial \varepsilon_{ij}} \quad (4.19)$$

These equations of motion can be solved to find both the displacement field $u(x,t)$ and phase field $s(x,t)$. The irreversibility condition $\Gamma(t) \subseteq \Gamma(t+\Delta t)$ is enforced in the strong form equations by introducing a strain history field, $\mathcal{H}$, which satisfies the Kuhn-Tucker conditions for loading and unloading:

$$\psi_e^+ - \mathcal{H} \leq 0, \quad \dot{\mathcal{H}} \geq 0, \quad \dot{\mathcal{H}}(\psi_e^+ - \mathcal{H}) = 0 \tag{4.20}$$

Substituting $\mathcal{H}$ for ψ_e^+ in (4.18) the modified strong form equations of motion are:

$$\begin{cases} \frac{\partial \sigma_{ij}}{\partial x_j} = \rho \ddot{u}_i & on\ \Omega \times]0,T[\\ \left(\frac{4l_0(1-k)\mathcal{H}}{\mathcal{G}_c} + 1\right) s - 4l_0^2 \frac{\partial^2 s}{\partial x_i^2} = 1 & on\ \Omega \times]0,T[\end{cases} \tag{4.21}$$

The equation of motion are subject to the boundary conditions:

$$\begin{cases} u_i = g_i & on\ \partial\Omega_{g_i} \times]0,T[\\ \sigma_{ij} n_j = h_i & on\ \partial\Omega_{h_i} \times]0,T[\\ \frac{\partial s}{\partial x_i} n_i = 0 & on\ \partial\Omega \times]0,T[\end{cases} \tag{4.22}$$

with $g_i(x,t)$ and $h_i(x,t)$ being prescribed on $\partial\Omega_{g_i}$ and $\partial\Omega_{h_i}$, respectively, for all $t \in]0,T[$, and with $n(x)$ being the outward-pointing normal vector of the boundary.

In addition, the equations of motion (4.21) are supplemented with initial conditions:

$$\begin{cases} u(x,0) = u_0(x) & x \in \Omega \\ \dot{u}(x,0) = v_0(x) & x \in \Omega \\ \mathcal{H}(x,0) = \mathcal{H}_0(x) & x \in \Omega \end{cases} \tag{4.23}$$

for both the displacement field and the strain history field, $\mathcal{H}_0(x)$, can be used to model pre-existing cracks or geometrical features.

4.4.2. Numerical formulation

The numerical formulation of (4.21) requires a spatial and temporal discretization. In this section the spatial discretization is formulated by means of the Galerkin method and a monolithic implicit scheme is introduced for the temporal discretization.

Continuous problem in the weak form

For the weak form of the problem it is defined a trial solution spaces $\mathcal{S}_t$ for the displacement and $\tilde{\mathcal{S}}_t$ for the phase field as:

$$\mathcal{S}_t = \left\{ u(t) \in \left(H^1(\Omega)\right)^d \mid u_i(t) = g_i \ \ on \ \partial\Omega_{g_i} \right\} \tag{4.24}$$

$$\tilde{\mathcal{S}}_t = \{ s(t) \in H^1(\Omega) \} \tag{4.25}$$

Similarly, the weighting function spaces are defined as:

$$\mathcal{v} = \{ w \in \} \left(H^1(\Omega)\right)^d \mid w_i = 0 \ \ on \ \ \partial\Omega_{g_i} \tag{4.26}$$

$$\tilde{v} = \{ q \in H^1(\Omega) \} \tag{4.27}$$

Multiplying the equations in (4.21) by appropriate weighting functions and applying integration by parts leads to the weak formulation:

$$
\begin{cases}
Given\ g, h, u_0, \dot{u}_0, and\ s_0\ find\ u(t) \in \mathcal{S}_t\ and\ s(t) \in \tilde{\mathcal{S}}_t, t \in [0,T], such\ that\ for\ all\ w \in \nu\ and\ for\ all\ q \in \tilde{\nu} \\
(\rho u,\ddot{w})_\Omega + (\sigma, \nabla w)_\Omega = (h, w)_{\partial\Omega_h} \\
\left(\left(\frac{4l_0(1-k)\mathcal{H}}{\mathcal{G}_c} + 1\right)s, q\right)_\Omega + (4l_0^2 \nabla s, \nabla q)_\Omega = (1, q)_\Omega \\
(\rho u(0), w)_\Omega = (\rho u_0, w)_\Omega \\
(\rho \dot{u}(0), w)_\Omega = (\rho \dot{u}_0, w)_\Omega \\
(s(0), q)_\Omega = (s_0, q)_\Omega
\end{cases}
\tag{4.28}
$$

where $(\cdot,\cdot)_\Omega$ is th$\mathcal{L}_2$e inner product on Ω.

The semidiscrete Galerkin form

Following the Galerkin method, $\mathcal{S}_t^h \subset \mathcal{S}_t, \nu^h \subset \nu, \check{\mathcal{S}}_t^h \subset \tilde{\mathcal{S}}_t$, and $\tilde{\nu}^h \subset \tilde{\nu}$ are the usual finite dimensional approximations to the function spaces of the weak form. The semidiscrete Galerkin form of the problem is then:

$$
\begin{cases}
Given\ g, h, u_0, \dot{u}_0, and\ s_0\ find\ u(t) \in \mathcal{S}_t\ and\ s(t) \in \tilde{\mathcal{S}}_t, t \in [0,T], such\ that\ for\ all\ w \in \nu\ and\ for\ all\ q \in \tilde{\nu} \\
(\rho u,\ddot{w})_\Omega + (\sigma, \nabla w)_\Omega = (h, w)_{\partial\Omega_h} \\
\left(\left(\frac{4l_0(1-k)\mathcal{H}}{\mathcal{G}_c} + 1\right)s, q\right)_\Omega + (4l_0^2 \nabla s, \nabla q)_\Omega = (1, q)_\Omega \\
(\rho u(0), w)_\Omega = (\rho u_0, w)_\Omega \\
(\rho \dot{u}(0), w)_\Omega = (\rho \dot{u}_0, w)_\Omega \\
(s(0), q)_\Omega = (s_0, q)_\Omega
\end{cases}
\tag{4.29}
$$

The explicit representations of u^h, w^h, s^h and q^h in terms of the basis functions and nodal variables are:

$$u_i^h = \sum_A^{n_b} N_A(x) d_{iA} \tag{4.30}$$

$$w_i^h = \sum_A^{n_b} N_A(x) c_{iA} \tag{4.31}$$

$$s^h = \sum_A^{n_b} N_A(x) \Phi_A \tag{4.32}$$

$$q^h = \sum_A^{n_b} N_A(x) \chi_A \tag{4.33}$$

where n_b is the dimension of the discrete space, the N_A's are the global basis functions, i is the special degree of freedom number, and d_{iA}, c_{iA}, Φ_A and χ_A are control variable degree of freedom. The same set of basis functions are used both for the finite dimensional trial solution and weighting function spaces.

4.4.3. Time discretization and numerical implementation

With this time discretization the momentum and phase field equations are solved independently. At a given time step, the momentum equation is solved first to get the displacements. Using the updated displacements, the phase field equation is solved. Here it is presented an algorithm that uses α methods to solve the momentum equation.

Defining the residual vectors for the momentum and phase field equations by:

$$R_{A,i}^u = (h, N_A e_i)_{\partial\Omega_h} - (\rho \ddot{u}^h, N_A e_i)_\Omega - \left(\sigma_{jk}, B_A^{ijk}\right)_\Omega \tag{4.34}$$

$$R_A^s = (1, N_A)_\Omega - \left(\left(\frac{4l_0(1-k)\mathcal{H}}{\mathcal{G}_c} + 1\right) s^h, N_A\right)_\Omega - \left(4l_0^2 \frac{\partial s^h}{\partial x_i}, \frac{\partial N_A}{\partial x_i}\right)_\Omega \tag{4.35}$$

And letting d and Φ be arrays of the control variable coefficients in (4.30) and (4.32), the staggered predictor/multicorrector time integration scheme is stated as follows: given (d_n, v_n, a_n, Φ_n), solve:

Predictor stage:

$$i = 0 \ (iteration\ counter) \tag{4.36a}$$

$$\tilde{v}_{n+1} = v_n + \Delta t(1-\gamma)a_n \tag{4.36b}$$

$$\tilde{d}_{n+1} = d_n + \Delta t v_n + \frac{(\Delta t)^2}{2}(1-2\beta)a_n \tag{4.36c}$$

$$a_{n+1}^{(i)} = 0 \tag{4.36d}$$

$$v_{n+1}^{(i)} = \tilde{v}_{n+1} \tag{4.36e}$$

$$d_{n+1}^{(i)} = \tilde{d}_{n+1} \tag{4.36f}$$

$$\Phi_{n+1}^{(i)} = \Phi_n \tag{4.36g}$$

Multicorrector stage

$$a_{n+\alpha_m}^{(i)} = a_n + \alpha_m\left(a_{n+1}^{(i)} - a_n\right) \tag{4.37a}$$

$$v_{n+\alpha_f}^{(i)} = v_n + \alpha_f\left(v_{n+1}^{(i)} - v_n\right) \tag{4.37b}$$

$$d_{n+\alpha_f}^{(i)} = d_n + \alpha_f\left(d_{n+1}^{(i)} - d_n\right) \tag{4.37c}$$

$$M^* \Delta a = R^u(d_{n+\alpha_f}^{(i)}, v_{n+\alpha_f}^{(i)}, a_{n+\alpha_m}^{(i)}, \Phi_{n+1}^{(i)}) \tag{4.37d}$$

$$a_{n+1}^{(i+1)} = a_{n+1}^{(i)} + \Delta a \tag{4.37e}$$

$$v_{n+1}^{(i+1)} = \tilde{v}_{n+1} + \Delta t \gamma a_{n+1}^{(i+1)} \tag{4.37f}$$

$$d_{n+1}^{(i+1)} = \tilde{d}_{n+1} + (\Delta t)^2 \beta a_{n+1}^{(i+1)} \tag{4.37g}$$

$$K^{ss} \Delta \Phi = F^s \tag{4.37h}$$

$$\Phi_{n+1}^{(i+1)} = \Delta \Phi \tag{4.37i}$$

The phase field arrays are defined as:

$$K^{ss} = [K_{AB}] \tag{4.38a}$$

$$K_{AB} = \left(\left(\frac{4 l_0 (1-k) \mathcal{H}}{\mathcal{G}_c} + 1 \right) N_B, N_A \right)_{\Omega} - \left(4 l_0^2 \frac{\partial N_B}{\partial x_i}, \frac{\partial N_A}{\partial x_i} \right)_{\Omega} \tag{4.38b}$$

$$F^s = \{F_A\} \tag{4.38c}$$

$$F_A = (1, N_A) \tag{4.38d}$$

and $\Delta t = t_{n+1} - t_n$ is the time step and parameters $\alpha_m, \alpha_f, \beta$ and γ, which define the method, are selected as described below.

If the linearized momentum equation is being solved implicitly then:

$$M^* = -\frac{\partial R_i^u}{\partial a_{n+1}} = \alpha_m M + \alpha_f \beta (\Delta t)^2 K \tag{4.39}$$

where M is the consistent mass matrix and

$$K = \left[K_{AB,ij}^{uu} \right] \tag{4.40}$$

$$K_{AB,ij}^{uu} = \left(\frac{\partial \sigma_{lk}}{\partial \varepsilon_{mn}} B_B^{jmn}, B_A^{ilk} \right)_{\Omega} \tag{4.41}$$

is the consistent damage-elastic tangent stiffness matrix.

The parameters are:

$$\alpha_m = 1 \tag{4.42a}$$

$$\alpha_f = 1 + \alpha \tag{4.42b}$$

$$\beta = \frac{(1-\alpha)^2}{4} \tag{4.42c}$$

$$\gamma = \frac{1-2\alpha}{2} \tag{4.42d}$$

$$\alpha \in \left[-\frac{1}{3}, 0\right] \tag{4.42e}$$

Chapter 5 – Examples and applications

5.1. Description of the global model

In this Chapter the final results of the union between the porous media theory and the phase field approach for fracture will be shown.

The aim is proving that a cohesion between the two is possible, permitting new future development in this research area.

The porous media implemented model descripted and validated in Chapters 2 and 3 is inserted as additional subroutine in the Matlab code supplied by the Department of Applied Mechanics of the TU Braunschweig, Germany (written: Marreddy Ambati, M.Sc. - Prof. Dr.-Ing. Laura De Lorenzis - Institut für Angewandte Mechanik -Technische Universität Braunschweig).

The logical passages of the implementation are:

1. Newton-Raphson cycle for phase field
   INPUT: displacements calculated at previous time step.
   OUTPUT: phase field, new displacements, new stiffness matrix.
2. Newton Raphson cycle for porous media
   INPUT: displacements and mechanical stiffness matrix given as an output by the previous N-R cycle, water pressures calculated at the previous time step.
   OUTPUT: new displacements, new water pressures.

Some examples are then carried on. In the next Section the results will be shown.

5.2. Examples and results

In this Section some tests will be described. All these cases have something in common: the creation of negative water pressures, that means the desaturation of the soil, and the formation of traction stresses and the consequent appearance of the fracture (phase field activation).

5.2.1. Exsiccation

With this test, the idea is to simulate the process of exsiccation.

On the Liakopoulis column (the same for geometry and material properties) the capillary pressure on the top is fixed at a value of 10000 Pa. Starting from a consolidated soil (hydrostatic pressure and relative displacements), the column will begin unsaturating, creating therefore a negative strain. This can activate the phase field value, which should slowly separate from the initial value 1, together with the crack formation.

The program is at first launched without the combination with the phase field, in order to evaluate the behaviour of the system and collect data for a comparison, and to check the creation of negative strains, essential for the activation of the phase field function.

After the first five minutes (30 time steps of 10 seconds), the situation in terms of strain is that described in Figure 5.1.

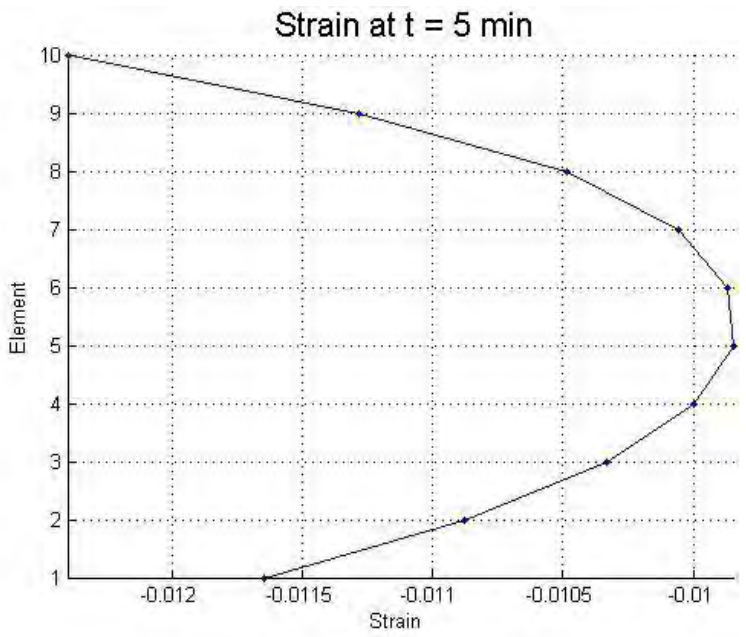

Figure 5. 1. Strain after five minutes.

Results for pressures and displacements are shown in Figures 5.2 and 5.3.

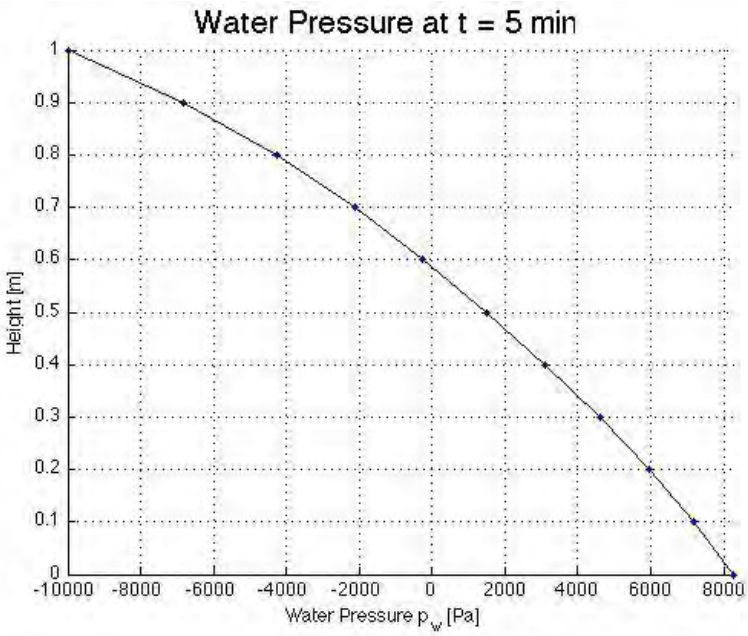

Figure 5. 2. Water pressure after five minutes.

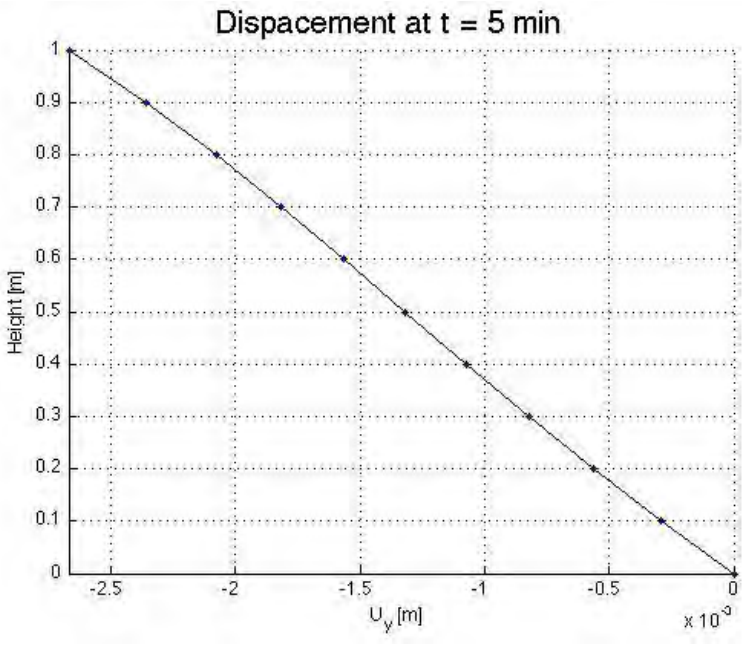

Figure 5. 3. Displacements after 5 minutes.

During the time steps the value of pressure should assume a linear trend with a maximum value on the top equal to the imposed value, and a minimum value at the bottom equal to the difference between the negative imposed pressure and the hydrostatic pressure at the base. This means:

$$p_w(nodes\ 1{,}2) = -10000 + 9806 = -194\ Pa$$

On the other hand, the trend of volumetric strains should settle in a linear one.

The changes during the time in terms of pressures, strains and displacements are shown in Figures 5.4, 5.5, 5.6.

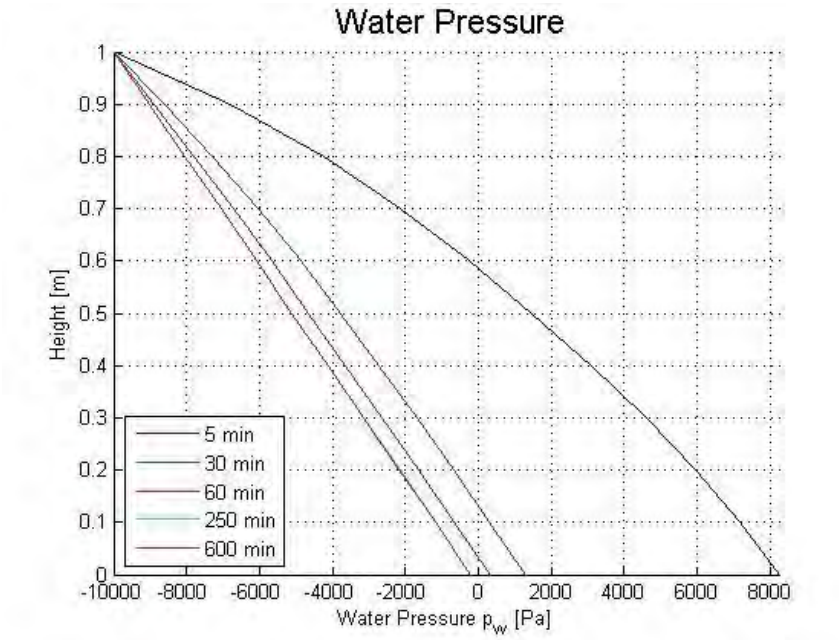

Figure 5. 4. Water pressure at different steps of time

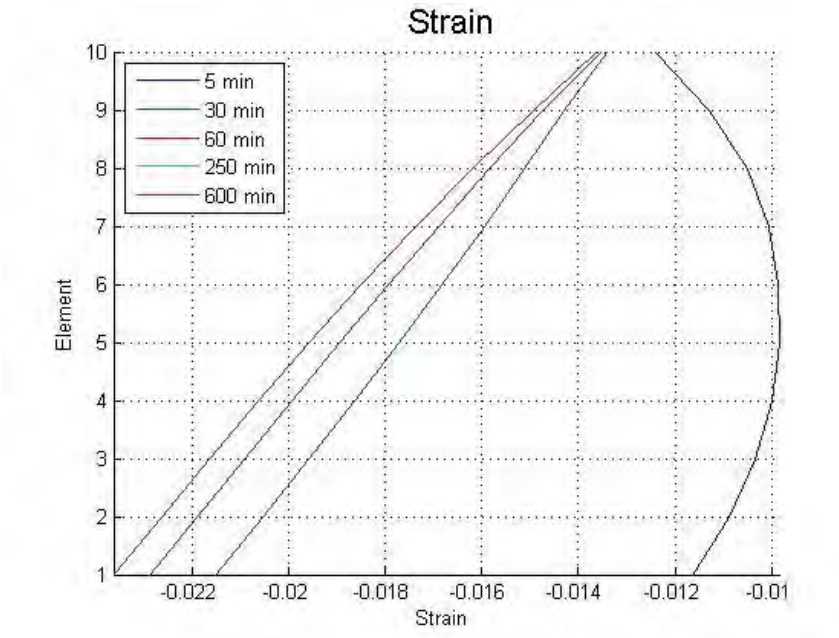

Figure 5. 5. Strain at different steps of time.

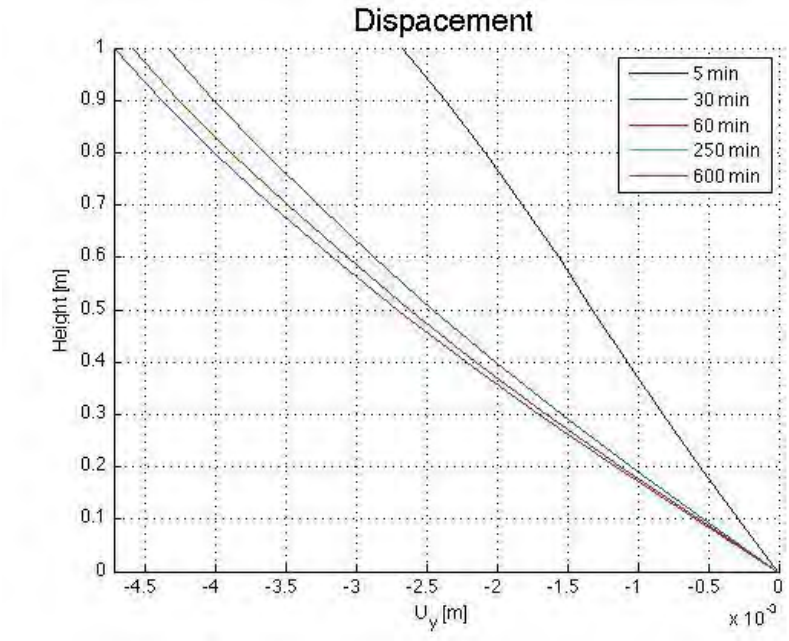

Figure 5. 6. Displacements at different steps of time.

The results are correct.

As additional example, the case of imposed positive capillary pressure on the top, not considering the gravity acceleration, is possible. In this case, after an adequate number of time steps, the pressure should become the same in each node of the column, and obviously equal to the imposed value. This is in fact what happens, as evident in Figure 5.7.

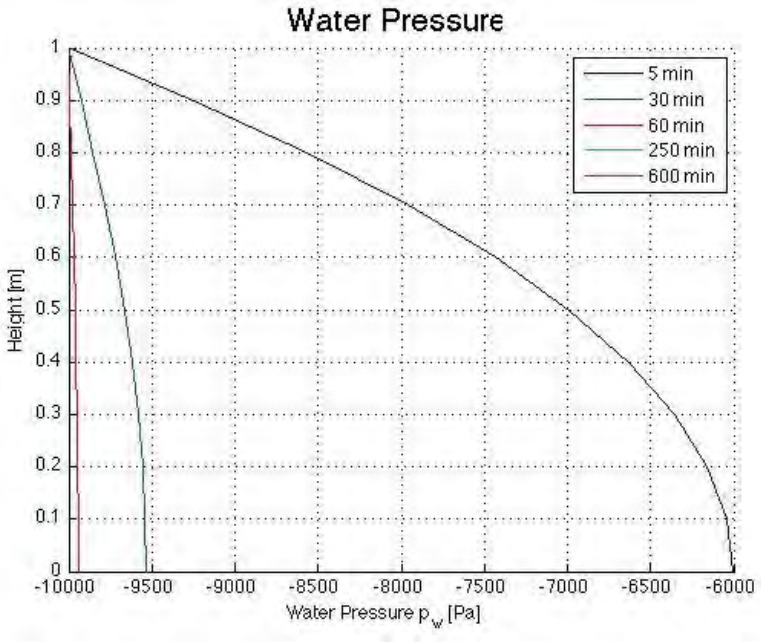

Figure 5. 7. Water pressure at different steps of time.

The insertion of the phase field function is therefore possible.

Effectively, after the first time step, thanks to the negative strains, the phase field moves away from the unit. The strains are however too low to permit a significant crack. The value of phase field after the first five minutes is

$$s = 9.999999999995791\ \mathrm{e}^{-01}$$

Essentially, the material is not broken yet.

The other variables at the same time step are shown in Figures 5.8, 5.9, 5.10.

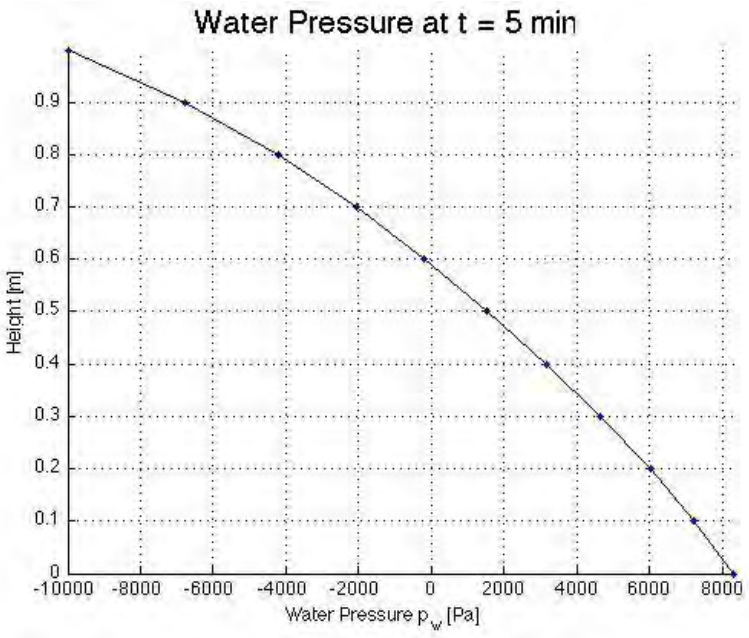

Figure 5. 8. Water pressure after five minutes.

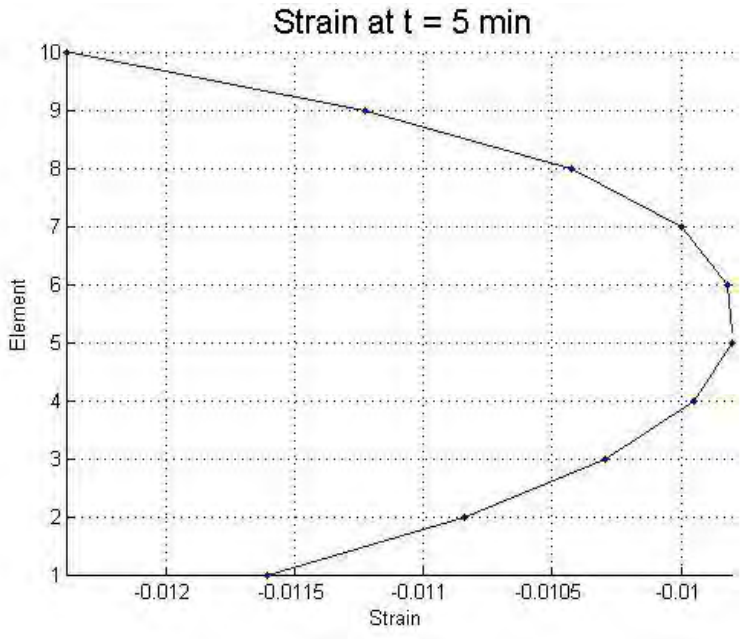

Figure 5. 9. Strain after five minutes.

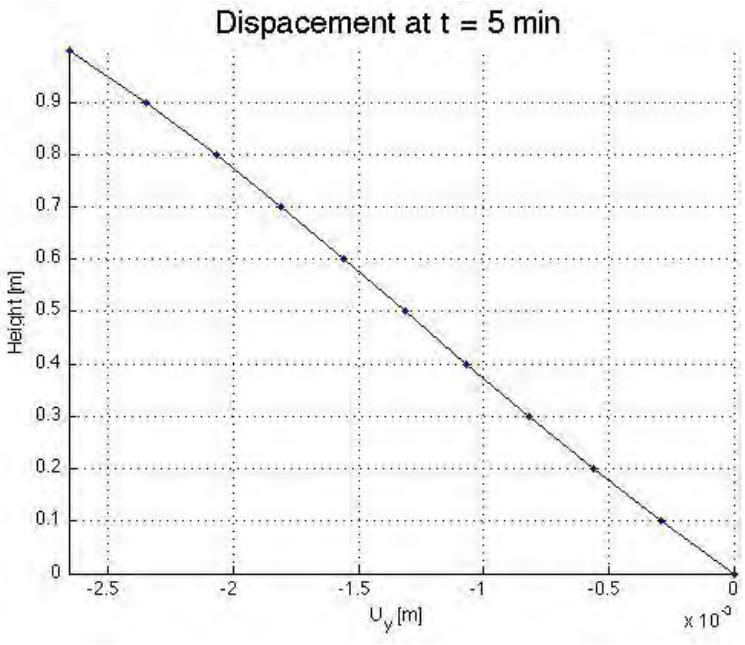

Figure 5. 10. Displacements after five minutes.

Going on with the time steps, displacements and strains lightly increase, but the order of magnitude remains about the same. The phase field variable remains for this reason unchanged during the evolution in time.

In the next graphs the trend of water pressures, strains and displacements at different time steps are plotted.

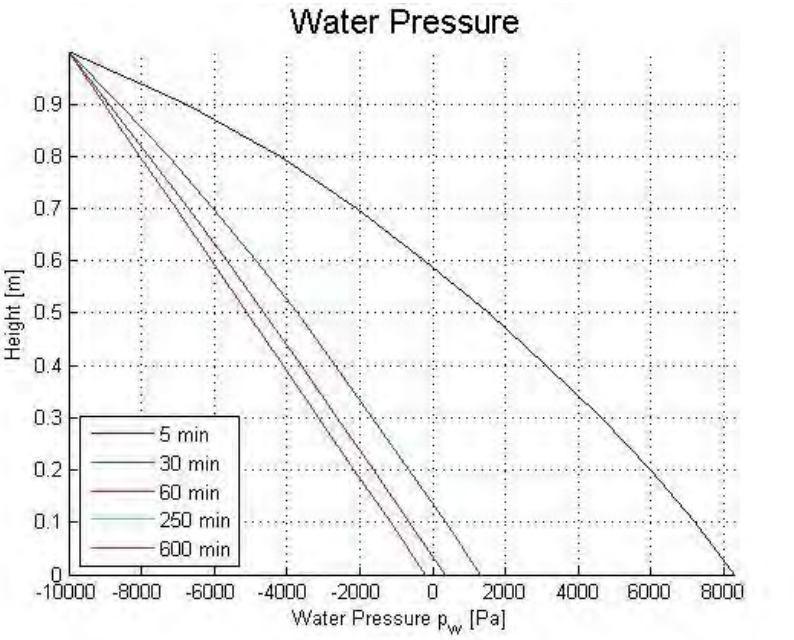

Figure 5. 10. Water pressure at different steps of time.

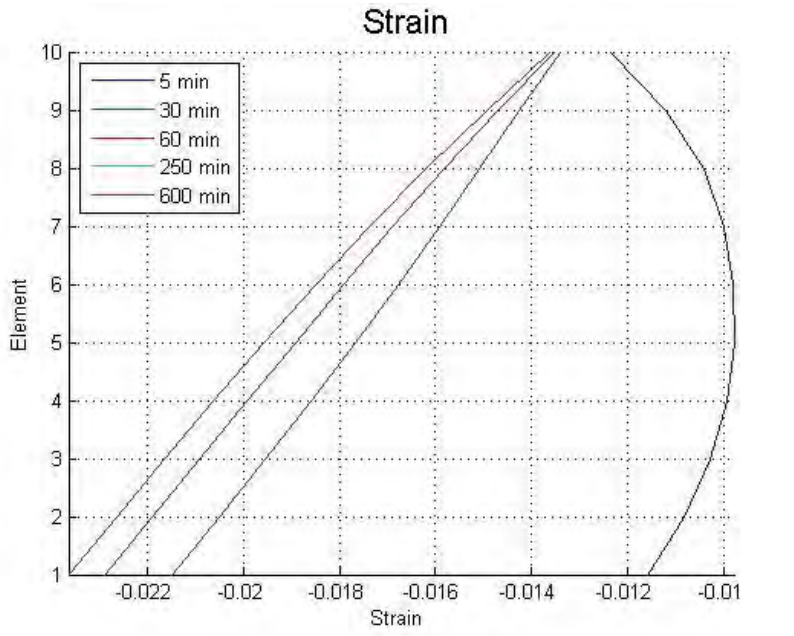

Figure 5. 11. Strain at different steps of time.

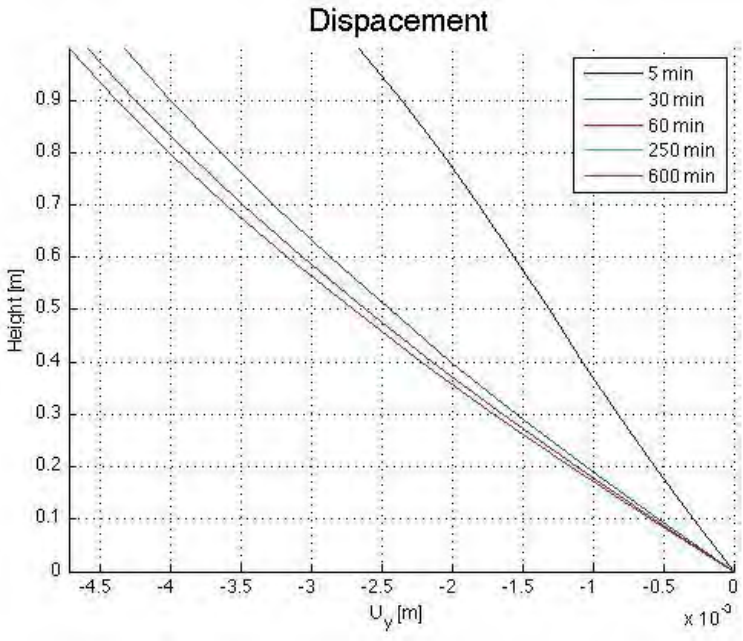

Figure 5. 12. Displacements at different steps of time.

Clearly, with the value of phase field constant and so closed to zero, the outputs with insertion of phase field calculation is essentially the same (or anyway not so different) of those calculated using the porous media model alone. This is clear in the next Figures 5.13, 5.14, with a comparison between the two at time t=5 $minutes$.

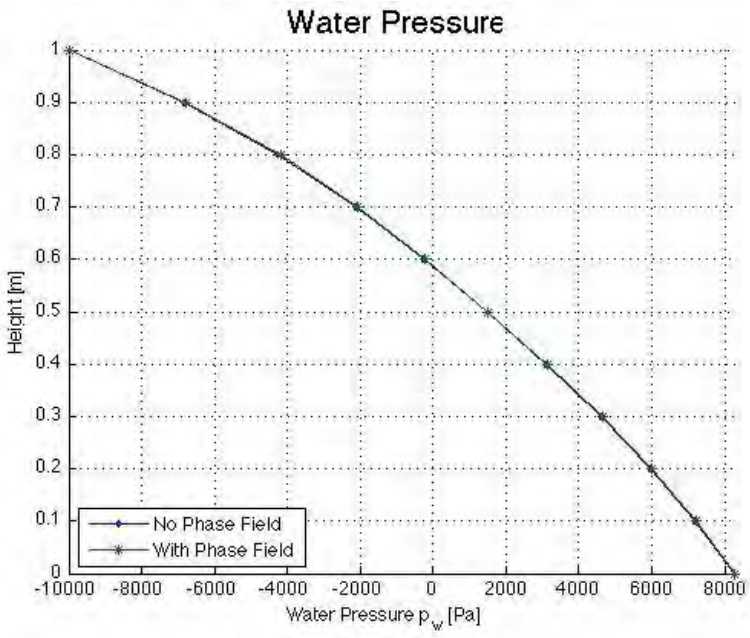

Figure 5. 13. Comparison of pressures with and without phase field.

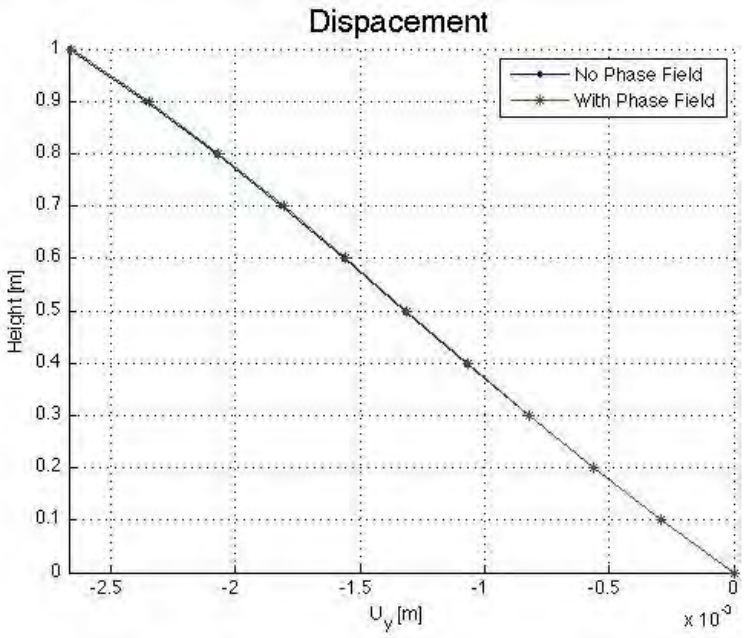

Figure 5. 14. Comparison of displacements with and without phase field.

It is not possible to increase the water pressure imposed on the top because of the limitation of the Liakopoulous laws for S_w, and consequently for pressure.

Liakopoulus test, because of its experimental nature, is valid in fact for saturation degrees not higher than 0,91. This corresponds to a value of water pressure, that cannot pass an intensity of about 9200 Pa. This example already lightly overpass the limit. It is not therefore possible to increase the capillary pressure on the top of the column.

5.2.2. Traction on the top. Ten elements-column.

The second example of union between phase field and the porous media is the following.

The geometry is the Liakopoulus' column with the same material parameters and the same constitutive relations.

On the top a displacement is imposed with an intensity 0,001m every time step. Water pressures on the bottom of the column are fixed at 9806 Pa. The starting point is the final results or the process of consolidation (for pressures and displacements).

Because of the same reasons explained in Section 5.2.1., the minimum water pressure that can be reached using the same constitutive relations of Liakopoulus test is -9200Pa.

After ten minutes, this limit is already overpassed.

In order to show the evolution of the variables (and in particular the decreasing of the phase field value) over these 10 minutes, the results are taken for a longer time. Reached the 40 minutes the values of the variables are clearly distorted.

In the following pages, the results in term of displacements, water pressure, saturation degree and phase field value, are described with graphs.

A comparison between the implementation with and without considering the phase field variable is made.

- **Displacements**

The evolution of displacements during the time taking into account the phase field (Figure 5.15a) and without considering it (Figure 5.16b) are shown.

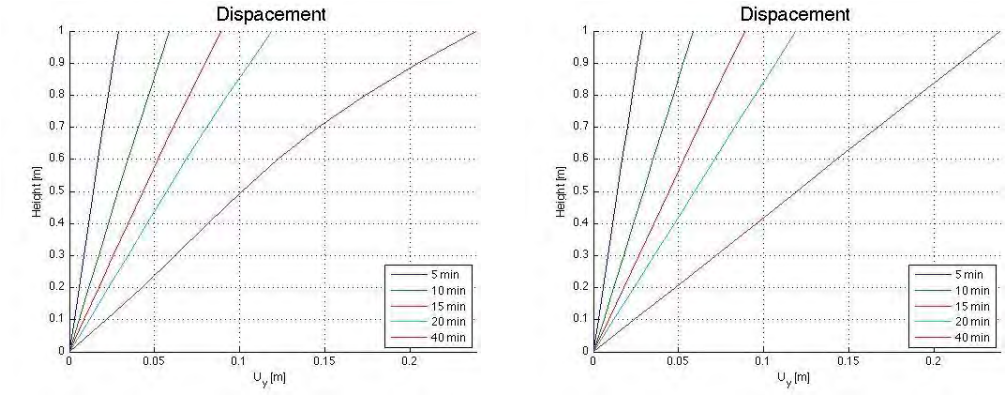

a) *b)*

Figure 5. 15. Displacements at different steps of time, with (a) and without (b) considering the phase field.

The comparison between final displacements considering or not considering the phase field at some different time steps (5,10,15 minutes) are now reported.

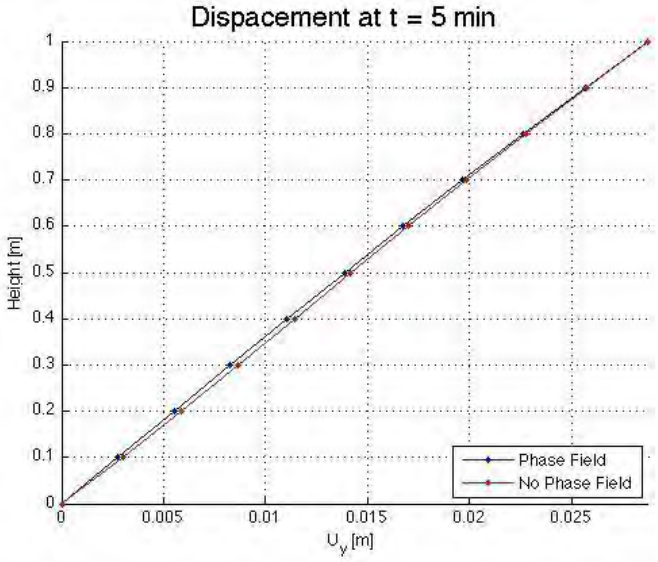

Figure 5. 16. Displacements after 5 minutes with and without considering the phase field.

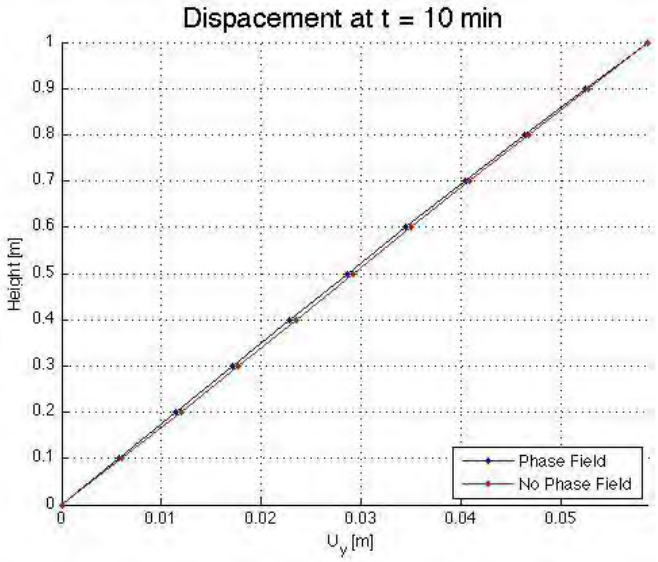

Figure 5. 17. Displacements after 10 minutes with and without considering the phase field.

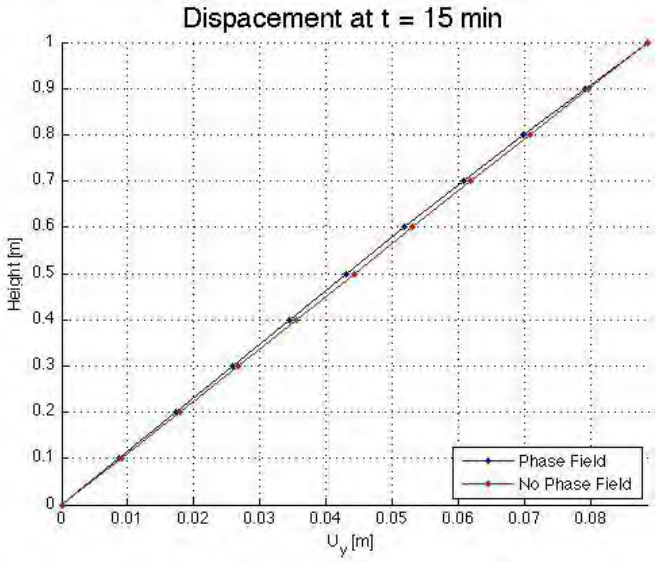

Figure 5. 18. Displacements after 15 minutes with and without considering the phase field.

As regards the displacements, the difference between those ones calculated without taking into account the phase field variable are not so different (but a little bit inferior) than the ones obtained from the complete model.

- **Water pressure**

Similarly to what was made for the displacements, also for water pressures the evolution in time is shown, both in the case complete with phase field and both in the case with the porous media alone.

The limit imposed for Liakopoulus constitutive laws is highlighted with a vertical red line (overpassed by the complete model after ten minutes).

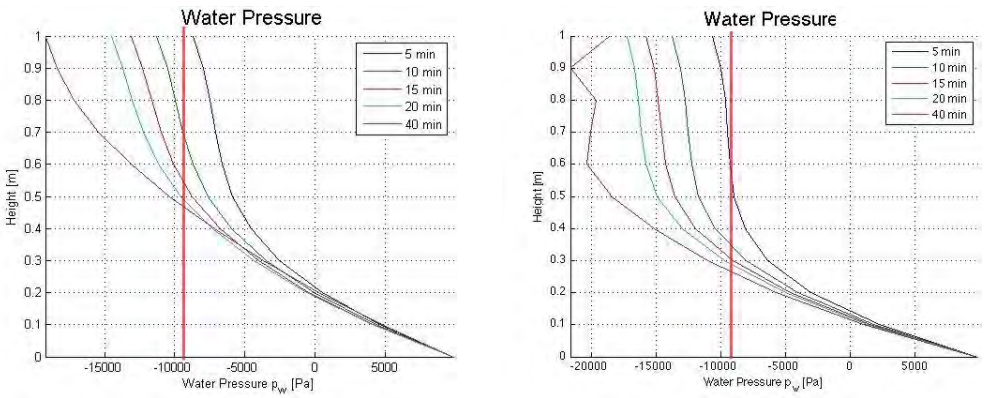

a) *b)*

Figure 5. 19. Water pressures at different steps of time, with (a) and without (b) considering the phase field.

The comparison between final displacements considering or not considering the phase field at some different time steps (5,10,15 minutes) are now reported.

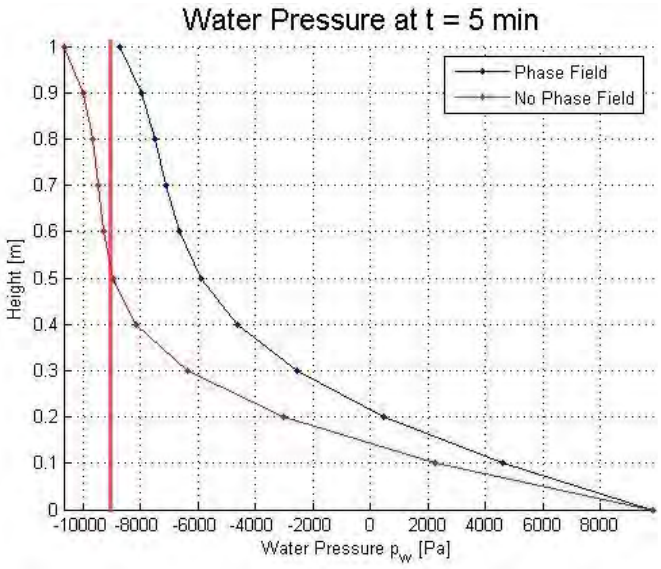

Figure 5. 20. Water pressures after 5 minutes with and without considering the phase field.

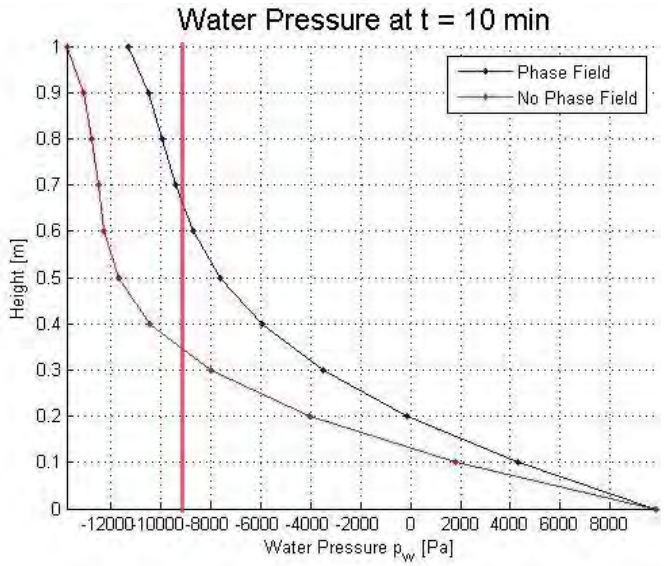

Figure 5. 21. Water pressures after 10 minutes with and without considering the phase field.

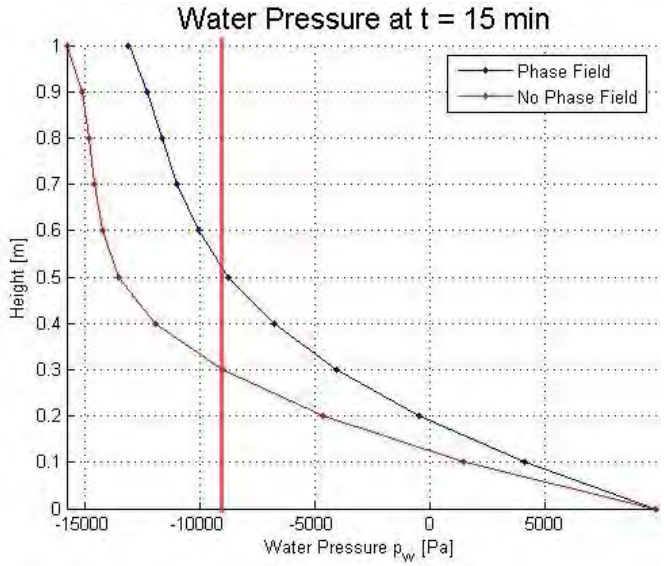

Figure 5. 22. Water pressures after 15 minutes with and without considering the phase field.

Observing the graphs above, the obvious conclusion that can be made is that water pressures in the complete model with phase field is lower in modulus. In fact the limit value (when every physical meaning of constitutive laws is lost) is reached before in the model without the phase field implementation (40 minutes).

In the complete model this limit is reached after 54 minutes, as shown in Figure 5.23.

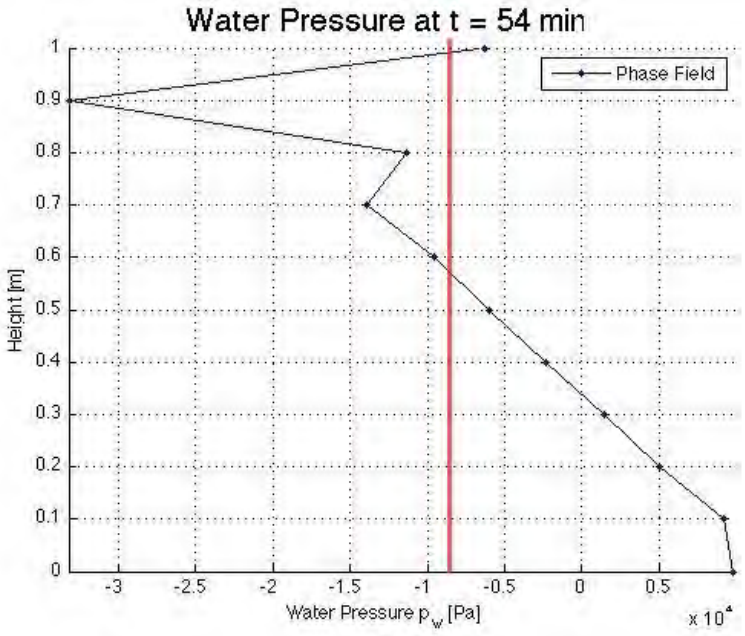

Figure 5. 23. Water pressures after 54 minutes in the complete model.

- **Saturation degree**

The evolution in time of Saturation degree is shown in Figure 5.24. In this case, the red vertical line indicates the limit for S_w, fixed at 0.91.

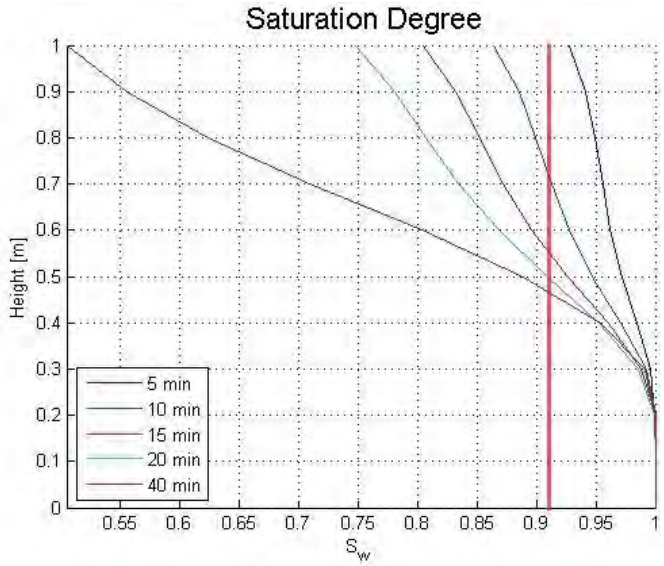

Figure 5. 24. Saturation degree at different steps of time.

Following, the results at some different time steps (5,10,15 minutes)

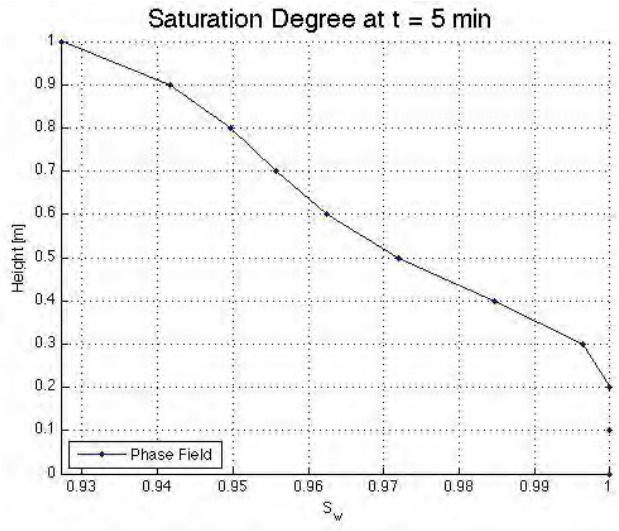

Figure 5. 25. Saturation degree after 5 minutes.

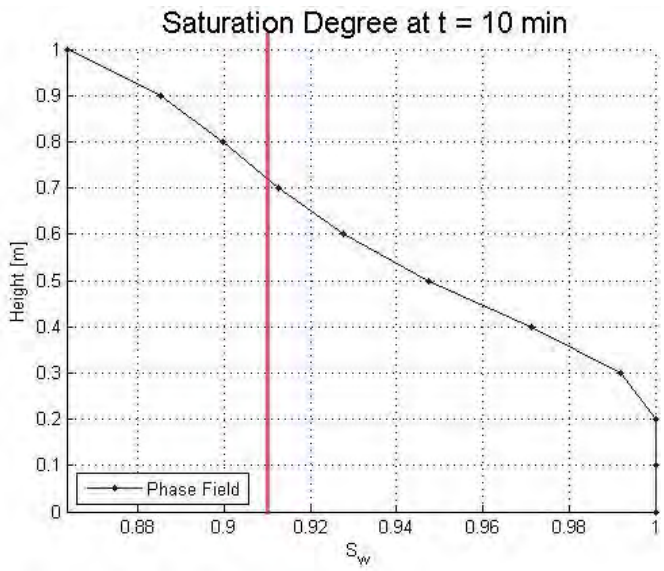

Figure 5. 26. Saturation degree after 10 minutes.

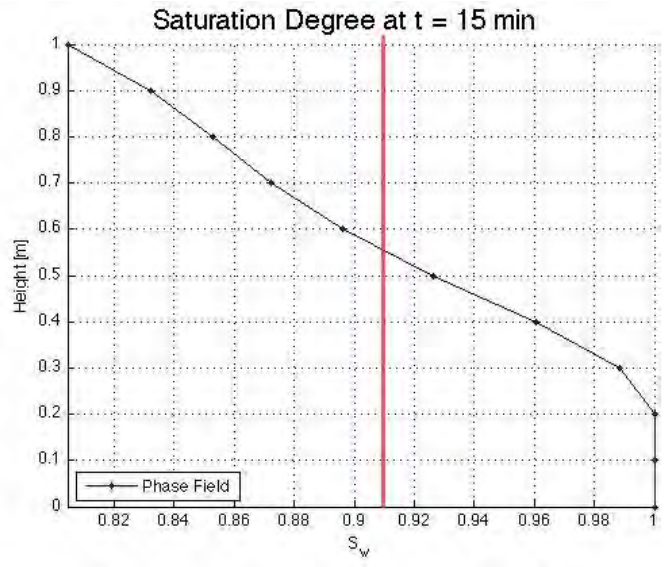

Figure 5. 27. Saturation degree after 15 minutes.

After 10 minutes, the Saturation degree at the top of the column begin to overpass the limit. In the case without the phase field implementation

this phenomenon appears earlier, already after the first five minutes, as evident from Figure 5.28.

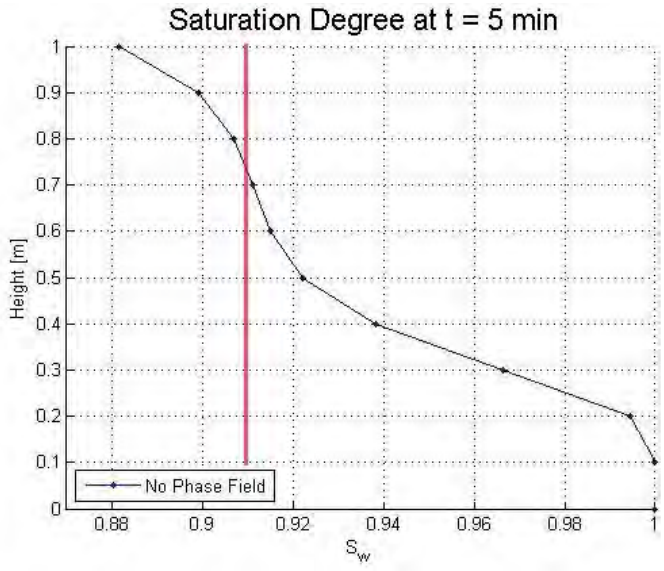

Figure 5. 28. Saturation degree after 5 minutes (no phase field).

- **Phase field**

The phase field parameter assumes the value zero at the beginning, when the material is unbroken. Step by step, its value tends to zero, value that corresponds to the broken material.

After 54 minutes the material (when our observations are forced to be stopped) is quite completely broken and the parameter is nearly zero. The evolution of this parameter is physically correct even if the laws are used over their theoretical limit.

Next, the evolution of phase field in time will be show (Figure 5.29).

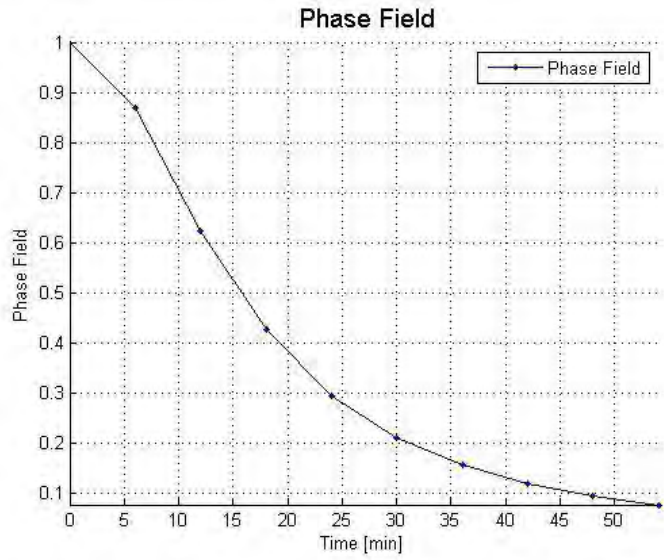

Figure 5. 29. Phase field vs time.

5.2.3. Traction on all the nodes on the top. 160 element-column

In order to collect more significant results, with a phase field changing along the column, from the top to the bottom of it, the mesh is better discretised. 160 elements, instead the previous ten, are used, creating a net of 4x40 elements, as described in Figure 5.30.

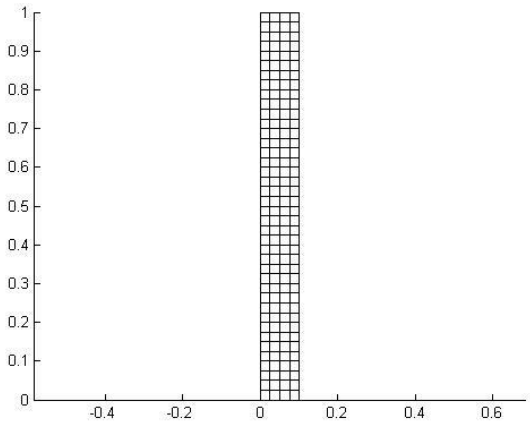

Figure 5. 30. Mesh with 160 elements.

The column is therefore loaded with incremental displacements (0.001 m each time step) applied on the five superior nodes.

Even in this case the limit pressure for the application of Liakopolus constitutive relations are overpassed, in order to catch the evolution of all the variables in time, even after reaching the limit point for pressures. The inevitable stop is after 35 minutes: after them the Liakopolus laws lose every physical meaning.

The results at each time step are shown below.

- **t = 5 minutes**

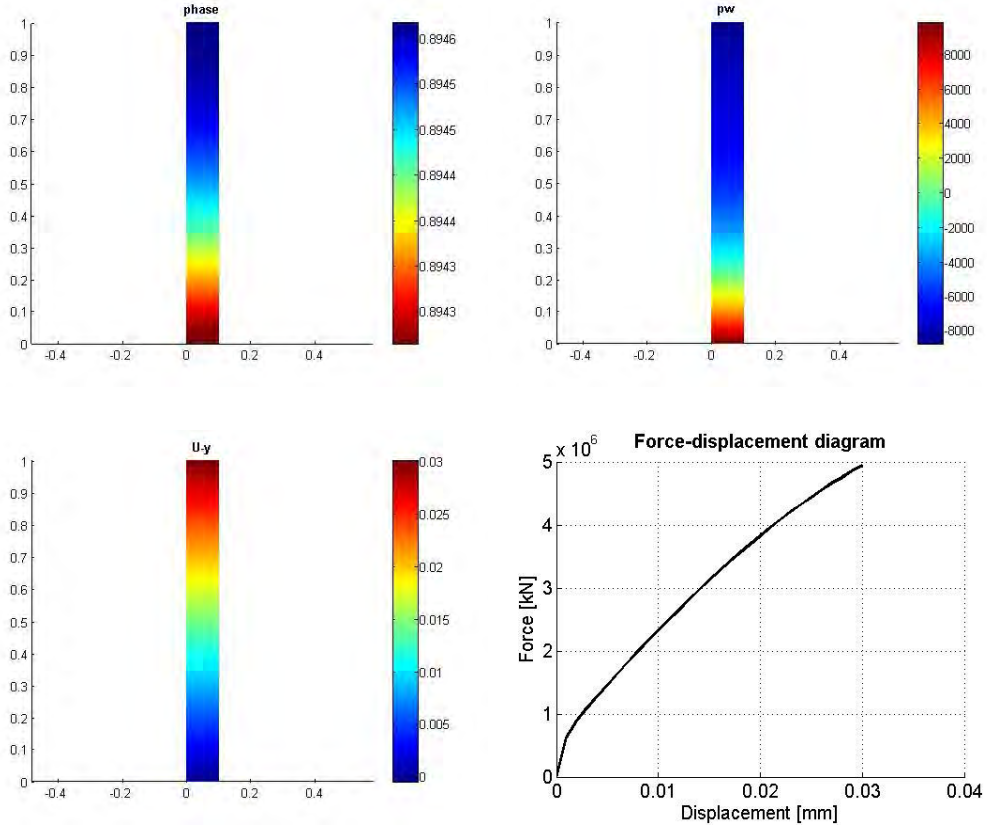

Figure 5.31.Results after 5 minutes.

- **t = 10 minutes**

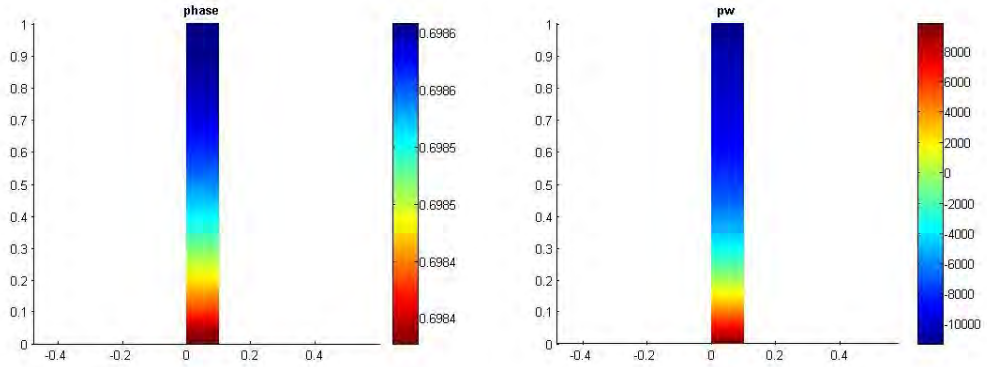

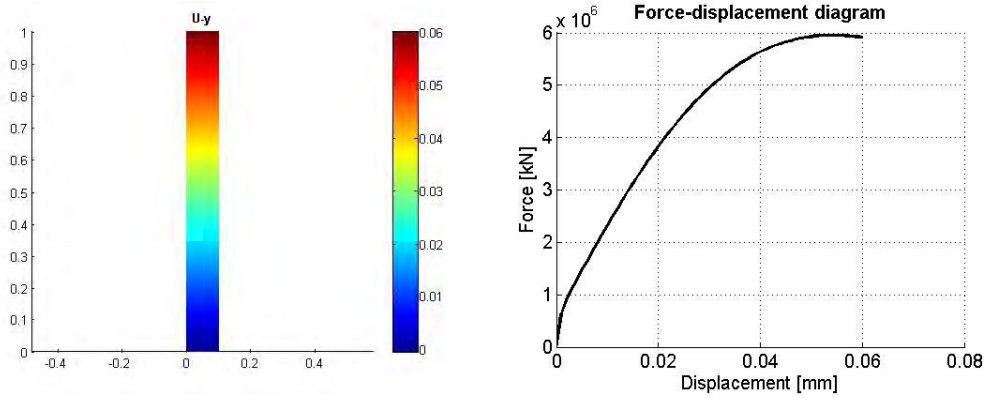

Figure 5. 32. Results after 10 minutes.

- **t = 15 minutes**

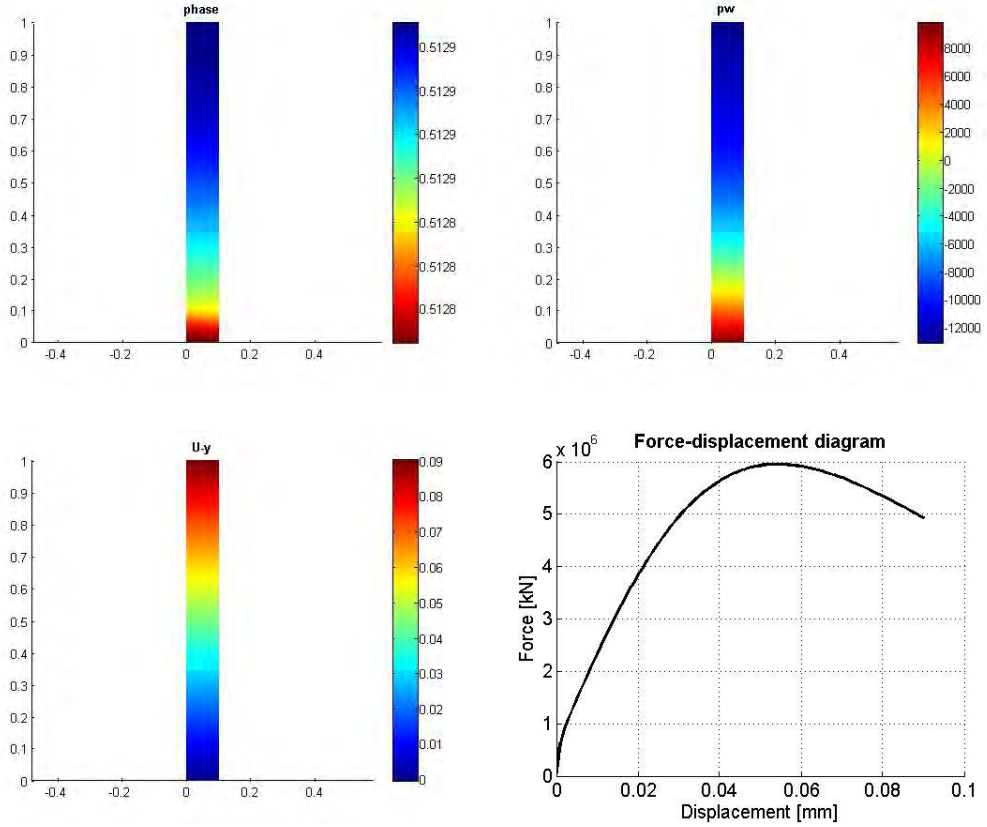

Figure 5. 33.Results after 15 minutes.

- **t = 20 minutes**

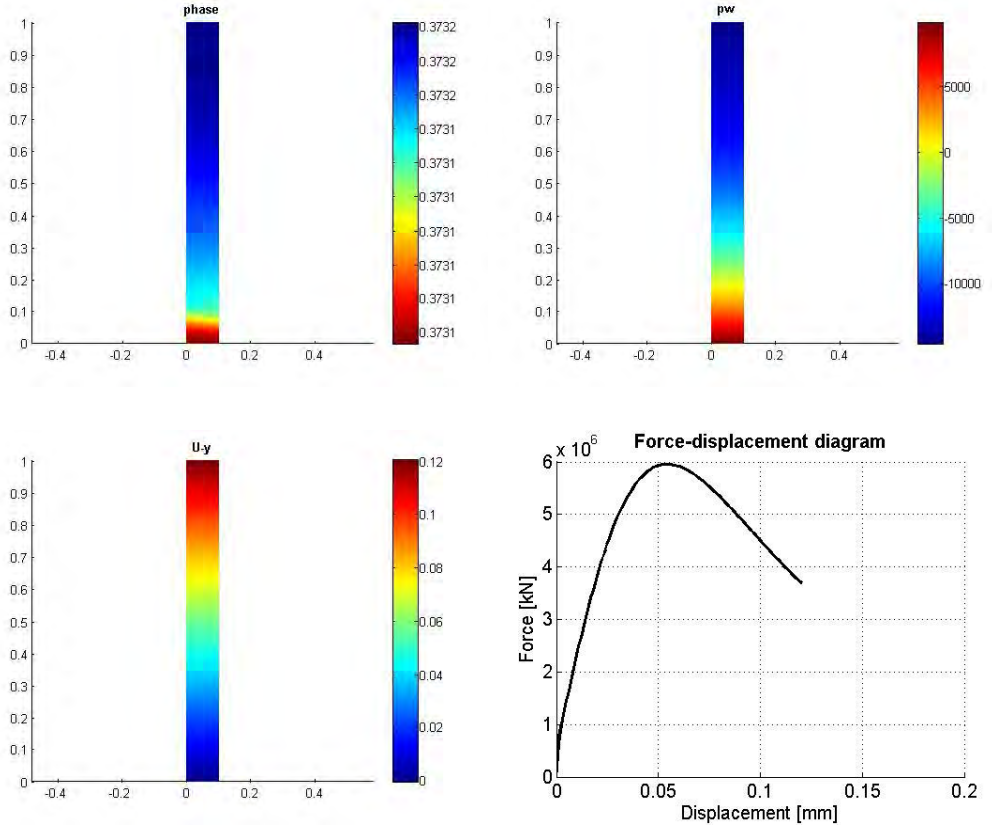

Figure 5. 34. Results after 20 minutes.

- **t = 25 minutes**

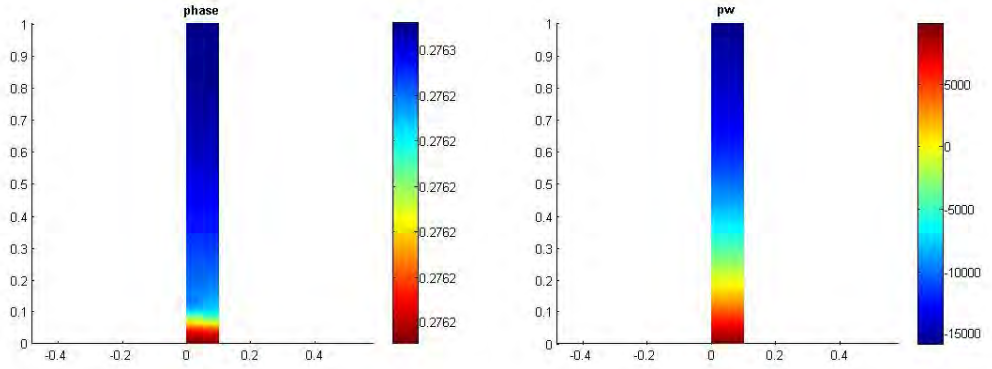

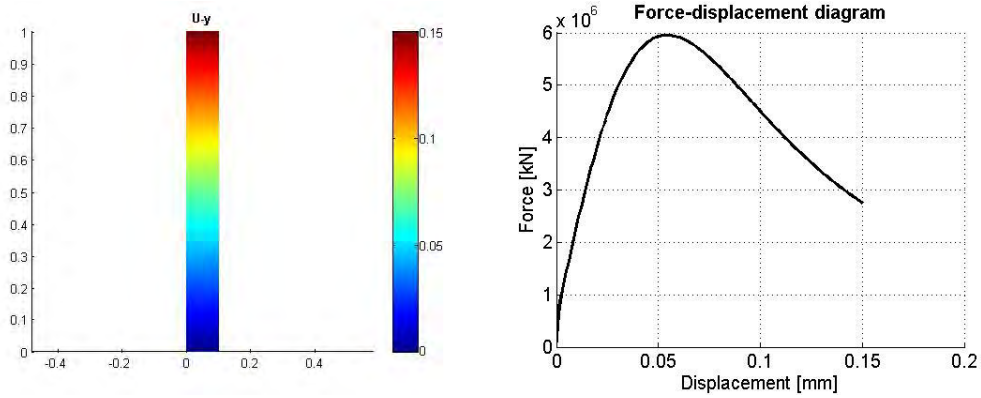

Figure 5. 35. Results after 25 minutes.

- **t = 30 minutes**

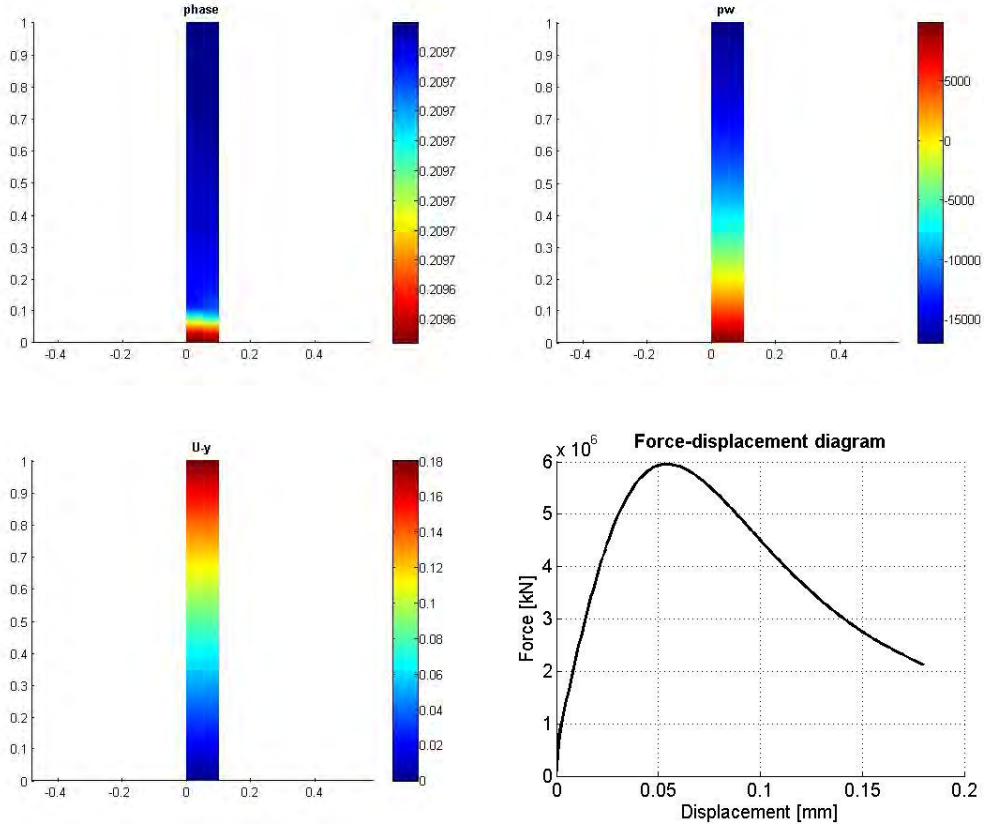

Figure 5. 36. Results after 30 minutes.

- **t = 35 minutes**

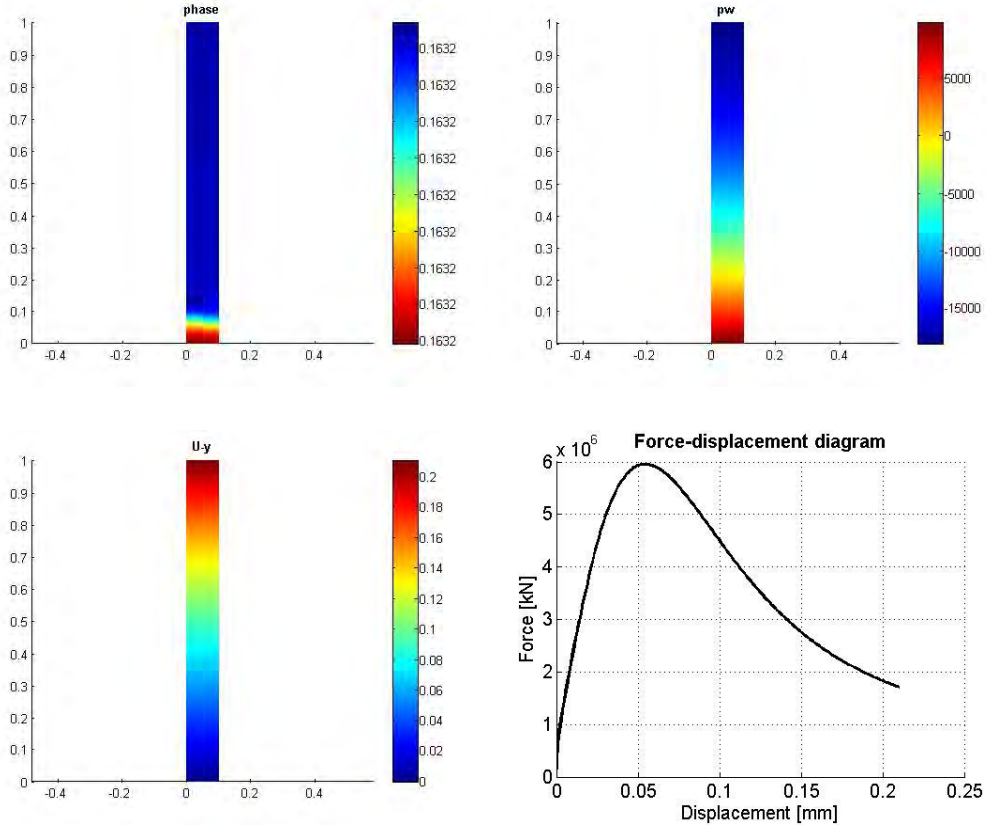

Figure 5. 37. Results after 35 minutes.

Final considerations

Values of phase field change from the top to the bottom of the column. Obviously the column breaks before in correspondence of the application of the load.

After the 35 minutes, the deformation of the column is the following:

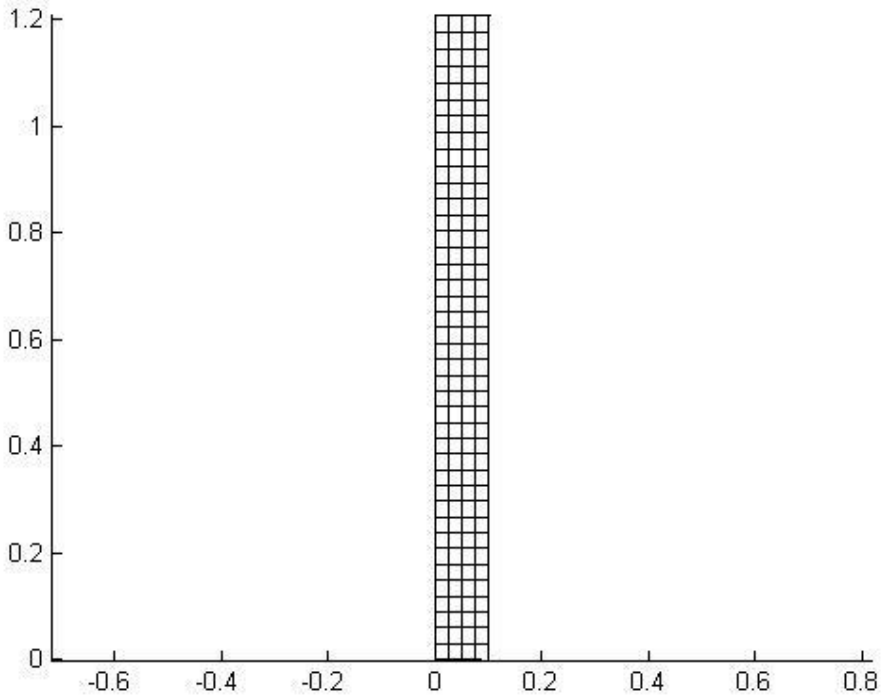

Figure 5. 38. Column configuration after 35 minutes.

The column is stretched, becoming 1.2 meters high: 0.2 meters more than in the initial conditions. Observing carefully the Figure 5.38, a different deformation of the elements can be noticed. In particular the element below are less stretched than the elements above.

An important observation is that after ten minutes water pressure values have already overpassed the limit pressure of Liakopoulus test.

At the last possible measure (35 minutes) the phase field value has however reached the value of 0,1632: the material can be considered almost totally broken.

The evolution of the phase field (calculated in one of the nodes of the top) in time is plotted in the next graph (Figure 5.39).

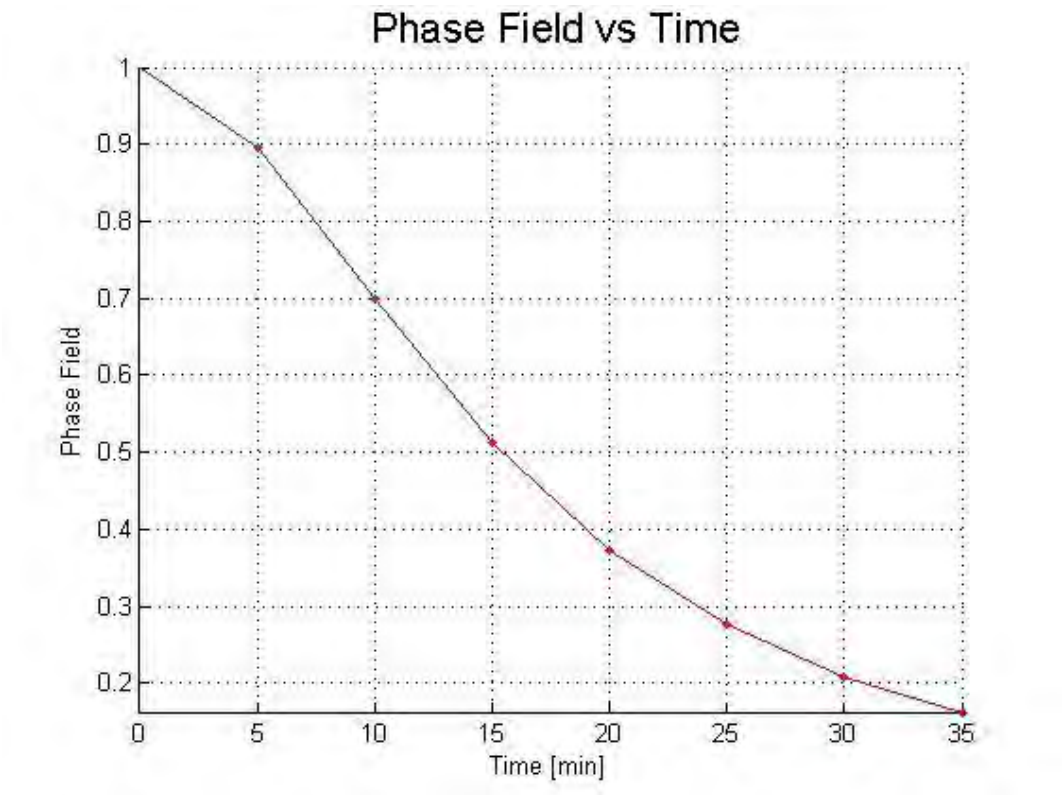

Figure 5. 39.Phase Field vs Time.

5.2.4. Traction on two the nodes on the top. 160 element-column

This example is a variation of the previous one. The mesh used is the same with 160 elements. The only difference is the point where the incremental displacements are applied. Instead of applying it to all the nodes on the top of the column, it is applied only to the two external nodes on the top. The aim is to notice a differentiation of strains and phase field variable even along the horizontal direction.

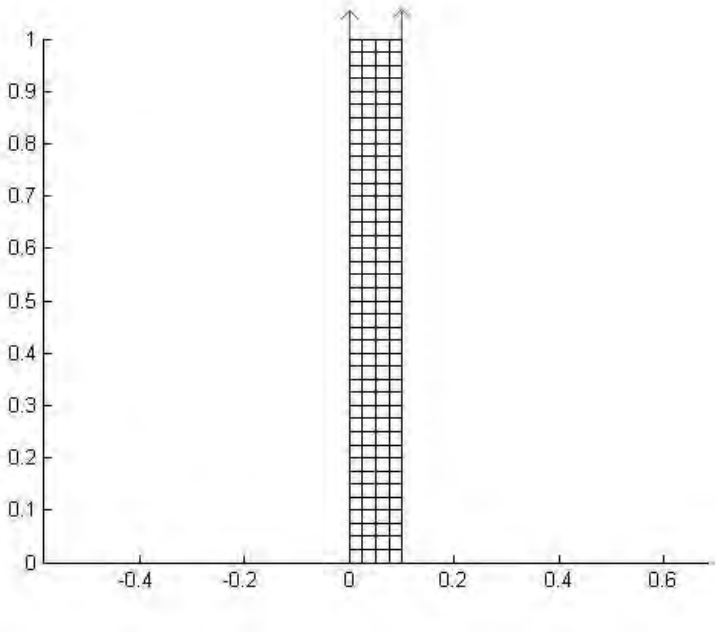

Figure 5. 40. Mesh and applied traction.

Also in this case the limit pressure for the application of Liakopolus constitutive relations are overpassed, in order to catch the evolution of all the variables in time, even after reaching the limit point for pressures. The inevitable stop is after 35 minutes: after them the Liakopolus laws lose every physical meaning.

The results at each time step are shown below.

- **t = 5 minutes**

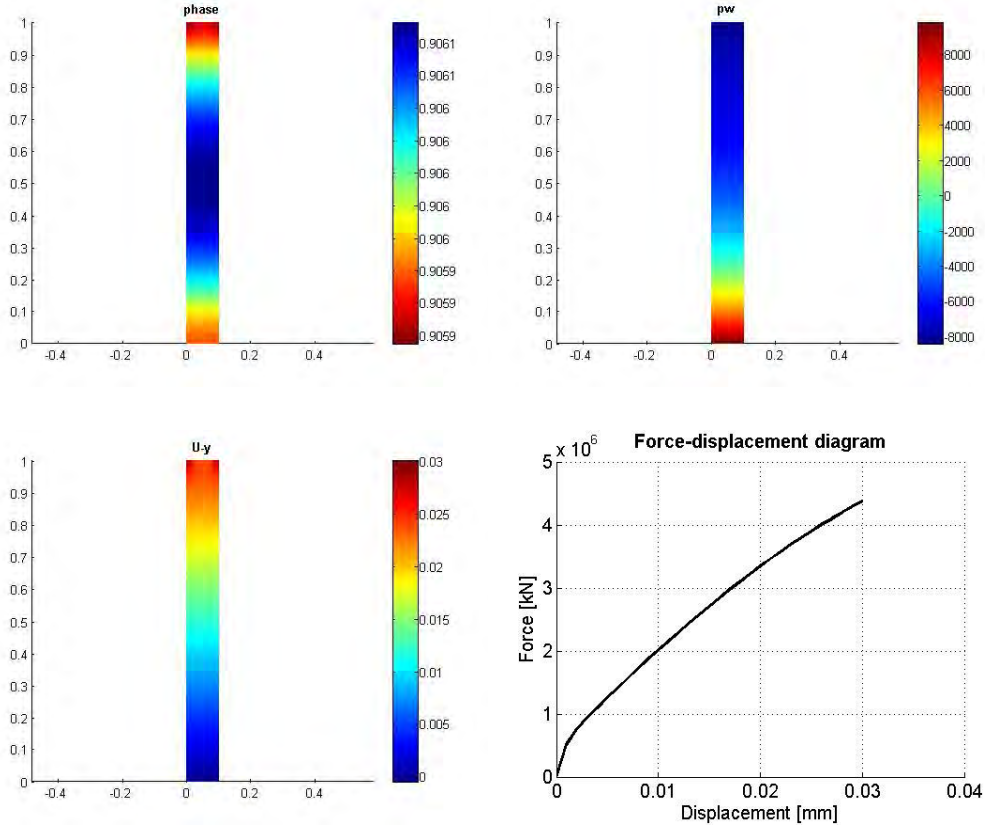

Figure 5. 41. Results after 15 minutes.

- **t = 10 minutes**

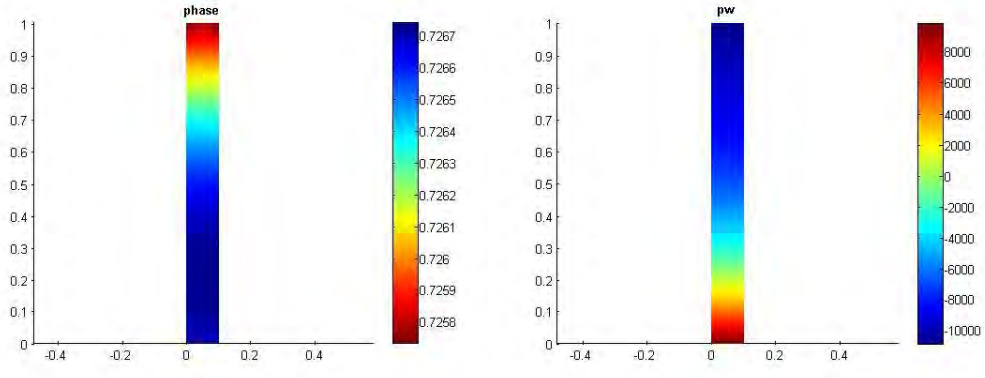

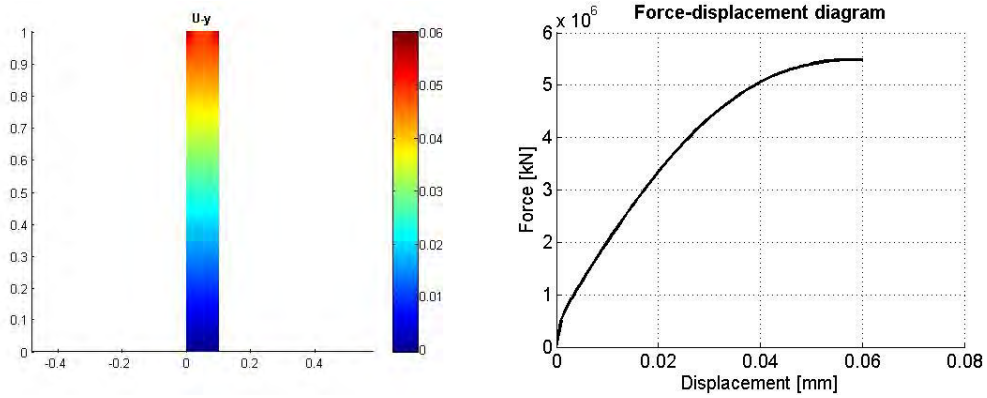

Figure 5. 42. Results after 10 minutes.

- **t = 15 minutes**

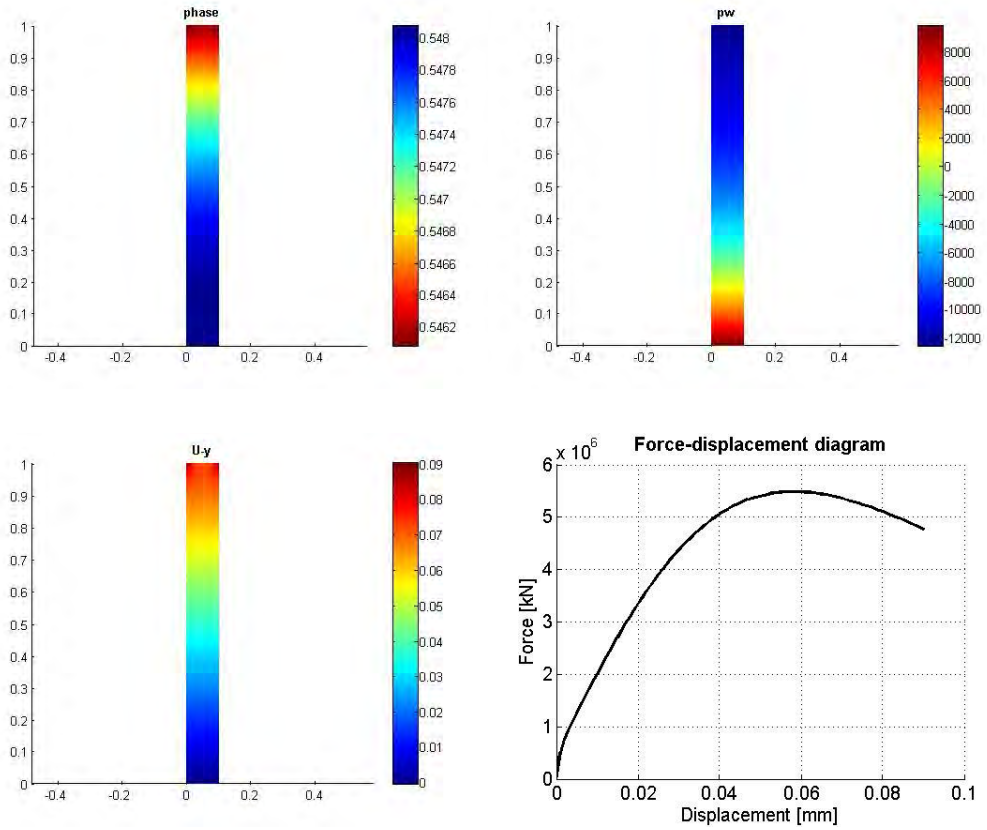

Figure 5. 43. Results after 15 minutes.

- **t = 20 minutes**

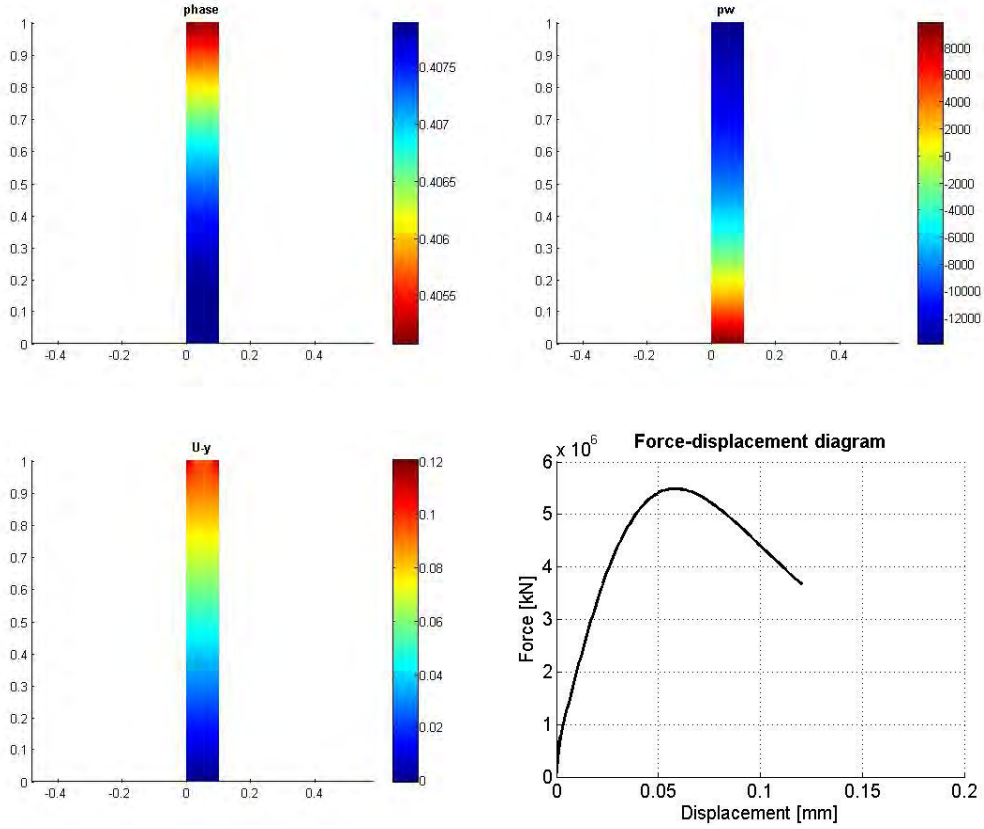

Figure 5. 44. Results after 20 minutes.

- **t = 25 minutes**

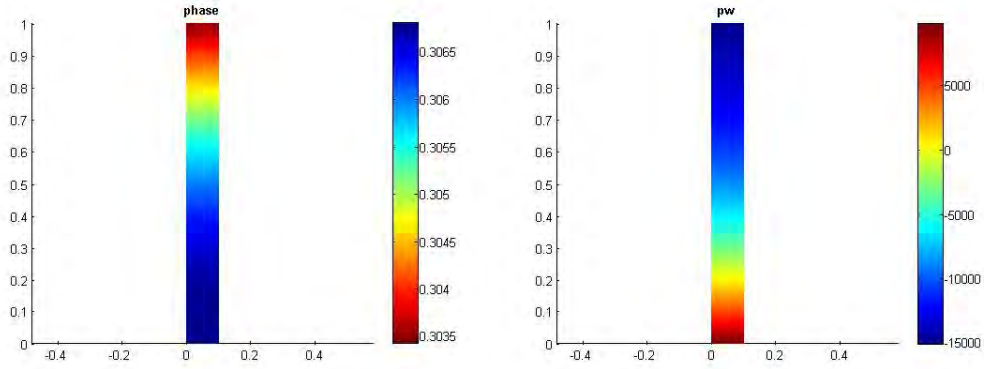

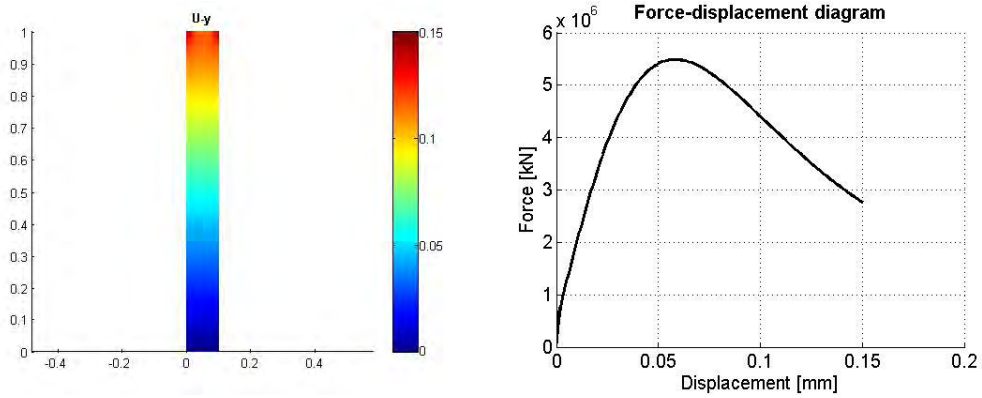

Figure 5. 45. Results after 25 minutes.

- **t = 30 minutes**

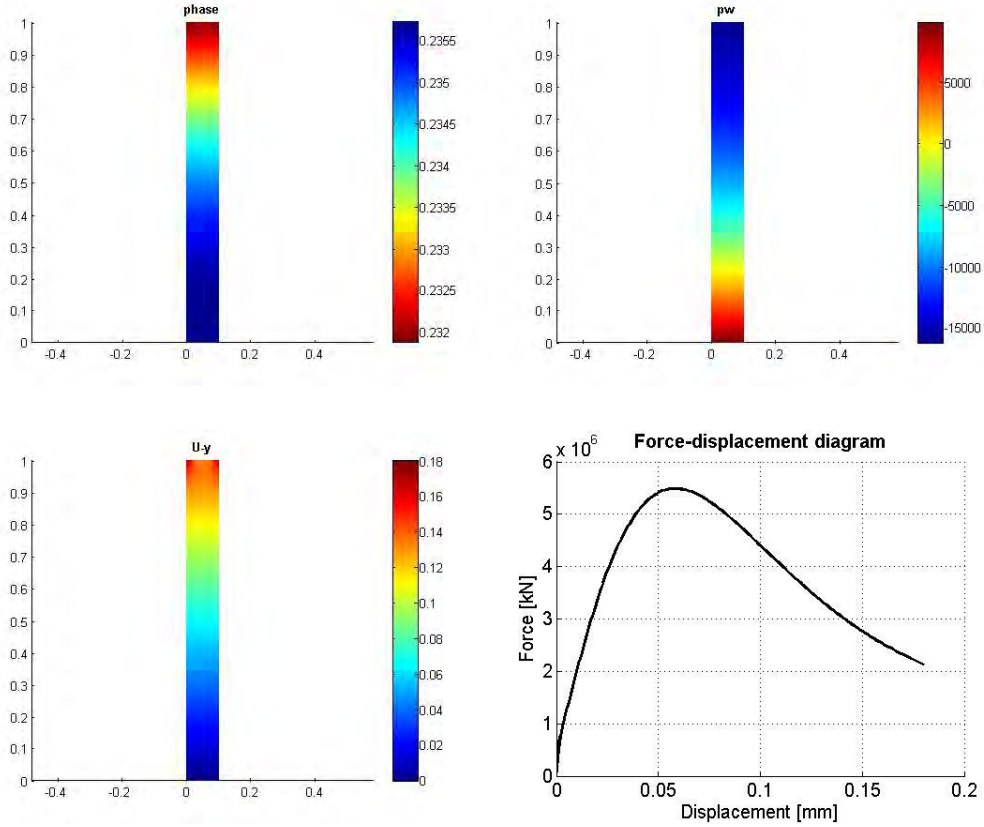

Figure 5. 46. Results after 30 minutes.

- **t = 35 minutes**

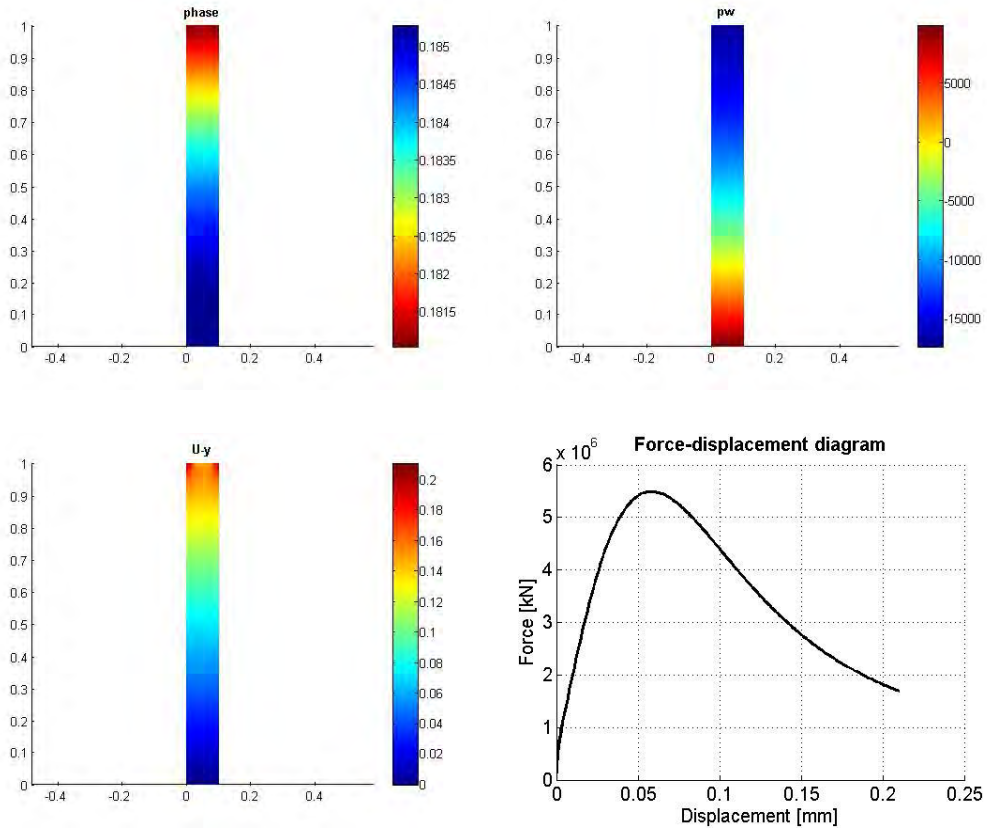

Figure 5. 47. Results after 35 minutes.

Final considerations

As evident from the graphs, the values of phase field (and consequently displacements), especially in correspondence of the elements more closed to the top, difference themselves also along the horizontal. They present peaks of value in correspondence of the nodes with an applied load.

After the 35 minutes, the deformation of the column is the following:

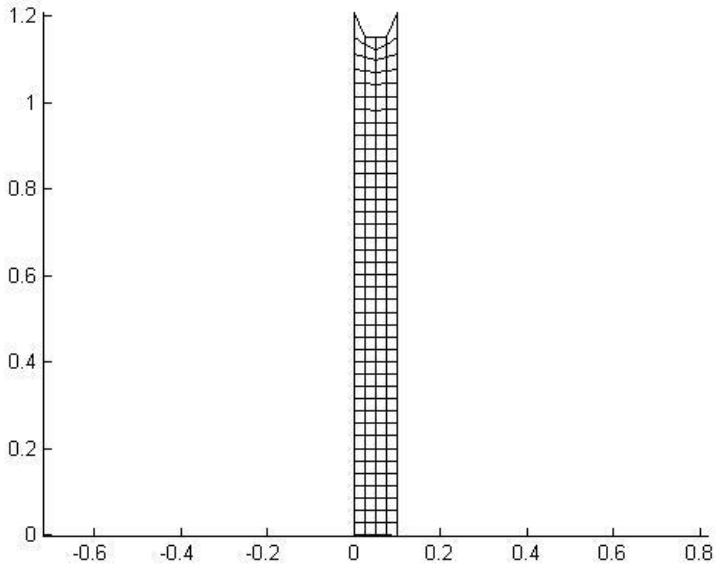

Figure 5. 48. Column configuration after 35 minutes.

At the last possible measure (35 minutes) the phase field value has however reached the value of 0,1815: the material can be considered almost totally broken.

The evolution of the phase field in time is plotted in the next graph (Figure 5.49).

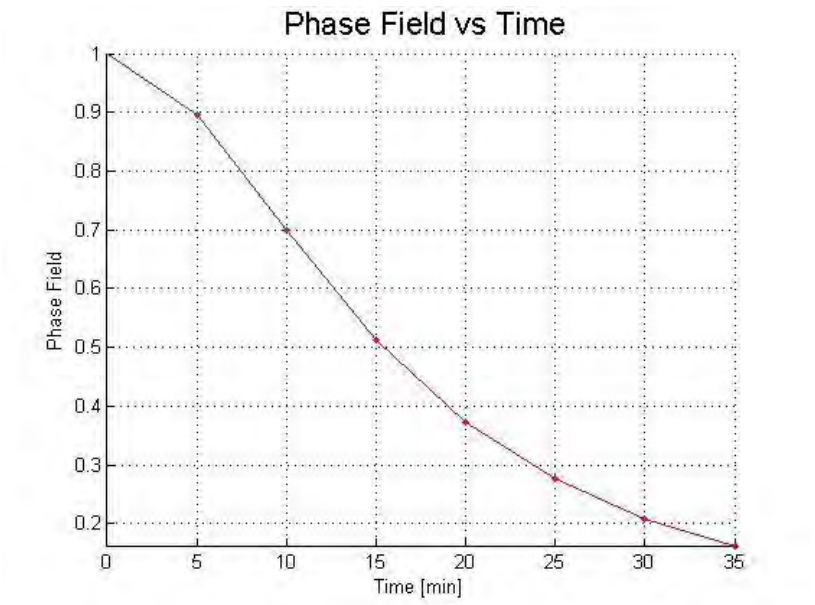

Figure 5. 49. Phase field vs Time.

It could be now interesting to compare the different evolution of phase field in the two last cases (traction applied on 5 nodes, or only on two nodes). This comparison is made in Figure 5.50.

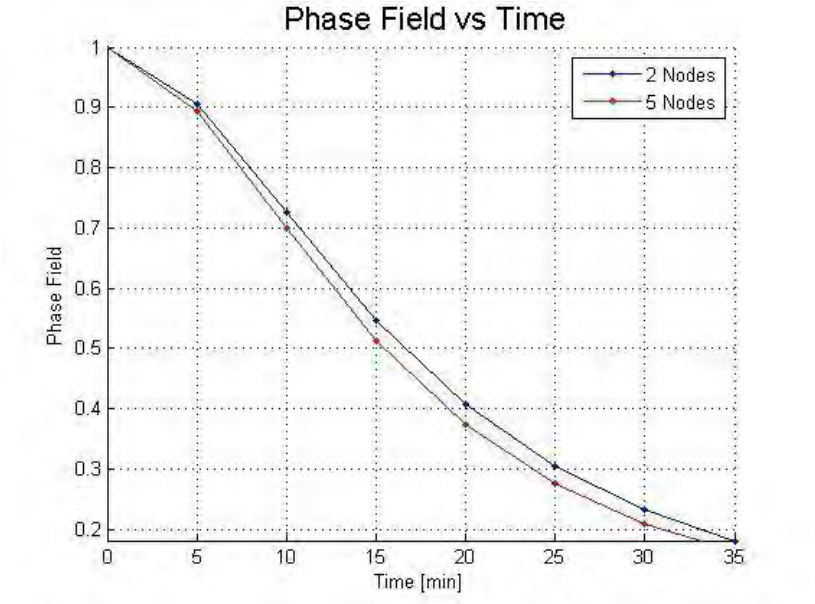

Figure 5. 50. Phase field vs Time – Comparison.

The phase field values in both cases are plotted in correspondence of one of the stretched nodes. The conclusion is that if less nodes are involved in the traction, they are consequently characterized by a highest value of phase field. They will arrive earlier to a fracture: this is comprehensible also from a physical point of view.

Chapter 6 – Conclusions

This work began with a carefully itinerary through the complex world of the phase field. The first weeks in Braunschweig have been devoted to the analysis of the phase field theory, as well as to the comprehension of its implementation in the Matlab code, kindly provided by the foreign Institute.

After that the attention was moved to the discovery of the porous media: their equations, their features and their laws. This was the indispensable step to implement a code able to perfectly describe the phenomena just studied.

Finally, the last stage: to find the right way to fit the two models together, not only from the point of view of a correct theoretical approach, but also from a numerical point of view.

The set goal for this master thesis was showing a proof that an union of the two big fields of research is possible and open the way for future investigations.

In fact, no studies have still leaded in this direction till now, and the way is still opened.

After this work, the result in this sense can be considered satisfactory. With the last examples of Chapter 5 is clear that the two models can combine in the right way and the number of tests and situation that can be simulated to examine in depth the subject is really ample.

In this work, some limits due to the applicability of the constitutive laws had to be taken into account. The first step for future analysis will be therefore the use of different laws which can better and more extensively describe the phenomena.

The way is opened, hopefully the future and the future studies will produce other proofs and deeper examples that this bond “porous media/phase field” is really possible.

Bibliography

Borden M.J. et al.; “A phase field description of dynamic brittle fracture”, Computer Methods Applied Mechanics and Engineering 217-220 (2012) 77-95

Durner W.;Flühler H.; “Soil Hydraulic Properties”, Encyclopedia of Hydrological Sciences. Edited by M G Anderson. 2005 John Wiley & Sons, Ltg.

Kuhn C.; “Investigation of a Phase Field Model for Fracture”,2013

Lewis R.W.; Schrefler B.A.; “The Finite Element Method in the Static and Dynamic Deformation and Consolidation of Porous Media”, 1998 John Wiley & Sons, Ltg.

Lu N.; Likos W.J.; “Unsaturated Soli Mechanics”, 1960 John Wiley & Sons, Ltg.

Miehe C. et al.; “A phase field model for rate-independent crack propagation: Robust algorithmic implementation based on operator splits”, Computer Methods Applied Mechanics and Engineering 199 (2010) 2765-2778

Xie

Zienkiewicz O.C.; Chan A.H.C.; Pastor M.; Schrefler B.A.; Shiomi T.; “Computational Geomechanics, with special Reference to Earthquake Engineering; John Wiley & Sons, Ltg.